ISSN: 2091-0304

JNCS

Journal of Nepal Chemical Society

JOURNAL OF NEPAL CHEMICAL SOCIETY

Volume 40, December 2019

Published by
Nepal Chemical Society
P.O.Box: 6145, Kathmandu, Nepal,
E-mail: info@ncs.org.np, Website: www.ncs.org.np

Published by

Regd. No. 8/042/43

Nepal Chemical Society

P.O.Box: 6145, Kathmandu, Nepal,

E-mail: info@ncs.org.np, Website: www.ncs.org.np

Regd. No. 8/042/043 **ISSN: 2091-0304**

Editorial Board

Chief Editor

Dr. Netra Lal Bhandari
Department of Chemistry, Tri-Chandra Multiple Campus
Tribhuvan University, Kathmandu Nepal
E-mail: chiefeditor@ncs.org.np

Editors

Dr. Bhushan Shakya
Amrit Science Campus, Tribhuvan University, Kathmandu Nepal
E-mail: bhusansakya@gmail.com

Dr. Lok Kumar Shrestha
National Institute for Materials Science (NIMS), Japan
E-mail: SHRESTHA.Lokkumar@nims.go.jp

Dr. Bijay Singh
Harvard University, Cambridge, USA
E-mail: singhbijay@ribb.org.np

Published by: Nepal Chemical Society, **GPO Box** 6145, Kathmandu, Nepal
E-mail: info@ncs.org.np, **Website:** www.ncs.org.np

December 2019

Executive Council of Nepal Chemical Society (2019/2021)

Contact Point

Central Department of Chemistry, Tribhuvan University, Kirtipur, Kathmandu, Nepal

GPO Box: 6145, Kathmandu, Nepal, **E-mail:** info@ncs.org.np, **Website:** www.ncs.org.np

JNCS
Journal of Nepal Chemical Society December 2019, Vol. 40

Contents

Author Guidelines-Journal of Nepal Chemical Society (JNCS)

Journal of Nepal Chemical Society (JNCS), publishes original research and review articles related to chemistry. The article should be concise, clear and written in English.

Scope: Journal of Nepal Chemical Society (JNCS) is a peer-reviewed chemistry journal published by Nepal Chemical Society (NCS), Kathmandu, NEPAL. JNCS publishes original research papers, review articles, short communications and research reports on topics related to different chemistry disciplines such as organic chemistry, inorganic chemistry, physical chemistry, analytical chemistry, pharmaceutical chemistry, nanochemistry and nanomaterials, polymer chemistry and polymer composites, biochemistry and bio molecules, environmental chemistry, geo-chemistry, and allied fields.

Authors are kindly requested to check final paper thoroughly before submitting–that you have fulfilled all requirements stated in the instructions.

Instructions for manuscript preparation

Manuscripts: JNCS publishes the original research articles and reviews related to chemistry. The manuscript should be written in English in a clear and concise manner and should follow the style of Nepal Chemical Society. The manuscript must be type written in Times New Roman-11 pt. font size with 1.5 line spacing, justified, in A4 size paper with 2 cm margins around.

A full-length paper should normally be divided into the following parts: **Title, Authors' name and affiliations** with corresponding E-mail. **Abstract** (not exceeding 250 words), Keywords (not exceeding 5 words), **Introduction, Experimental Methods (Materials and Methods), Results and Discussion, Conclusion, Acknowledgements, References** and Annexures if any.

Enter the page number on every page. Language should be precise, clear without redundant words. Binomial names of organisms and other acronyms should be spelled full in the first use. The length of the paper including tables and figures should be preferably within 5-10 typed pages for original article, 8-16 pages for review and 3-4 pages for short communications. The SI system units and symbols are recommended. Manuscript should be free from plagiarisms. The journal follows a blind submission policy and articles will anonymously be reviewed by peers. The editorial board will assume no responsibility for the statements and opinions forwarded by the contributors. The decision of the Editorial Board will be final for processing and publication.

Title: Titles should represent the content of the manuscript, correlates the conclusion, serve as a guide to reference librarians, and facilitate communication. It should be concise, meaningful and clear. Subtitles may be used whenever needed. Title text should be centred, 14 pt. boldface with initial capitals, and subtitles 12 pt., boldface and sentence case.

Author(s) and Author(s) affiliations: The full name of the author(s) should be written in 11 pt. bold, centre aligned and below the title. Authors' list should include only those who have made a substantial contribution to design, execution of the work and manuscript preparation. Author(s) affiliations represent the official institutional address of authors. It should be typed in 11 pt. italics, left aligned.

Abstract: Abstract should summarize and briefly explain the major findings of the paper. It must contain experimental question, importance, method, major findings, conclusions and applications preferably not exceeding 250 words followed by 5 keywords.

Introduction: The purpose of your research should appear in the introduction. Stat the questions you sought to answer, and provide pertinent information of previous findings for those questions including brief and latest literatures survey.

Materials and Methods: Provide sufficient information clearly to allow someone to repeat your work. Clear descriptions of experimental design, sampling procedures, and statistical tools have to be mentioned. Give the model number and company for equipment used (if any).

Results and Discussion: Results should be stated concisely, do not misinterpret your findings. Differentiate the results of your study from data obtained from other secondary sources. Interpret your results, relate them to the results of previous research, and discuss the implications of results.

Conclusion: State clearly the main conclusions of the research and give a clear explanation of the importance, relevance and applications.

Acknowledgements: Acknowledge only those who have made an important contribution to the study. Many contributions justify acknowledgement such as technical help, financial support, source of materials and persons who have contributed intellectually to the development of the manuscript. Do not acknowledge anyone who has no contribution.

References: Author(s) take the full responsibility for the accuracy of their references. The format of references must be uniform and consistent with the instructions below. All publications cited in the text should be referred to by a number in square brackets (e.g. [1]). Note that only one reference belongs to one number. List all cited references in chronological order using Arabic numerals.

Tables, Figures, Pictures, Equations: The tables and figures should be clearly marked with self-explanatory notes and figure legends. Figure and table captions should be given below and above respectively. Figures and illustrations are expected in JPEG/TIFF (at least 300 dpi resolution) format. Figure and table captions are typed in 10 pt., Times New Roman and in italic. Each figure and table should be linked with the text. Figure and Table number should be in sequence, using Arabic numerals, i.e. Figure 1. 2., 3., etc., Table 1., 2., 3., etc.). They should be clearly numbered. All the new symbols must be clearly explained. Metric units for all kind of measurements would be preferred. Figures include photographs, drawing and graphs, and they should be made in an appropriate size of about 3 inch height and 4 inch width. Legends for table and figure should be typed separately.

Reference Style: ***Journals articles;*** [Authors name; R. Robinson, …], [title of paper], [*journal name*], [year], [**volume**], [page range.], [DOI]

1. J-M. Seo, H-J. Noh, H. Y. Jeong and J-B. Baek, Converting unstable imine-linked network into stable aromatic benzoxazole-linked one via post-oxidative cyclization, *Journal of the American Chemical Society,* 2019, **141**(30), 11786-11790. (DOI: 10.1021/jacs.9b05244).
2. S. Y. Park, A. K. Lytton-Jean, B. Lee, S. Weigand, G. C. Schatz and C. A. Mirkin, DNA-programmable nanoparticle crystallization, *Nature*, 2008, **451**, 553-556. (DOI: 10.1038/nature06508)

Books; [Author], [*book title*], [edition], [publisher], [country], [year], [chapter], [page nos.].

Vogel's Text Book of Practical Organic Chemistry, 5th Ed. Logmans Group, UK, Limited, 1989, 968-988.

An electronic copy of manuscript both in Microsoft word and portable document format (pdf) should be send to Editor-in-Chief at E-mail: chiefeditor@ncs.org.np/nlbhandari@yahoo.com.

Further information may be provided on request to the Editor-in-Chief, Journal of Nepal Chemical Society, GPO Box 6145, Kathmandu, NEPAL.

JNCS
Journal of Nepal Chemical Society December 2019, Vol. 40, 1-4
ISSN: 2091-0304 (print)
DOI: https://doi.org:10.3126/jncs.v40i0.27270
RESEARCH ARTICLE

Anti-inflammatory Compounds Camphor and Methylsalicylate from Traditionally Used Pain Curing Plant *Equisetum arvense L.*

Achyut Adhikari[1*], Silan Bhandari[1], Durga Prasad Pandey[2]

[1]Central Department of Chemistry, Tribhuvan University, Kirtipur, Kathmandu, Nepal
[2]Research Centre for Applied Science and Technology (RECAST), Tribhuvan University, Kirtipur, Kathmandu, Nepal

[*]Corresponding E-mail: adhikarimine@yahoo.com
(Received: Sept. 11, 2019; Revised: Dec. 25, 2019 & Accepted: Dec. 27, 2019)

Abstract

Equiseum arvense L. is a bushy perennial herb commonly called field horsetail distributed in the northern part of Nepal and used against curing muscle and bone pain and other many diseases. This research work was performed to analyze the possible cause of the anti-inflammatory activity of this plant. Out of four different fractions, dichloromethane (DCM) fraction showed the presence of compounds on TLC and was subjected to column chromatography to isolate and identify pure compounds. D_2 and D_{20} fractions eluted from column gave single and distinguished spots so that these fractions were subjected to gas chromatography analysis. The GC analysis of the pure fraction D_2 obtained from column revealed the presence of a major compound major compounds camphor (92.53%) and other minor compounds; (+)-2-Bornanone, Camphor, Carvone<(z)-, dihydro->, Benzoic acid, 2-(1-oxopropyl)- and GC report from D_{20} fraction showed two compounds; Salicylate<methyl-> and Benzoic acid, 2-(1-oxopropyl)-. The major compounds camphor (92.53%) and methyl salicylate (66.87%) have been reported being potent anti-inflammatory activity and their synergetic effect is more prominent for the same.

Keywords: *Equisetum arvense*, anti-inflammatory, camphor, methyl salicylate.

Introduction

Equisetum arvense L. is the bushy perennial herb, commonly called field horsetail which is usually distributed in the northern hemisphere throughout Canada, USA, Europe, and Asia south to Turkey, Iran, the Himalayas, and across China, Korea and Japan [1]. In Nepal, it is found in moist places of the country at about 2000 m and commonly known as "Kurkure Jhar".

Horsetail consists of the creeping, string-like rootstock and roots at the nodes that produce numerous hollow, and conspicuously jointed stems. Two different types of the stem; the sterile stems are green bottle brush-like and tend to be much taller and bushier, with the jointed segments being around one inch long with a diameter of about 1/20th of an inch. The fertile stems are generally half as tall as the sterile stems and also tend to be more succulent. Fertile stems bearing spore clusters at its tip appears in early spring and are usually thick and succulent, brownish to whitish, 10 – 30 cm tall [2].

In folk medicine, *Equisetum arvense* is used for tuberculosis, for catarrh in the kidney and bladder regions, as a hemostatic for profuse menstruation, nasal, pulmonary and gastric hemorrhages, for brittle fingernails and loss of hair, for rheumatic diseases, gout, poorly healing wounds and ulcers, swelling and fractures and for frostbite (PDR for herbal medicines) [1]. The commonly known phytochemical compounds in *E. arvense* are alkaloids, phytosterols, tannin, triterpenoids and phenolics such as flavonoids, styrylpyrones and phenolic acids [3]. *Equisetum arvense* exhibits a significant antioxidant and antimicrobial activity [4]. The water extract from sterile stems of *Equisetum arvense L.* has dose-dependent cytotoxic effects on human leukemic U 937 cells [5].

FHMDO Monte *et al.* (2004) experimented on mice

by applying the hydroalcoholic extract of horsetail to mice which resulted that *Equisetum arvense* extract has an antinociceptive (pain-relieving) and anti-inflammatory agent [6]. Due to the anti-inflammatory action of *Equisetum arvense*, it is used for arthritis, chilblains, cystitis, gout, inflammation of the lower urinary tract, renal gravel and also for benign enlargement of the prostate gland. Horsetail tea is used as a gargle for mouth and gum inflammation [7]. In Nepal horsetail is used against Burns, scabies, malarial fever (Manandhar 2002, Bhattarai 2007). In the hilly area of Nepal, dried plants of horsetail are pounded and paste is then applied in bone fracture, aches, and pains of the muscles, joints, and backaches [8].

The present study is focused to determine the phytoconstituents of *Equisetum arvense* and responsible for anti-inflammatory activity.

Materials and Methods

Collection of plants

The whole plant of *Equisetum arvense* was collected from the bank of Ghatte Khola at an altitude of 2000 m from Siddeswor VDC of Bhojpur district and the collected plant material was identified by D.R. Kandel, 3-5-2019, National Herbarium and Botanical laboratory, (KATH), Godawari, Nepal. The collected plant materials were washed, shade-dried and was ground into powder.

Instruments

Buchi Rotavapour R-200, Grinder, Digital weighing machine (GT 210), GC-MS-QP 2010 Ultra SHIMADZU, Column Chromatography, water bath (Buchi 461)

Chemicals used

All reagents and solvents used were of laboratory grade from E. Merck, T. Fisher Scientific, and Qualigens Chemical Companies, India. Solvents used were hexane and dichloromethane (DCM), Silica of 60-120 mesh, Silica gel-G, Pre-coated TLC aluminum plates with a thickness of 0.2 mm.

Extraction process

Two hundred grams powdered plant was dissolved in 500 mL of hexane in clean and dry conical flasks and was kept for two days with frequent shaking and the mixtures were decanted and filtered and thus obtained residue was dried and another solvent DCM was added to the dried residue and kept for 2 days with frequent shaking and the mixtures were decanted and filtered. Finally, the obtained filtrates were concentrated with the help of a rotary evaporator below 40 ºC. Finally, a semi-solid extract of hexane and DCM extract was obtained.

Isolation of compounds

DCM soluble fraction was subjected for column chromatography because good separation and a large number of spots were seen in TLC. A slurry of the DCM fraction (1.8 g) was made with a double (1: 2) amount of silica gel, which was loaded on to a column packed with silica gel (200 g, E-Merck, 60-120 mesh). The column had an internal diameter of 4.5 cm and a height of 60 cm. The column was eluted with 100% hexane at first and then gradually polarity was increased by adding ethyl acetate in hexane with 2%, 3%, 4%, 6% ,10%,15%, 20%, 25%, 30%, 35%, 40%, 50%, 60% gradients. After obtaining each fraction TLC was checked. The number of spots observed in TLC was visualized under UV-Visible light and iodine chamber. After column chromatography, TLC of each eluted fraction was performed. Fractions having similar TLC were mixed.

Analytic conditions for GC

The GC-MS analysis was performed at the Department of plant resources, Thapathali and was performed on GCMS-QP 2010 under the following conditions: injection volume 1 µL with slit ratio 1:90. Helium as a carrier gas with a RTX-5 MS column of dimension 60 m × 0.32 mm × 0.25 µm, temperature-programmed at 50, 150 and 250 °C with a hold time of 0.0 and 4.0 min identification was accomplished by comparison of retention time with those reported in NIST 2017 and FFNSC 1.3 libraries and test method used was IS O:7609:1985.

Results and Discussion

The fraction D_2 obtained from column chromatography of DCM extract revealed the presence of a major compound camphor (92.53%) and other minor compounds (+)-2-bornanone (2.32%), carvone<(z)-, dihydro->(0.55%), and benzoic acid, 2-(1-oxopropyl)- (4.59%). The GC-MS analysis of another fraction D_{20} revealed the presence of four chemical compounds out of which only two are identified. They are Salicylate<methyl-> (66.87%) and Benzoic acid,

2-(1-oxopropyl)-(21.77%). Among them, Salicylate < methyl-> is the major component with a percentage area of 66.87%. The results are shown in the table below:

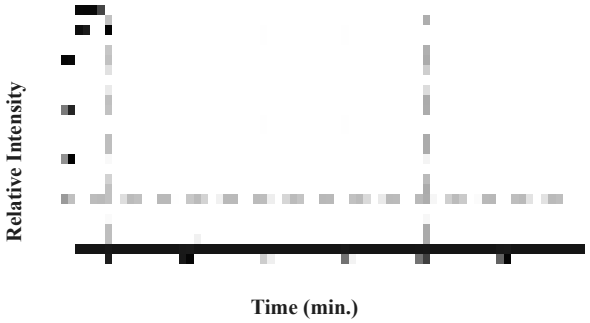

Figure 1: *Gas chromatogram of DCM extract (D_2) of Equisetum arvense.*

From the above review facts, dry horsetail is traditionally used as a fine powder paste in bone fracture, aches, and pains of the muscles, joints, and backaches. The result of GC showed that DCM extract of *Equisetum arvense* has a high content of camphor and methyl salicylate that are potent anti-inflammatory compounds. The camphor used as OFCMT (Oily formulation of camphor, menthol, and thymol) has shown tremendous protection from pain and inflammation [9] while Multum (2018) reported that methyl salicylate is a nonsteroidal anti-inflammatory drug (NSAID) which when used with a combination of camphor and lidocaine works by reducing the substances in the body that cause pain and inflammation and provide temporary relief from aches and pains of the muscles, joints, and backaches.

Table1: *Compounds detected in GC analysis of D_2 fraction of Equisetum arvense.*

S.N.	Compounds	Retention time (min.)	Percentage area	Molecular weight (g/mole)
1	(+)-2-Bornanone	21.530	2.32	152.23
2	Camphor	23.474	92.53	152.23
3	Carvone<(z)-,dihydro->	25.916	0.55	152.23
4	Benzoic acid,2-(1-oxopropyl)-	43.040	4.59	178.18

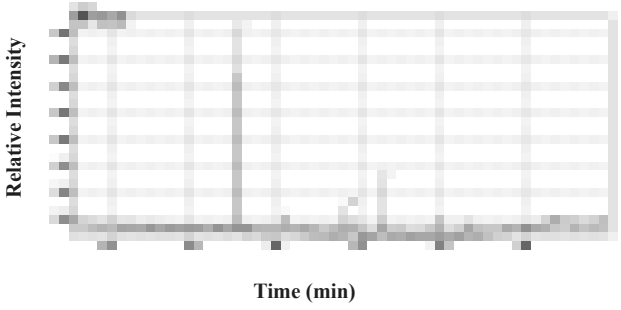

Figure 2: *Gas chromatogram of DCM extract (D_{20}) of Equisetum arvense*

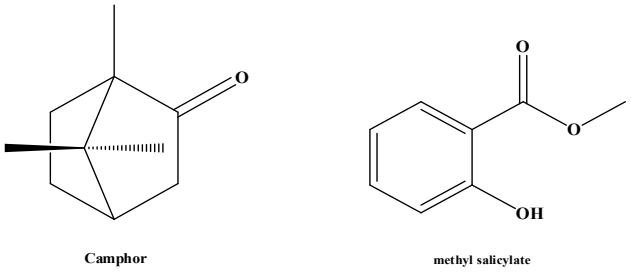

Figure 3: *Structure of the major compounds identified by GC*

Table 2: *Compounds detected in GC analysis of D_{20} fraction of the DCM extract.*

S.N.	Compounds	Retention time (min.)	Percentage area	Molecular weight (g/mole)
1	Salicylate<methyl->	25.782	66.87	152.15
2	Benzoic acid,2-(1-oxopropyl)-	42.997	21.77	178.18

Conclusion

The main compounds that were isolated from DCM extract of *Equisetum arvense L.* by column chromatography after subjected to FTIR and GC-MS analysis were Camphor (92.53%) and methylsalicylate (66.87%), which are potent anti-inflammatory compounds and using them as a mixture is more effective against inflammation. Hence, ethnomedicinal practice of the plant *Equisetum arvense* to cure pain is scientifically validated.

Acknowledgment

We are thankful to the Department of Plant Resources, Thapathali, Kathmandu, Nepal for providing a GC-MS facility.

References

1. N. S. Sandhu, S. Kaur and D. Chopra, *Equisetum arvense*: pharmacology and phytochemistry-a review, *Asian Journal of Pharmaceutical & Clinical Research,* 2010, **3,** 146-150.
2. A. E. Al-Snafi, The pharmacology of *Equisetum arvense* -A review, *IOSR Journal of Pharmacy,* 2017, **7,** 31-42.
3. H. J. Altameme, I. H. Hameed and N. A. Abu-Serag, Analysis of bioactive phytochemical compounds of two medicinal plants, *Equisetum arvense* and *Alchemila valgaris* seed using gas chromatography- mass spectrometry and fourier-transform infrared spectroscopy, *Malaysian Applied Biology,* 2015, **44,** 47-58.
4. Z. Kukrić, L. Topalić-Trivunović, S. Pavičić, M. Žabić, S. Matoš and A. Davidović, Total phenolic content, antioxidant and antimicrobial activity of *Equisetum arvense L.*, *Chemical Industry and Chemical Engineering Quarterly/ CICEQ,* 2013, **19,** 37-43.
5. V. Alexandru, D. N. Petrusca and E. Gille, Investigation of pro-apoptotic activity of *Equisetum arvense L.* water extract on human leukemia U 937 cells, *Romanian Biotechnological Letters,* 2007, **12,** 3139.
6. A. S. Hoque, G. Bithika, N. Rimlee, S. B. Roy, K. Pallab, and D. B. Kumar, Pharmacognostical evaluation and phytochemical screening of the plant *Equisetum Arvense L.*, *World Journal of Pharmacy & Pharmaceutical Sciences,* 2016, **5,** 1537-1543.
7. F. H. Do Monte, J. G. Dos Santos, M. Russi, V. M. Lanziotti, L. K. Leal and G. M. Cunha, Antinociceptive and anti-inflammatory properties of the hydroalcoholic extract of stems from *Equisetum arvense L.* in mice, *Pharmacology Research,* 2004, **49,** 239- 243.
8. K. Joshi, R. Joshi and A. R. Joshi, Indigenous knowledge and uses of medicinal plants in Macchegaun, Nepal, *Indian Journal of traditional knowledge,* 2011**, 10,** 281- 286.
9. S. S. Ghori, M. I. Ahmed, M. Arifuddin and M. S. Khateeb, Evaluation of analgesic and anti-inflammatory activities of formulation containing camphor, menthol and thymol, *International Journal of Pharmacy & Pharmaceutical Science,* 2016, **8**, 271-274.

JNCS
Journal of Nepal Chemical Society December 2019, Vol. 40, 5-10
ISSN: 2091-0304 (print)
DOI: https://doi.org:10.3126/jncs.v40i0.27271
RESEARCH ARTICLE

Synthesis, Characterizations and Antimicrobial Activity of Cuprous Oxide (Cu_2O) Nanoparticles

Amrit Regmi[1], Janak Bhandari[1], Sitaram Bhattarai[2], Surendra K. Gautam[1]*

[1]Department of Chemistry, Tri-Chandra Multiple Campus, Tribhuvan University, Kathmandu, Nepal
[2]Center for Nanomaterials, Sogang University, Seoul, South Korea

**Corresponding E-mail: sgautam2055@yahoo.com*
(Received: Sept. 17, 2019; Revised: Dec. 23, 2019 & Accepted: Dec. 24, 2019)

Abstract

Cuprous oxide nanoparticles were synthesized by the reduction of copper sulphate pentahydrate salt at different concentration using sodium borohydride as a reducing agent, polyethylene glycol-6000 as a stabilizer by simple, chemical co-precipitation methods and the effect of concentration on particle size were also studied. The crystalline size and phase of Cu_2O nanoparticles (NPs) were authenticated by X-ray diffraction (XRD), morphology and structure by scanning electron microscopy (SEM), transmission electron microscopy (TEM), and elemental analysis was carried out by energy-dispersive X-ray spectroscopy (EDX). The concentration-dependent antimicrobial properties of Cu_2O NPs were studied for a different strain of bacteria. XRD and selected area electron diffraction studies (SAED) patterns confirmed the formation of face-centered-cubic Cu_2O nanoparticles with size 4.77 nm and 8.02 nm at two different concentrations of 0.01 M and 0.1 M $CuSO_4$, respectively. SEM and TEM images showed that the nanoparticles were uniform, in the form of clusters, and homogeneously distributed. EDX confirmed that synthesized nanoparticles were in pure form having copper and oxygen ratio 3:1 based on the atomic percentage of the chemical species. Cu_2O nanoparticles showed excellent antibacterial activity against both bacterial strains Gram-positive (*Staphylococcus aureus*) and Gram-negative *(Escherichia coli*). The antibacterial activities of Cu_2O NPs were found to be concentration-dependents and large bactericidal effect were seen for Gram-positive (*Staphylococcus aureus*) bacteria at higher concentrations of Cu_2O NPs.

Keywords: Bactericidal, co-precipitation, EDX, Gram-positive, XRD

Introduction

P-type semiconductor [1] Cu_2O NPs have gained huge attention in scientific society due to captivating properties such as high critical temperature superconductors [1], direct bandgap of 2.2 eV [2], antimicrobial activity [1], low toxicity [3], photocatalytic activity [4], low cost and most abundant source materials [2], etc. Because of such practically applicable properties, Cu_2O nanoparticles have been broadly studied in the various application fields like batteries [1], catalysis [5], gas sensor, biosensors [2], magnetic storage devices [6], medical, anti-fouling coating [6], photo¬voltaic and photocatalytic degradation of most of the organic pollutants [3,7].

Cu_2O nanoparticles have excellent optical, physical, electrical, magnetic, and biological properties compared to the bulk and microparticles because of the large surface area to volume ratio [4, 8]. These novel properties are strongly related to the synthetic processes [4] and there are numerous synthesis techniques like mechanical milling, vacuum vapor deposition, pulsed laser ablation, and pulsed wire discharge, microemulsion techniques, wet-chemistry route, electrochemical, sonochemical, microwave-assisted, thermal decomposition and hydrothermal methods, liquid hydrolysis, etc [1-8]. Among all those synthesizes methods, chemical co-precipitation method is superior because of following advantages as it can be performed even in room temperature and pressure, it is inexpensive, and also not required specialized equipment and organic solvents in the

reaction [9].

The metal nanoparticles such as Ag, Cu, etc. are found to have antibacterial activity [9,10]. The antibacterial effect of copper nanoparticles has been credited to their small size and high surface to volume ratio which allows them to interact closely with microbial membranes [11]. Although the mechanisms behind the antimicrobial activity of copper nanoparticles are still mystified, the most accepted hypothetical mechanisms, first pileup, and dissolution of nanoparticles in the bacterial membrane changing its permeability causes the degeneracy of the proton motive force across the plasma membrane, and successive discharge of lipo-polysaccharides, intracellular biomolecules, membrane proteins [12,13] and next is uptake of metallic ions derived from NPs or entirely NPs into cells, causing depletion of intracellular ATP production and disruption of DNA replication [14,15].

Materials and Methods

a. Synthesis of Cu_2O nanoparticles

Chemicals like copper sulphate pentahydrate salt ($CuSO_4.5H_2O$), polyethylene glycol-6000 (PEG-6000), were obtained from Merck, sodium borohydride (NaBH4) was obtained from Sigma-Aldrich, and all chemicals were laboratory grade of reagent and used directly to synthesize Cu_2O nanoparticles by co-precipitation method without further purification.

0.01 M and 0.1 M solution of $CuSO_4.5H_2O$ were prepared using double ionized water, PEG-6000 were added and magnetically stirred for half an hour. After that 0.1 M $NaBH_4$ solutions were added drop by drop till the color of the solution changed to black. The black color of the solution indicates the start of the reduction reaction; the solution was further magnetically stirred for one hour and left overnight for aging. Dry particles of Cu_2O nanoparticles were obtained in the Whatman filter paper after filtering the aging solution.

b. Characterization techniques

The average particle size and surface morphology of the Cu_2O were estimated by TEM images (Tecnai G^2 20 electron microscope) and SEM image (JEOL model JSM-7600F) whereas the elemental compositions (purity) of the synthesized nanoparticles were studied by EDX (JEOL model JSM-7600F). Crystalline size and crystallite structure of Cu_2O nanoparticles were determined by XRD (Rigaku ultima IV model) employing CuKα radiation (λ = 0.15406 nm). The average crystallite size "D" of nanoparticles was calculated using Debye-Scherrer's equation:

$$D = 0.94 \lambda / \beta \cos \theta$$

Where, λ is the X-ray wavelength (0.15406 nm), β is the full width at half maximum in radian and θ is the Bragg's diffraction angle.

c. Antimicrobial activity of Cu_2O nanoparticles

Two bacterial strains, namely Staphylococcus aureus and Escherichia coli a Gram-positive and Gram-negative bacteria respectively, were taken from the Central Department of Biotechnology, Tribhuvan University, and were grown in LB Agar (Luria Bertani) and stored at 4°C. The media plates were made of Muller Hinton Agar (MHA). Bacterial lawn cultures were prepared by taking the respective bacteria for the different Petri plates labeled accordingly with the help of a cotton swab.

10 mg per mL stock solution of the synthesized Cu_2O NPs synthesized using 0.01 M $CuSO_4$ solutions were taken and diluted to (0.1, 0.5, 0.75 and 1) mg per mL in dimethyl sulfoxide (DMSO) and was also used as a negative control sample. 50 µL of each sample solution was introduced very carefully in the wells of labeled Petri plates, respectively with the help of micropipette and were left for a while to diffuse the sample through Media. Finally, these plates were incubated at 37 °C for 24 hrs.

Results and Discussion

i. Crystalline analysis

XRD data of the synthesized Cu_2O nanoparticles were plotted in figure 1 from 25º to 80º which revealed the structures were crystalline. In figure 1, there are six distinct peaks appearing at 2Θ values of 29.68º, 36.68º, 42.6º, 61.76º, 73.98º and 77.8º corresponding to the hkl values (110), (111), (200), (220), (311) and (222), respectively and peaks also matches with the (JCPDS 05-669) reference standard XRD spectrum of Cu_2O NPs [1]. Besides, no extra peaks of impurity are detected, indicating the synthesized Cu_2O nanoparticles are pure, crystalline with cubic crystal structures. The average crystalline size of Cu_2O nanoparticles was calculated from the most intense peak labeled 111 at 36.44º using Debye-

Scherrer's equation and was found to be 4.77 nm and 8.02 nm, 0.01 M and 0.1 M precursor concentrations, respectively. As the concentration of precursor increases, the hydrodynamic size of particles also increases. When the concentration of $CuSO_4.5H_2O$ increases, the stabilizer finds difficulty in fully covering the particles and consequently increases the part of the uncovered area of nanoparticles, which elevates the tendency of particles to interact with each other [16]. So, crystal sizes of Cu_2O were found more significant at higher concentrations.

Figure 1: *XRD patterns of Cu_2O NPs synthesized using two different concentration (a) 0.01 M and (b) 0.1M $CuSO_4$ and reducing agent $NaBH_4$.*

Figure 2: *SAED pattern of Cu_2O NPs synthesized using 0.01 M $CuSO_4$ and reducing agent $NaBH_4$.*

The SAED patterns of the Cu_2O NPs in figure 2 shows the characteristic diffraction rings corresponding to (111), (200) and (220) of the face-centered-cubic (FCC) phase which also well supported the crystalline phase obtained from XRD.

ii Morphology analyses

Scanning electron microscopy (SEM) and transmission electron microscopy (TEM) images of synthesized Cu_2O nanoparticles using the precursor of 0.01 M $CuSO_4.5H_2O$ solution is shown in figures 3 and 4, respectively.

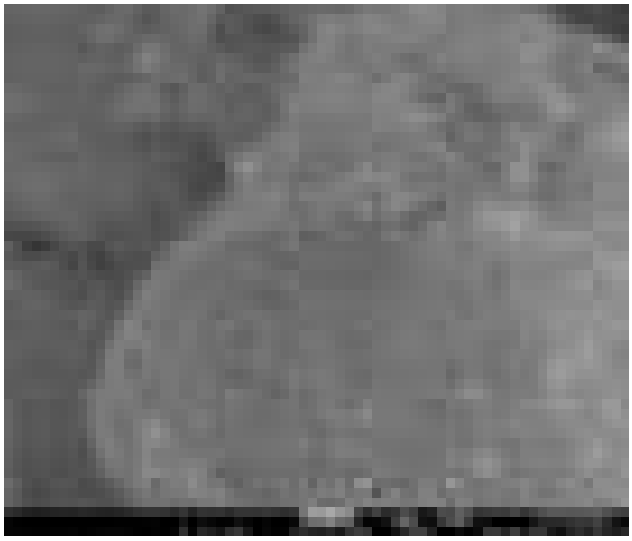

Figure 3: *SEM image of Cu_2O NPs synthesized using 0.01 M $CuSO_4$ and reducing agent $NaBH_4$*

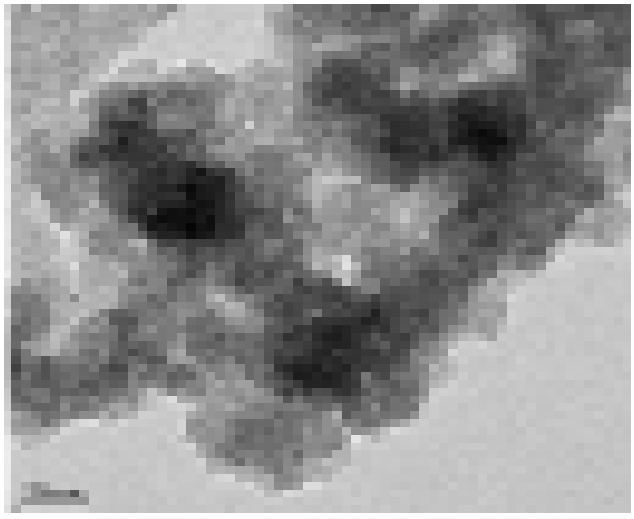

Figure 4: *TEM image Cu_2O NPs synthesized using 0.01 M $CuSO_4$ and reducing agent $NaBH_4$*

SEM and TEM images reveal that the primary particles aggregate into secondary particles because of their small dimensions and high surface energy called Ostwald ripening process [17]. The images show that all NPs are uniform in size, in clusters form, homogeneously, and evenly distributed.

iii Elemental analyses

The EDX curve in figure 5 reveal the presence of copper, oxygen, carbon, and platinum as major elements and found in the sample 60.93 %, 20.34 %, 5.68 %, and 4.59 %, respectively on the basis of atomic percentage of the chemical species and also other trace elemental impurities such as aluminum, silicon, sulphur, zinc, and zirconium. Pure and stable copper oxide nanoparticles are formed with copper

Figure 5: *EDX of Cu_2O NPs synthesized using 0.01 M $CuSO_4$ and reducing agent $NaBH_4$*

and oxygen in the ratio of 3:1 by atomic percentage. Impurities like platinum were recorded because samples were coated by platinum to prevent the sample from charging during the sample analysis, a recognizable amount of carbons were present in samples because polyethylene glycol-6000 were used as a stabilizing agent during Cu_2O NPs synthesis and other impurities are due to the laboratory-grade of reagent used without further purification.

iv Antibacterial analyses

The antibacterial activities of synthesized Cu_2O nanoparticles using the precursor of 0.01 M $CuSO_4.5H_2O$ solution were screened with one Gram-negative (*Escherichia coli*) and one Gram-positive (*Staphylococcus aureus*) bacteria are shown in figures 6 and 7, respectively. The zones of inhibition of the Cu_2O NPs at different concentration and standard tetracycline antibiotics were measured for both Gram-positive and Gram-negative bacteria were summarized in table 1. The antimicrobial properties of copper oxide mainly depend on the release of Cu^+, Cu^{2+} ions and also on radicals like ·OH, and O^{2-} generated from photocatalysis activity. These

Figure 6: *Antibacterial activities shown by Cu_2O NPs synthesized using 0.01 M $CuSO_4$ and reducing agent $NaBH_4$ in Escherichia coli.*

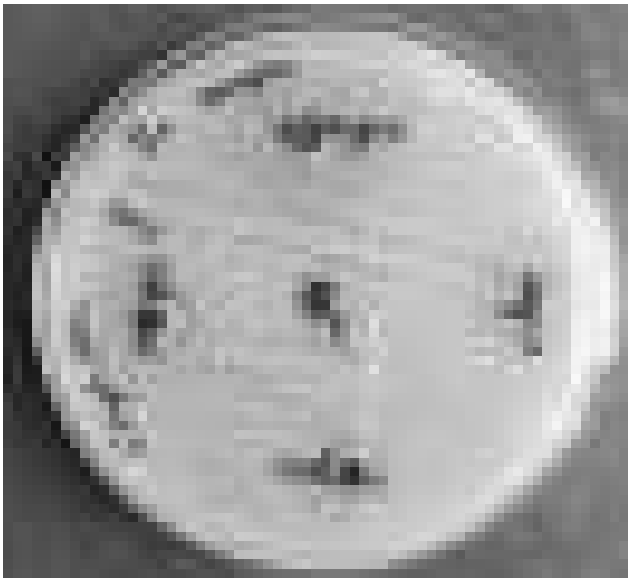

Figure 7: *Antibacterial activities shown by Cu_2O NPs synthesized using 0.01 M $CuSO_4$ and reducing agent $NaBH_4$ in Staphylococcus aureus.*

Table 1: *Comparison of antimicrobial activity of Cu_2O NPs with standard antibiotics tetracycline [18]*

Pathogen	Zone of inhibition (mm) Concentration (mg/ml)				Standard Tetracycline (5 µg/disc)
	0.1	0.5	0.75	1	
Escherichia coli	5	10	14	17	22
Staphylococcus aureus	7.5	13	17	19	22

ions and radicals are responsible to injure cellular structure and disturb the physiological activity of microorganisms [7]. Cu_2O NPs show that broad-spectrum activity and antimicrobial activity increases with an increase in concentrations of the NPs. While comparing two different microorganisms, it is seen that the antibacterial activity of Cu_2O NPs is more in Gram-positive (*S. aureus*) bacteria than in Gram-negative bacteria.

Conclusion

Cu_2O NPs have been synthesized successfully at two different concentration of copper precursors by the co-precipitation method using $NaBH_4$ as a reducing agent and (PEG-6000) as a stabilizer. As the concentration of precursor increase from 0.01 M to 0.1 M, the particle size of Cu_2O also increases from 4.77 nm to 8.02 nm. Morphology, particle size, and purity of synthesized Cu_2O obtained from XRD, SAED, SEM, TEM, EDX, corroborate each other. Bactericidal activity of copper oxide performed on both Gram-positive and Gram-negative strain bacteria displays the effectiveness of Cu_2O NPs against bacterial growth and antibacterial activity increases with increasing the concentration of copper oxide. Moreover, the antibacterial activity of Cu_2O NPs was high for Gram-positive (*Staphylococcus aureus*) compare to Gram-negative (*Escherichia coli*) bacteria.

Acknowledgments

Authors are grateful to acknowledge the Department of Chemistry, Tri-Chandra Multiple Campus, and Central Department of Biotechnology, Tribhuvan University, Kathmandu, Nepal for providing lab facilities and necessary materials. We are also thankful to Indira Pokhrel, Center for Nanomaterials, Sogang University, Seoul, South Korea for SEM, SAED, TEM and EDX, and Dr. S. P. Singh, Research professor, Nanotechnology and Advanced Materials Engineering, Sejong University, Seoul, South Korea for XRD.

References

1. M. A. Khan, M. Ullah, T. Iqbal, H. Mahmood, A. A. Khan, M. Shafique, A. Majid, A. Ahmed and N. A. Khan, Surfactant assisted synthesis of cuprous oxide (Cu_2O) nanoparticles via solvothermal process, *Nanoscience and Nanotechnology Research*, 2015, **3**(1) 16-22. (DOI: 10.12691/nnr-3-1-3).
2. S. S. Sawant, A. D. Bhagwat and C. M. Maharjan, Synthesis of cuprous oxide (Cu_2O) nanoparticles – a review, *Journal of Nano and Electronic Physics*, 2016, **8**(1), 1035-1040. (DOI:10.21272/jnep.8(1).01035).
3. M. Bagherzadeha, N. Mousavi, M. Amini, S. Gautam, J. P. Singh and K. H. Chae, Cu_2O nanocrystals with various morphology: synthesis, characterization and catalytic properties, *Chinese Chemical Letters*, 2017, **28**, 1125–1130. (DOI:10.1016/j.cclet.2017.01.022).
4. P. Li, W. Lv and S. Ai, Green and gentle synthesis of Cu_2O nanoparticles using lignin as reducing and capping reagent with antibacterial properties, *Journal of Experimental Nanoscience*, 2016, **11**(1), 18-27. (DOI:10.1080/17458080.2015.1015462).
5. Y. Qian, F. Ye, J. Xu, and Z. G. Le, Synthesis of cuprous oxide (Cu_2O) nanoparticles/graphene composite with an excellent electrocatalytic activity towards glucose, *International Journal of Electrochemical Science*, 2012, **7**, 10063-10073.
6. M. Behera, G. Giri, Green synthesis and characterization of cuprous oxide nanoparticles in presence of a bio-surfactant, *Materials Science-Poland*, 2014, **32**(4), 702-708. (DOI:10.2478/s13536-014-0255-4).
7. B. D. Du, D. V. Phu, L. A. Quoc and N. Q. Hien, Synthesis and investigation of antimicrobial

activity of Cu_2O nanoparticles/zeolite, *Journal of Nanoparticles*, 2017, **2017**, 1-6. (DOI:10.1155/2017/7056864).

8. M. S. Usman, M. E. E. Zowalaty, K. Shameli, N. Zainuddin, M. Salama and N. A. Ibrahim, Synthesis, characterization, and antimicrobial properties of copper nanoparticles, *International Journal of Nanomedicine*, 2013, **8**, 4467–4479.
9. K. Jhansi, S. Chandralingam, N. R. Manohar, P. Suvarna, C. Ashok and K. R. Venkateswara, CuO nanoparticles synthesis and characterization for humidity sensor application, *Journal of Nanotechnology and Materials Science*, 2016, **3**(1), 10- 14. (DOI: 10.15436/2377-1372.16.020).
10. A. K. Chatterjee, R. Chakraborty and T. Basu, Mechanism of antibacterial activity of copper nanoparticles, *Nanotechnology,* 2014, **25**, 135101-135113. (DOI:10.1088/0957-4484/25/13/135101).
11. J. Ramyadevi, K. Jeyasubramanian, A. Marikani, G. Rajakumar and A. A. Rahuman, Synthesis and antimicrobial activity of copper nanoparticles, *Materials Letters,* 2012, **71**, 114-116.
12. A. Azam, A. Ahmed, M. Oves, M. Khan and A. Memic, Size dependent antimicrobial properties of CuO nanoparticles against gram positive and negative bacterial strains, *International Journal of Nanomedicine*, 2012, **7**, 3527–3533.
13. N. A. Amro, L.P. Kotra, K. Wadu-Mesthrige, A. Bulychev, S. Mobashery and G. Y. Liu, High resolution atomic force microscopy studies of the *E. coli* outer membrane: structural basis for permeability, *Langmuir,* 2000, **16**, 2789–2796.
14. I. Sondi, and B. Salopek-Sondi, Silver nanoparticles as antimicrobial agent: a case study on *E. coli* as a model for gram negative bacteria, *Colloids*, 2004, **275**, 177–182. (DOI:10.1016/j.jcis.2004.02.012).
15. C. N. Lok, C. M. Ho,R. Chen, Q. Y. He, W.Y. Yu, H. Sun, P. K. Tam, J. F. Chiu and C. M. Che, Proteomic analysis of the mode of antibacterial action of silver nanoparticles, *Journal of Proteome Research*, 2006, **5**, 916–924. (DOI 10.1007/s00775-007-0208-z).
16. N. Ahmad, B. C. Ang, M. A. Amalina and C. W. Bong, Influence of precursor concentration and temperature on the formation of nanosilver in chemical reduction method, *Sains Malaysiana,* 2018, **47**(1), 157-168.(DOI:10.17576/jsm-2018-4701-19).
17. N. Topnani, S. Kushwaha and T. Athar, Wet synthesis of copper oxide nanopowder, *International Journal of Green Nanotechnology: Materials Science & Engineering*, 2010, **1**(2), M67-M73. (DOI:10.1080/19430840903430220).
18. K. Muthulakshmi and C. Uma, Antimicrobial activity of *Bacillus subtilis* silver nanoparticles, *Frontiers in Bioscience* (Elite Ed.), 2019, **11**, 89-101.

JNCS
Journal of Nepal Chemical Society December 2019, Vol. 40, 11-18
ISSN: 2091-0304 (print)
DOI: https://doi.org:10.3126/jncs.v40i0.27272
RESEARCH ARTICLE

Antioxidant and Antimicrobial Efficacy of Various Solvent Extracts of Seed of Rudrakshya (*Elaeocarpus ganitrus*) from Ilam District of Nepal

Bishan Datt Bhatt*, Purushottam Dahal

Department of Chemistry, Tri-Chandra Multiple Campus, Tribhuvan University, Kathmandu, Nepal

**Corresponding E-mail: bdbhatta@gmail.com*

(Received: Sept. 30, 2019; Revised: Dec. 21, 2019 & Accepted: Dec. 22, 2019)

Abstract

Elaeocarpus ganitrus (Rudrakshya) is an evergreen tree found in tropical and sub-tropical regions and has been commonly used in traditional medicine against various diseases. In the present study, phytochemical constituents, antimicrobial activity and antioxidant property of seed of *Elaeocarpus ganitrus* have been evaluated in hexane, ethyl acetate, acetone and methanol extracts. The phytochemical screening showed the presence of alkaloids, flavonoids, phenols, tannins, steroids, carbohydrates, saponins, terpenoids etc. The antibacterial test showed a significant zone of inhibition against *Escherichia coli, Salmonella typhi* and *Staphylococcus aureus* with the maximum zone of inhibition of 20mm. The study showed that these extracts can be used as antimicrobialsubstances against various bacteria. Antioxidant activity of the methanol, acetone and ethyl acetate extract were studied by DPPH radical scavenging assay. The extracts showed significant antioxidant activity. Among the IC_{50} values of different extractson DPPH assay for antioxidant determination, methanol seed extract showed the lowest value of 28.09µg/mL. This means methanol extract of seed showed the significantly high antioxidant properties. Calculation of total phenolic content showed a significant amount of phenolic content in different solvent extracts. Methanol seed extract showed the highest total phenolic content of 174.6 mgGAE/g. Similarly, methanol seed extract showed the highest total flavonoid content of 107.13 mgQE/g. These results suggest that the seeds of the *Elaeocarpus ganitrus* (Rudrakshya) plant from the Ilam district of Nepal possess high antimicrobial and antioxidant properties and thus, the plant can be used in the discovery of new bioactive natural products.

Keywords: Antibacterial, antioxidant, *Elaeocarpus ganitrus*, phytochemical analysis.

Introduction

Elaeocarpus ganitrus belongs to family *Elaeocarpeceae*, and it generally grows in the Himalayan region. It is commonly known Rudrakshya in Nepal. The family *Elaeocarpeceae* has about 360 species and is mainly found in Nepal, India, Australia, Indonesia and East Asia. About 120 species of *Elaeocarpus* are found in Asia, among which *Elaeocarpus ganitrus* is one of the important species with high medicinal value [1]. It is an evergreen tree found in tropical and sub-tropical regions at the altitude up to 2000 meters from sea level. The height of Rudrakshya tree ranges from 50-200 feet with large sized green leaves [2].

Elaeocarpus ganitrus is a common perennial tree which grows on tropical, sub-tropical and hilly region of Nepal and other countries including India, Malaysia, China, Japan, Australia, Newzealand, Fiji and Hawaii [3]. In Nepal, it is widely distributed in Eastern hilly and terai districts like Ilam, Pachthar, Jhapa, Morang, Dhankuta, Sankhwasabha, Bhojpur, Terhathum etc.It is a large evergreen broad-leaved tree which grows in the area of gangetic plain to the foothills of high Himalaya. Tree has a pyramidal shape and starts giving fruit in seven years. The mature fruit is a drupe and stone beads are enclosed by an outer shell which is blue colored on ripening and hence they are also called blueberry beads. Beads are hard in nature. *Elaeocarpus ganitrus* grows in a suitable climatic condition of temperature ranging from 20-30 ^{o}C.

According to Hindu mythology, Rudrakshya bead bears a great religious, spiritual and materialistic

significance. The Hindu mythology considers Rudrakshya as the symbol of linkage between the earth and heaven and is believed to contain the secrets of the evolution of cosmos within itself [4]. It has a significant position in the Hindu religion and in Ayurveda, the ancient Hindu system of medicine. *Elaeocarpus ganitrus* is the king of herbal medicine working effectively and has many spiritual and medicinal values both as defensive and remedial. It is used in folk medicine in treatment of stress, anxiety, depression, palpitation, nerve pain, epilepsy, migraine, lack of concentration, asthma, hypertension, arthritis, liver diseases and is effective antimicrobial agent [5].

Elaeocarpus ganitrus is a source of various pharmacologically and medicinally significant chemicals such as triterpenes, tannins like geranin and 3,4,5-trimethoxy geranin, indolizilidine alkaloids, grandisines, rudrakine, and flavonoid quercetin [6]. *Elaeocarpus ganitrus* plant, having ethno medicinal claims with regard to their phytoconstituents, pharmacological profile and other allied activities, has been claimed to exhibit antiaging, antianxiety, antidepressant, antidiabetic, anti-inflammatory, sedative, anticonvulsive, antihypertensive and antimicrobial properties. The beads of *Elaeocarpus ganitrus* helps in therapeutic healing of body diseases chronically due to its electromagnetic properties also by virtue of acupressure and bio magnetic therapy and piezoelectric consequences. It has the ability to generate an electric charges in the response to applied mechanical stress [7]. The beads, bark and leaves of *Elaeocarpus ganitrus* have immense importance in the Ayurvedic medicine system and have been described to cure ailments like mental disorder, headache, fever, skin diseases, palpitation, insomnia, infertility etc [8]. The bark of the *Elaeocarpus ganitrus* found to contain various bioactive metabolites, responsible for its various medicinal uses [9]. *Elaeocarpus ganitrus* beads help in the therapeutic healing of various body diseases due to its electromagnetic property [10]. It is an important medicinal plant with several curative properties, that's why it is used in traditional systems of medicine [11].

Despite so many applications of the plants, no extensive studies on evaluation of phytochemicals, and study on the relation of various phytochemicals with their bioactivity efficacy, have been done from the seeds of Nepal specially Ilam district. Also, there is no comparative investigation in the biological efficacy of extracts in different solvents like hexane, ethyl acetate, acetone and methanol. The present study aims to evaluate the various phytochemicals, total phenolic content, total flavonoid content, antimicrobial activity and antioxidant property of various solvent extracts of seed of this useful plant of Ilam district. The study will be utilized to correlate the total phenolic and flavonoid contents and phytochemical screening with its antimicrobial and antioxidant efficacy.

Materials and Method

Collection of plant materials

The seeds of *Elaeocarpus ganitrus* were collected,in the month of June, from Rong rural municipality of the Ilam district, Nepal. They were then washed shade dried and crushed into a fine powder using mortar.

Extraction of plant materials

The powdered seed was extracted using soxhlet extractor in the solvent hexane, ethyl acetate, acetone and methanol successively at 30 ºC. Then the sample was collected separately, evaporated using a rotatory evaporator and the dry extract was used for further study.

Phytochemical analysis

The dry extract was analyzed by color reactions, different phytochemicals were studied and the presence of different groups of phytochemicals was noted.

Antibacterial activity

The activity of various bioactive compounds from the plants has led to the discovery of new medicinal drugs. Antibacterial activity of the plant extract was performed by agar well diffusion method. The effectiveness of antimicrobial activity was evaluated by determining the zone of inhibition. The microbial strains obtained from MED-MICRO Nepal laboratory Kathmandu were inoculated in agar medium. The studied strains include a Gram-positive bacterium (*Staphylococcus aureus* ATCC 25923) Cocci-grapes like structure, a Gram negative bacterium (*Escherichia coli* ATCC 25922) short rod shape structure and another Gram-negative bacterium (*Salmonella typhi*) pink in color. Six wells were made in each incubated media plates with the help of sterile cork borer no.6. Sothe diameter of the well was 6 mm and was labeled

properly. Then 50 µL of the working solution of the plant extract, DMSO as the negative control (Nc) and 25 µL of Ofloxacin (antibiotic- ear and eye drop) as the positive control (Pc) at the same time in separated well were loaded into the respective wells with the help of micropipette. The plates were subsequently left for half an hour with the lid closed so that the extract diffused into the media. The plates were incubated for 24 hours at 37 ºC. After 24 hours of incubation, the plates were observed for the presence of inhibition of bacterial growth which was indicated by a clear zone around the wells. The size of the zone of inhibition was measured and the antibacterial activity was expressed in terms of the average diameter of the zone of inhibition in millimeters. The absence of the zone of inhibition was interpreted as the absence of the activity. The zone of inhibition (ZOI) was measured with the help of a millimeter ruler and the mean was recorded.

Antioxidant activity

The numerous methods used to measure the antioxidant activity of the plants can give varying results depending on the specific free radical being used as a reactant. An efficient method to measure antioxidant capacity involves the use of the free radical, 2, 2-diphenyl-1-picrylhydrazyl (DPPH). The antioxidant capacity of ethyl acetate extract, acetone extract and methanol extract were evaluated using standard DPPH assay [12]. The percentage of DPPH free radical scavenging activity was calculated by using the following equation:

Radical scavenging (%) = $[(A_o-A_s)/A_o]\times100$

Where, A_o=Absorbance of the control (DPPH solution + methanol),

A_s =Absorbance of the test sample

The IC_{50} (50% inhibitory concentration) value is indicated as the effective concentration of the sample which is required to scavenge 50% of the DPPH free radicals. IC_{50} values were calculated using the inhibition curve by plotting extract concentration versus the corresponding scavenging effect.

Preparation of the 0.2 mM DPPH solution

DPPH has a molecular mass of 394.32 g/mol. Thus, 100 mL of 0.2 mM solution of DPPH was prepared by weighing the 0.0078 g of the DPPH carefully and dissolving it on methanol and finally maintaining the volume to 100 mL. The solution was kept in dark place until the use. Different concentrations of test samples of 20, 40, 60, 80 and 100 µg/mL were made from stock solutions. Then 2 mL of all the test solutions were mixed to 2mL of DPPH solution. The test tubes were shaken vigorously for the uniform mixing and the solutions were kept for 30 minutes in the dark place at room temperature. The control was prepared by mixing methanol and DPPH solution without the plant extracts (methanol + DPPH). After 30 minutes, the absorbance of the entire sample was measured at 517 nm using a UV-visible spectrophotometer. The ascorbic acid of the same concentration was prepared as a standard and its absorbance was also taken spectrophotometrically at 517 nm and the calibration curve was constructed. Using ascorbic acid as the positive control, the percent radical scavenging activity was determined by comparison with the methanol treated control group.

Total phenolic content (TPC) determination

The total phenolic content of all selected plant extracts were estimated using Folin-Ciocalteu reagent involving gallic acid standard based on oxidation-reduction reaction. The procedure carried out for the total phenol content was based on the standard procedure using gallic acid as standard. Gallic acid stock solution was prepared by dissolving 10 mg of gallic acid in 1 mL of methanol. Various concentrations of gallic acid such as 20, 40, 60, 80 and 100 µg/mL were prepared. An aliquot of 1 mL gallic acid of each concentration in methanol was poured to a 20 mL test tube. To that 5 mL of folin-ciocalteau (FCR) (10%, 1:10 v/v diluted in distilled water) and 4 mL of 7% Na_2CO_3 were added to get a total volume of 10 mL. The blue-colored solution was shaken well and then incubated for 30 minutes at 40 ºC in a water bath. After this, the absorbance was accurately measured at 760 nm against a blank containing all reagents except gallic acid. The average absorbance values obtained at these different concentrations of gallic acid were used to plot the calibration curve. By the serial dilutions, samples with the concentrations of 20, 40, 60, 80 and 100 µg/mL were prepared. To these diluted solutions, 10% FCR and 7% Na_2CO_3 were added and incubated for 30 minutes as in the case of gallic acid and absorbance was measured at 760 nm against blank for each concentration.

Total flavonoid content (TFC) determination

Total flavonoid content of the seed extracts was determined according to the aluminum chloride colorimetric method involving quercetin as standard [13]. Quercetin stock solution was prepared by dissolving 10 mg of quercetin in 1 mL of methanol. Various concentrations of quercetin such as 20, 40, 60, 80 and 100 µg/mL were prepared. An aliquot of 1 mL quercetin of each concentration in methanol was poured to 20 mL test tube containing 4 mL of double-distilled water. At the zero time, 0.3 mL 5% $NaNO_2$ was added to the test tube. After a minute, 0.3 mL of 10% $AlCl_3$ was added. After 6 minutes, 2 mL of 1 M NaOH was added to the mixture. Immediately, the total volume of the mixture was made up to 10 mL by the addition of 2.4 mL of double distilled water and mixed thoroughly. The absorbance of the pink color mixture was determined at 510 nm versus blank containing all the reagents except quercetin. All the experiments were carried out in triplicate. The average absorbance values obtained at different concentrations of quercetin were used to plot the calibration curve. The stock solutions of all the extracts were prepared by dissolving 10 mg in 1 mL of methanol (10 mg/mL). Serial dilutions were carried out to get the concentration of 20, 40, 60, 80 and 100 µg/mL. Following the procedure as for quercetin as described above, absorbance for each concentration of the extract was measured at 510 nm.

Results and Discussion

Phytochemical analysis

Different phytochemical constituents present in the extract were identified by the color reaction with different reagents following the standard phytochemical screening methods. The main objective of phytochemical screening was to identify the different groups of chemical constituents present in the different plant extracts. The screening of phytochemicals showed the presence of alkaloids, carbohydrates, flavonoids, terpenoids, lactones, tannins, phenols, quinines, etc. The main phytochemicals obtained as a result of the phytochemical screening of the seed of *Elaeocarpus ganitrus* are summarized in table 1.

The above results show the presence of several important phytochemicals in nearly all the extracts. Moreover, acetone and methanol extracts have been found to contain most of the phytochemicals under study. These results show that the plant can be used as a potential source of several natural products.

Table1: *Phytochemical constituents of different solvent extracts of seed of Elaeocarpus ganitrus.*

S.N	Phytochemicals	Name of test	H. E	E.E	A.E	M.E
1	Alkaloids	a) Mayer's test	-	+	+	+
		b) Wagner's test	+	+	+	+
		c)Dragendroff's test	-	+	+	+
2	Carbohydrates	a) Fehling's test	+	+	+	+
		b) Molisch's test	+	+	+	+
3	Glycosides	a) Alkaline reagent test	+	+	+	+
		b) Legal test	+	+	+	+
4	Lactones	a) Kedde test	+	+	+	+
		b)Baljel test	+	+	+	+
5	Proteins &	a) Xanthoprotic test	-	-	-	-
	Amino acids	b) Biuret test	-	-	-	-
6	Fatty acids	a) Spot test	-	+	+	+
7	Flavonoids	a) Shinoda test	+	+	+	+
		b) Shibata test	+	+	+	+
		c) Lead acetate test	+	+	+	+
8	Steroids	a) Salkowski test	+	-	+	+
9	Terpenoids	a) Salkowski test	+	+	+	+
		b) Tschugajen test	+	+	+	+
10	Saponins	a) Froth test	-	-	+	+
11	Tannins	a) Lead acetate test	+	+	+	+
12	Phenols	a) Braymerm test	+	+	+	+
13	Phlabotannins	a) Precipitate test	-	-	-	-
17	Anthraquinones	a) Alkaline reagent test	+	+	+	+
18	Quinones	a) Brontiager test	+	+	+	+

H.E= Hexane extract, E.E= Ethyl acetate extract, A.E=Acetone extract, M.E=Methanol extract, (+) = Presence, (-) = Absence

Table 2: *Antibacterial analysis of hexane, ethyl acetate, acetone and methanol extracts of seed of Elaeocarpus ganitrus.*

S.N	Plant extract	Bacteria	ZOI of extract 1%10%		ZOI of ofloxacin
1	Hexane Extract	*S. aureus*	0	8	32
		E. coli	9	12	30
		S. typhi	0	8	22
2	Ethyl acetate Extract	*S. aureus*	0	12	34
		E. coli	12	12	30
		S. typhi	0	15	25
3	Acetone Extract	*S. aureus*	8	10	33
		E. coli	12	12	30
		S. typhi	18	20	23
4	Methanol Extract	*S. aureus*	8	10	32
		E. coli	13	16	30
		S. typhi	18	20	22

Table 3*: Absorbance values of ethyl acetate, acetone and methanol extracts of the seed of Elaeocarpus ganitrus measured at 517nm in the DPPH assay.*

S.N	Samples	Concentration (µg/mL)	Absorbance	% inhibition	IC_{50}
1.	Ethyl acetate extract	20	0.2756	60.43	35.65
		40	0.2393	65.64	
		60	0.2079	70.15	
		80	0.1454	79.12	
		100	0.1156	83.40	
2.	Acetone extract	20	0.2602	62.64	36.72
		40	0.2432	65.08	
		60	0.2241	67.82	
		80	0.1854	73.38	
		100	0.1295	81.40	
3.	Methanol extract	20	0.2288	67.14	28.09
		40	0.1741	75.00	
		60	0.1452	79.14	
		80	0.1205	82.69	
		100	0.0673	90.34	

Antibacterial Activity

The zone of inhibition (ZOI) produced by the plant extract on particular bacteria was measured for the estimation of its antibacterial activity. Zone of inhibition created by hexane, ethyl acetate, acetone and methanol extracts were studied and their effects against Gram-positive bacteria Staphylococcus aureus and Gram-negative bacteria Escherichia coli and *Salmonella typhi* were evaluated. Results obtained from the antibacterial analysis of different extracts have been tabulated in table 2.

The above result shows that the acetone and methanol extracts exhibit significant antimicrobial activities against bacteria under investigation. Acetone and methanol extracts have been found highly effective against *S. typhi*.

DPPH free radical scavenging activity

In this study, the antioxidant activity of each plant extract was measured by using 1,1-diphenyl-2-picryl hydrazyl radical (DPPH). In this assay, the mixture of DPPH with different concentrations of extract solutions and ascorbic acid were separately incubated at room temperature and absorbance was recorded at 517 nm by a spectrophotometer. The calibration curve was constructed by measuring the absorbance of ascorbic acid in order to calculate the IC_{50} value. The value obtained from plant extract was compared with ascorbic acid. The observed absorbance values with the different concentrations have been tabulated in table 3 and graphically represented in figure 1.

(MS=Methanol seed, AS= Acetone seed, ES= Ethyl acetate seed.)

Figure 1: *A bar diagram of IC_{50} values of different seed extracts of Elaeocarpus ganitrus and ascorbic acid*

The above results show that the methanol extract is found to contain the lowest IC_{50} value, which is close to the value of ascorbic acid. This result shows its efficacy as a good antioxidant.

Total phenolic content (TPC)

The TPC in plant extract was estimated by using the FCR colorimetric method based onoxidation reduction reaction. Gallic acid was used as a standard compound for the construction of calibration curve. The TPC values of different extracts have been depicted in table 4.

Table 4*: Total Phenolic content of different solvent extracts of Elaeocarpus ganitrus seed.*

S. N.	Sample	Extract	TPC(mgGAE/g)
1	AS	Acetone Seed	146.15
2	ES	Ethyl acetate Seed	143.90
3	MS	Methanol Seed	174.60

More conveniently, total phenolic content in different plant extracts has been represented in the bar diagram in figure 2.

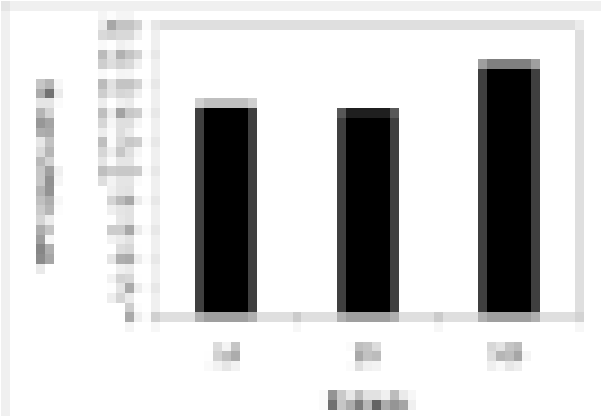

(MS=Methanol seed, AS= Acetone seed, ES= Ethyl acetate seed.)

Figure 2: *Total phenolic content of seed of Elaeocarpus ganitrus in different solvents.*

The result demonstrated that among the studied samples, the total phenolic content was the highest in the methanol extract, though all the extracts were found to contain a significant amount of phenolic contents. These TPC values match with the results obtained in phytochemical screening.

Total flavonoid content (TFC)

The aluminum chloride colorimetric assay was used for the estimation of total flavonoid present in the

seed extract in a different solvent according to the standard procedure involving quercetin as standard. The flavonoids of the plant extracts in the presence of aluminum chloride forms an acid liable complex, has an intense yellow fluorescence which can be observed under UV spectrophotometer at 510 nm. The intensity of light absorption at that wavelength is proportional to the concentration of flavonoids and was determined using quercetin as standard. The TFC values of different plant extracts (mg quercetin equivalent per g dry extract) have been tabulated in table 5.

Table 5: *Total flavonoid content of different extracts of seed of Elaeocarpus ganitrus.*

S. N.	Sample	Extract	TFC (mgQE/g)
1	AS	Acetone Seed	78.92
2	ES	Ethyl acetate Seed	66.88
3	MS	Methanol Seed	107.13

The results have been represented as a bar diagram in figure 3.

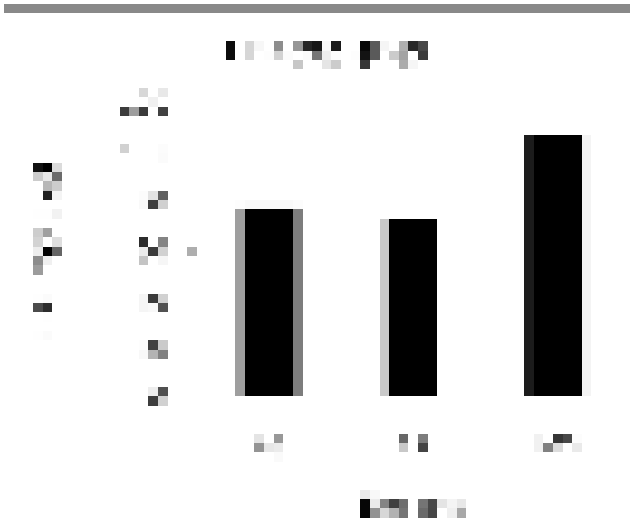

(MS=Methanol seed, AS= Acetone seed, ES= Ethyl acetate seed.)

Figure 3: *Total flavonoid content of seed of Elaeocarpus ganitrus in different solvents.*

The result demonstrated that among the studied samples, the total flavonoid content was highest in the methanol extract, followed by acetone extract of seed. Acetone and ethyl acetate extracts also showed a significant amount of total flavonoid content.

Conclusion

Phytochemical investigation of the seed extract of Elaeocarpus ganitrus showed the presence of various bioactive substances such as alkaloids, phenols and tannins, terpenoids, carbohydrates, quinones, flavonoids, glycosides in various solvents. These results show the use of this plant as a potential source of several bioactive natural products.

All the extracts of the seed of Elaeocarpus ganitrus showed significant antibacterial activity with different values of the zone of inhibitions. The methanol extract was found to be highly effective against Salmonella typhi. These results show the efficacy of the plant as a source of antimicrobial substances.

Methanol seed extract shows the low value of IC50 (28.09µg/mL) in antioxidant DPPH assay which is close to that of ascorbic acid (23.06µg/mL). A significant amount of total phenolic compound was obtained in the various extracts, methanol extract being highest with total phenolic content of 174.6 mgGAE/g extract. Similarly, the highest total flavonoid content (107.13 mgQE/g) was found in methanol seed extract. Other extracts also showed a significant amount of total phenolic content as well as total flavonoid content.

Different previous pharmacological studies in this plant show the presence of different phytochemicals and their antibacterial efficacy. The different zone of inhibitions in these studies may be due to the different areas of samples as well as different solvents used for extraction. Similarly, IC50 value 78-72 µg/mL in antioxidant DPPH assay [11] is slightly different than the present study, due to the difference in the geographical region, climatic condition as well as the time of sample collection.

In the present study, it has also been found that high antioxidant activity is shown by the extracts which have higher phenolic and flavonoid contents. Phenolic compounds and flavonoids play important role in antioxidant activity. These all the facts highly support the use of Elaeocarpus ganitrus (Rudrakshya) in the traditional medicinal system as well as in homemade medicines.

References

1. H. Swati, B. B. Nandy and K. Kumar, *Elaeocarpus ganitrus* (Rudrakshya): A reservoir plant with their pharmacological effects, *International Journal of Pharmaceutical Science,* 2015, **34**(1), 645-649.
2. S. Tripathy, A. Middhaa and S. Swain, *Elaeocarpus ganitrus,* the amazing electromagnetic bead of nature to redeem mankind from disease, sickness and medicinal problem, *World Journal of Pharmacy and Pharmaceutical Science*, 2016, **5**(9), 1079-1099.
3. S. Hardainian, B. C. Nandy and R. Saxena, Phytochemical investigation of fruit extract of *Elaeocarpus ganitrus, International Journal of Pharmacy and Pharmaceutical Sciences,* 2015, **7**(6), 415-418.
4. K. Pandey, M. Singh and A. Upadhyaya, Preliminary phytochemical screening and antimicrobial activities of plant extract of *Elaeocarpus ganitrus*, *International Journal of Bioassay*, 2016, **5**(9), 4885-4889.
5. A. Tilak, S. Gangwar and R. N. Thakur, Preliminary phytochemical screening and antimicrobial activities of plant extract of *Elaeocarpus ganitrus Roxb*., *Imperial Journal of Interdisciplinary Research*, 2017, **3**(1), 1531-1538.
6. T. J. Dennis, Rudrakshya- not just a spiritual symbol but also a medicinal remedy, *Sachitra Ayurved,* 1993, **46**(2), 142-146.
7. H. N. Mastura and A. Germano, Plant alkaloids: main features, toxicity and mechanism of action, *Researchgate,* 2015, **10**(7), 94-102.
8. L. Yang and J. Stocktigt, Trends for diverse production strategies of plant, medicinal alkaloids, *Natural Product Report*, 2010, **27**(6), 1469-1479.
9. N. Talukdar, A. M. Dutta, R. Chakraborty and K. Das, Screening of phytochemicals, antioxidant and inhibitory effect on alpha-amylase by ethanolic extract of *Elaeocarpus ganitrus* bark, *International Journal of Pharmaceutical Sciences and Research,* 2017, **8**(12), 5270-5275.
10. A. Tilak, S. Gangwar, and R. N. Thakur, Elaeocarpus ganitrus medicinal use in modern time, *Imperial Journal of Interdisciplinary Research,* 2017, **3**(1), 1531-1538.
11. A. Marisetti and S. Kolli, In-vitro anti-oxidant and thrombolytic activity of *Elaeocarpus ganitrus* bark extracts, *World Journal of Pharmacy and Pharmaceutical Sciences,* 2016, **5**(10),1312-1320.
12. W. B. Williams, M. E. Cuveliar and C. Berset, Use of free radical method to evaluate antioxidant activity, *Food Science Technology*, 1995, **28**(1), 25-30.
13. M. Mazur and J. Telser, Free radicals and antioxidants in normal physiological functions and human disease, *The International Journal of Biochemistry and Cell Biology*, 2007, **39**, 44-84.

JNCS
Journal of Nepal Chemical Society December 2019, Vol. 40, 19-24
ISSN: 2091-0304 (print)
DOI: https://doi.org:10.3126/jncs.v40i0.27273
RESEARCH ARTICLE

Phytochemical Screening and Cytotoxicity Evaluation of Ethanolic Extract of *Hypericum cordifolium* (choisy) Leaves

Deepak Basyal[1], Netra Lal Bhandari[2*]

[1]*Department of Pharmacy, Maharajgunj Medical Campus, Institute of Medicine, Tribhuvan University, Kathmandu, Nepal*

[2]*Department of Chemistry, Tri-Chandra Multiple Campus, Tribhuvan University, Kathmandu, Nepal*

[*]*Corresponding E-mail: netra.tu.edu@gmail.com*

(Received: Sept. 03, 2019; Revised: Dec. 24, 2019 & Accepted: Dec. 26, 2019)

Abstract

Hypericum cordifolium is a medicinal plant traditionally used for the treatment of the menstrual disorder, backache, dislocation of bone, fever, diarrhea and dysentery due to the presence of potential bioactive secondary metabolites. Ethanolic extract of dried leaf powder was prepared using the Soxhlet apparatus, followed by qualitative phytochemical screening with different reagents. In-vitro cytotoxicity assay was screened by using brine shrimp bioassay and LC_{50} was calculated by probit analysis. Alkaloids, glycosides, amino acids, and fixed oils were present at very minute level whereas saponin, phenolics and flavonoids were present at significant level. Cytotoxicity assay of the leaf extract showed useful results ($p<0.05$). LC_{50} of 273 ppm, which was less than 1000 ppm, showing that the plant is toxic. The study revealed that the plant possessed medicinal values, that could justify the traditional medicinal practices. This research has pointed out further possibilities of works to be done on this virgin plant creating the opportunity for scientific researches to give birth of potent lead molecules.

Keywords: *Hypericum cordifolium*, phytochemical screening, probit analysis, LC_{50}.

Introduction

Medicinal plants have been the important source of medicine amongst traditional tribal healers worldwide since antiquity [1]. From the earliest times, herbs have been prized for their relieving and healing abilities, and today we still curative properties of plants [2]. According to WHO, 80% of the people living in rural areas depend on medicinal herbs as the primary healthcare system and 25% of prescribed drugs are derived from plants [2,3]. Hence, drug discovery by investigating on bioactive natural products has been most significant strategy for new drug development [4].

Cancer is one of the leading causes of death in the world, and the number of individuals infected with cancer is continuing to expand [5]. It is a group of diseases caused by loss of cell cycle control and associated with abnormal, uncontrolled cell growth. It is caused by both external factors (tobacco, chemicals, radiation and infectious organisms) and internal factors (inherited-mutations, hormones, immune conditions, the mutation that occur from metabolism) [6]. Hence, it is a significant worldwide public health problem generally due to lack of widespread and comprehensive early detection method, the associated poor prognosis of a diagnosis of disease in patients [7].

Anticancer activity means reversal, suppression or prevention of carcinogenic progression by using bioactive natural and synthetic agents [8]. Treatment options of cancer are typically expensive and unavailable in developing countries [9]. In most cases, drugs used for the treatment of cancer are not effective or have an unpleasant side effect [10]. Therefore, new drug discovery and development is necessary for further treatment option to combat these diseases.

In the present study, one of the ethnomedicinally important plants has been selected, having very few supportive scientific researches *Hypericum cordifolium*, for exploration of its cytotoxicity. *H. cordifolium* is an endemic plant, well-distributed from the altitude of 900 m-1700 m in the central development region and some part of the western development region [11]. This plant has some ethnomedical records as a remedy for the menstrual disorder, back pain, fever. This is the most attractive indication to draw our attention for this project to discover toxicity of leaves in cattle [12]. Results show that it possess some cytotoxic molecules for this action.

Being endemic, very limited international and also national publication on this plant is available. This indicates that the real potency of *H. cordifolium* has not been justified scientifically. Hence, research aimed to explore cytotoxicity of the plant. As other *Hypericum species* have shown their potentiality as anticancer drugs, the *H. cordifolium* could be an alternative species with much more potentiality that can meet today's need for a drug with minimum adverse effect and maximum efficacy.

Materials and Methods

Plant collection and identification

Young leaves of *Hypericum cordifolium* (approx. 8 kg) were collected from wild, slopy areas of Ashapuri village of Bhaktapur district in August. The plant was identified in the Pharmacognosy laboratory of the Pharmacy Department, Maharajgunj Medical Campus, Tribhuvan University, Kathmandu, Nepal.

Processing of crude drug

The leaves were stripped from the plant by carefully discarding the damaged ones. Then the leaves were thoroughly washed with water to remove the impurities and again washed with 1% saline solution. Water was strained from the leaves in the perforated bucket transferred in trays for room drying.

Leaves were thinly spread in the mosquito net in a well-ventilated room. This room was an insect, rodent, and dust proof. Air circulation was maintained through room ventilations, but the direct air towards the leaves was avoided, as it could increase the contamination with germs in the air. It was dried for 15 days followed by milling using a mixture grinder. The milled leaves were sieved with the sieve of mesh size 2 mm to get uniform powder. It was dried at 50 ºC for 30 minutes to reduce moisture content considerably below 7.5% and was stored.

Solvent extraction

The obtained powder was subjected to pre-soxhlet maceration for 6 hours, with 90% ethanol. Then the mixture was soxhleted for 48 hours with 90% ethanol with a solvent to sample ratio of 10:1 (v/w). Each extract was filtered by vacuum filtration then evaporated to near dryness using a rotary evaporator. Lastly, the percentage yield of extract was calculated and stored in container (inside the refrigerator) for further studies.

Phytochemical screening

Phytochemical screening of alkaloids, saponins, tannins, flavonoids, terpenoids, resins, phenols, protein and aminoacids, phytosterol, carbohydrate, glycosides, fixedoils, and fats were carried out for ethanolic extracts as per the standard methods [13,14].

Brine shrimp lethality assay (cytotoxic activity)

Brine shrimp lethality assay was conducted as per the standard method [15,16]. The brine shrimp bioassay is based on the ability to kill laboratory-cultured *Artemia nauplii.* Brine shrimp (*A. salina*) belongs to phylum arthropod and class crustacean. Brine shrimp are marine invertebrates about 1 mm in size. The eggs of brine shrimp remain viable for years in the dry state. Brine shrimp method provides a quick and economical alternative to vertebrate testing. It determines LC_{50} values in ug/mL of test samples against *nauplii* in the brine medium.

Two unequal halves (Larger and smaller compartment) was made with a plastic divider in a 22 x 32 cm rectangular dish with several holes and filled with artificial seawater (28g sea salt/L). The smaller compartment was illuminated the light. About 15 mg eggs of *A. salina* were sprinkled larger compartment. After 24 hours, phototropic *nauplii* were collected using a Pasteur pipette from the smaller compartment. 10 shrimps were transferred to each vial containing 2 mL of seawater and 0.2 mL of 1000, 500, 250 and

125 ppm concentration of the extract prepared in 1% DMSO. The control vials were treated with 1 % DMSO (negative control) instead of extract. Each concentration replicates was performed in triplicates. All the vials were placed under illumination at room temp, and after 24 hours, the number of survivors was counted and the percentage of deaths was calculated. Larvae not exhibiting any internal and external movement during multiple observations were considered dead. The number of death if occurred in the control was also counted and, the data were corrected using the following formula. LC_{50} was calculated by plotting concentration and % mortality (Probit analysis).

Statistical analysis

Cytotoxicity of ethanolic extracts was carried out in various concentrations (triplicate). Data were analysed by One-way ANOVA followed by Post-Hoc Tuckey test using SPSS version 20 (SPSS Inc, Chicago).

Results and Discussion

The extractive value of ethanol was found to be highest (45%) when compared with water (35%) and ether (5%). Hence the selection of ethanol as a solvent for extraction will give the highest yield i.e. a large number of compounds. The lowest extractive value of ether indicated that there is the fewer amount of non-polar constituents but the highest extractive value of ethanol, indicated a higher amount of polar constituents in leaves powder and also ethanol has the ability to extract many non-polar constituents. Water could be a choice of solvent for economic and easy extraction but there is the chance of microbial contamination on storage and extraction of only polar constituents. Hence, ethanol due to its high extraction ability and less chance of contamination, it will be the best option in solvent selection.

Table 1: *Phytochemical screening of ethanolic extract of plant leaves*

SN	Detection	Test name	Reference	Observation	Result
1	**pH test**	Blue litmus paper Red litmus paper P^Hvalue	Turns to red if acidic Turn to blue if basic	Red No change	Acidic 4.72
2	**Alkaloids**	Hager's test	Yellow ppt	No yellow ppt.	-
		Wagner's test	Yellow /brown ppt	Brown ppt.	+
		Mayer's test	White/Pale yellow ppt.	No yellow ppt.	-
3	**Saponin**	Foam test	Foam persist for 10 min	Foam persist for more than 10 mins	+++
4	**Tannin**	5 % $FeCl_3$	Blue, Violet or Purple colour	Blue colour	+++
		Gelatin test	White ppt.	White ppt.	+++
5	**Flavonoids**	Zinc HCl reduction test	Purplish pink	Purplish pink	++
		Alkaline reagent	Intense yellow color by 10% NaOH and colorless by few drops of dilute HCL	Colorless	++
6	**Terpenoids**	Copper acetate -di-terpenoids	Emerald green color	Emerald green	++
7	**Resin**	Acetone-water test	Turbidity	No turbidity	-
8	**Phenol**	Ferric chloride test	Bluish Black color	Bluish black	+++
9	**Proteins and Amino acid**	Xanthoproteic test	Yellow color (Proteins)	Yellow color	++
		Ninhydrin test	Blue color (Amino acids)	No blue color	-
10	**Phytosterols**	Salkowski test	Golden yellow (tritepenes)	Golden color	++
		Tshugajeu test	Eosin red color (triterpenes)	Eosin red color	+++
11	**Carbohydrate**	Benedicts test	Brick red ppt	Red color	+
		Fehling test	Red/Brick red ppt.	No red ppt.	-
12	**Glycosides**	Molischs test	Red violet ring appears which disappears on the addition of alkali	Nocolor change	-

The alkaloid was present in trace amount with the positive result only in Wagner's test, but there was a negative result for other two; Hager's and Mayer's test. The various study performed in other species of *Hypericum* claimed xanthone only alkaloid at very minute level [17] and flavonoid and phenol as the major constituent components [18]. The screening indicated the presence of flavonoid and phenol in major amount. The test indicated a huge amount of saponin and researches showed that saponins are important therapeutically as they are shown to have hypolipidemic and anticancer activity. There was an appreciable amount of terpenoid in the extract. However, in contrast to available study which shows the appreciable amount of anthrone derivatives as hypericin, pseudohypericin, etc. in other species [19], It was found only in a minute or trace amount. Such a result might be because of a very less amount of glycosides due to loss on storage or drying or the available test might not be suitable. There was an absence of resin but the presence of a very trace amount of fixed oil. The carbohydrate gave positive results only for the Benedict's test but negative for Fehling's and Molisch test. Similarly, amino acid also exhibits dual result giving a positive result for xanthotropic whereas negative for the ninhydrin test. These dual findings might be due to inherent color leaf extract that led to confusion in observations and limited sensitivity of the test methods utilized [20].

Brine shrimp cytotoxicity assay

Figure 1: *Brine shrimp cytotoxicity of different concerntation extract*

Cytotoxicity of the extract in various concentrations was examined by Brine shrimp cytotoxicity assay and results expressed in LC_{50} as presented in the above figure. In the present study, the lowest concentration of 125 ppm has also shown some range cytotoxic activity causing 33.34% mortality, whereas the highest concentration of 1000 ppm results highest toxicity of 96.67% mortality. The LC_{50} from the table was obtained on the concentration of 273 ppm, which was less than 1000 ppm that verified that the plant is toxic. From the One-Way ANOVA followed by the Post-Hoc Tuckey test, it was found that there was a significant difference between different concentrations and activity at the significant level of 0.05.

No specific molecule from this plant has been identified but hypericin-c from *H. riparium* shows potent cytotoxic activity in brine shrimp lethality bioassay and hyperuralone A from *H. uralum* exhibited cytotoxic activity against five human cancer cell line in-vitro with IC_{50} of 4.6-14.4 μM. As brine shrimp cytotoxic assay has been considered as a pre-screening assay for antimicrobial, antitumor, antimalarial, antifungal, and insecticidal activities and a positive correlation exist between brine shrimp lethality and human carcinoma [21-23], hence efforts have been made to determine the preliminary in-vitro anticancer activity of the extract.

Conclusion

This study concludes that ethanolic extract of this plant possessed medicinal values, that could justify the ethnomedicinal importance. Likewise, this research results have pointed out further possibilities of works on this virgin plant creating an opportunity for scientific researches to give birth of potent lead molecules as a remedy of cancer and a gift for the welfare of humanity. There is a need for further studies in this plant to clarify the *in-vivo* potential of this plant in the management of cancer. That was a subject of investigation in our group. Fractionation of the extract to identify bioactive fractions and further isolation and characterization of compounds are in progress.

Acknowledgment

The authors are thankful to Department of Pharmacy, Maharajgunj Medical Campus, Institute of Medicine, Tribhuvan University, Kathmandu, Nepal for providing the facilities for carrying out this research work.

References

1. M. S. Butler, The role of natural product chemistry in drug discovery, *Journal of Natural Products,* 2004, **67**(12), 2141-2153. (DOI: 10.1021/np040106y).
2. A. S. Rajesh, N. S. Kiran, P. C. Tripathi and K. Verma, In vitro cytotoxicity of *Moringa oleifera* against different human cancer cell lines, *Asian Journal of Pharmaceutical and Clinical Research*, 2012, **5**(4), 271-2.
3. R. Dipasquale, The aboca museum: Displaying the histroy of herbal medicine in Italy and Europe, *The Journal of American Botanical Council,* 2005, **65,** 50-57.
4. S. P. Rout, K. A. Choudary, D. M. Kar, L. O. Das and A. Jain, Plants in traditional medicinal system-future source of new drugs, *International Journal of Pharmacy and Pharmaceutical Sciences*, 2009, **1**(1), 1-23.
5. R. S. Kumar, B. Rajkapoor and P. Perumal, Antitumor and cytotoxic activities of methanol extract of *Indigofera linnaei Ali*., *Asian Pacific Journal of Cancer Prevention,* 2011, **12**(3), 613-8.
6. S. Chanda and K. Nagani, In vitro and in vivo methods for anticancer activity evaluation and some Indian medicinal plants possessing anticancer properties: an overview, *Journal of Pharmacognosy and Phytochemistry,* 2013, **2**(2).
7. M. H. Teiten, F. Gaascht, M. Dicato and M. Diederich, Anticancer bioactivity of compounds from medicinal plants used in European medieval traditions, *Biochemical Pharmacology,* 2013, **86**(9), 1239-1247. (DOI: 10.1016/j. bcp.2013.08.007).
8. J. Alzeer, B. R. Vummidi, R. Arafeh, W. Rimawi, H. Saleem and N. W. Luedtke, The influence of extraction solvents on the anticancer activities of Palestinian medicinal plants, *Journal of Medicinal Plants Research,* 2014, **8**(9), 408-415. (DOI: 10.5897/JMPR2013.5044).
9. A. Eghdami, H. Piri, M. Sirati-Sabet and D. Ilghari, Investigation of anti proliferative properties and antioxidant activity of aerial parts ethanolic extract of *Hypericum perforatum L*. by breast cancer 4T1 cell lines, *International Journal of Biosciences,* 2013, **3**(12), 265-72. (DOI: 10.12692/ijb/3.12.265-272).
10. P. S. Coker, J. Radecke, C. Guy and N. D. Camper, Potato disc tumor induction assay: a multiple mode of drug action assay, *Phytomedicine,* 2003, **10**(2-3),133-138. (DOI: 10.1078/094471103321659834)
11. N. P. Manandhar, *Plants and People of Nepal, Timber Press,* 2002.
12. P. K. Mukherjee, R. Verpoorte and B. Suresh, Evaluation of in-vivo wound healing activity of *Hypericum patulum* (Family: *Hypericaceae)* leaf extract on different wound model in rats, *Journal of Ethnopharmacology*, 2000, **70**(3), 315-321. (DOI: 10.1016/S0378-8741(99)00172-5).
13. P. Tiwari, B. Kumar, M. Kaur, G. Kaur and H. Kaur, Phytochemical screening and, extraction: a review, *Internationale Pharmaceutica Sciencia*, 2011,**1**(1), 98-106.
14. A. Pandey and S. Tripathi, Concept of standardization, extraction and pre phytochemical screening strategies for herbal drug, *Journal of Pharmacognosy and Phytochemistry*, 2014, **2**(5).
15. S. B. Gaikwad, M. G. Krishna, and S. J. Anerthe, Antimitotic activity and brine shrimp lethality test of *Tectona grandis Linn*. bark, *Research Journal of Pharmaceutical, Biological and Chemical Science,* 2011, **2**(4), 1014-1022.
16. A. P. Peron, R. G. Mariucci, I. V. de Almeida, E. Düsman, M. S. Mantovani and V. E. Vicentini, Evaluation of the cytotoxicity, mutagenicity and antimutagenicity of a natural antidepressant, *Hypericum perforatum L.* (St. John's wort), on vegetal and animal test systems, *BMC Complementary and Alternative Medicine*, 2013, **13**(1), 97. (DOI: 10.1016/S0278-6915(01)00053-9).

17. I. A. Nawchoo, In vitro antibacterial activity and phytochemical studies of methanolic extract of leaves of *Hypericum perforatum L.* growing wild in Kashmir Himalaya, *Asian Journal of Plant Science and Research,* 2012, **2**(4), 414-420. (ISSN : 2249-7412).

18. G. Çelen, S. Özkan, and F. Ayhan, The phenolic compounds from *Hypericum perforatum* and their antimicrobial activities, *Hacettepe Journal Of Biology And Chemistry*, 2008, **36**(4), 339-345. (DOI: 10.1055/s-2002-20053).

19. U. M. Vattikuti and V. Ciddi, An overview on *Hypericum perforatum Linn., Natural Product Radiance,* 2005, **4**(5), 368-381.

20. K. S. Vidyalakshmi, D. A. Chales and H. R. Vasanthi, Anti–mitotic and cytotoxic effect of *Mussaenda queensirkit*, *Journal of Pharmacology and Toxicology,* 2007, **2**(7), 660-5. (DOI: 10.3923/jpt.2007.660.665).

21. A. V. Krishnaraju, T. V. Rao, D. Sundararaju, M. Vanisree, H. S. Tsay and G. V. Subbaraju, Assessment of bioactivity of Indian medicinal plants using brine shrimp (*Artemia salina*) lethality assay, *International Journal of Applied Science and Engineering,* 2005, **3**(2), 125-134. (DOI: 10.1.1.613.7777).

22. B. Jaki, J. Orjala, H. R. Bürgi and O. Sticher, Biological screening of cyanobacteria for antimicrobial and molluscicidal activity, brine shrimp lethality and cytotoxicity, *Pharmaceutical Biology,* 1999, **37**(2), 138-143. (DOI: 10.1076/phbi.37.2.138.6092).

23. R. Padmaja, P. C. Arun, D. Prashanth, M. Deepak, A. Amit and M. Anjana, Brine shrimp lethality bioassay of selected Indian medicinal plants, *Fitoterapia,* 2002, **73**(6), 508-510. (DOI: 10.1016/S0367-326X(02)00182-X).

JNCS
Journal of Nepal Chemical Society December 2019, Vol. 40, 25-29
ISSN: 2091-0304 (print)
DOI: https://doi.org:10.3126/jncs.v40i0.27274
RESEARCH ARTICLE

Corrosion Inhibition of Bark Extract of *Euphorbia royleana* on Mild Steel in 1M HCl

Bishal Thapa[1], Dipak Kumar Gupta[1,2], Amar Prasad Yadav[1*]

[1]*Central Department of Chemistry, Tribhuvan University, Kirtipur, Kathmandu, Nepal*

[2]*Department of Chemistry, Tri-Chandra Multiple Campus, Tribhuvan University, Kathmandu, Nepal*

**Corresponding E-mail: amar2y@yahoo.com*

(Received: Aug. 26, 2019; Revised: Dec. 24, 2019 & Accepted: Dec. 25, 2019)

Abstract

The bark extract of *Euphorbia royleana* as a green corrosion inhibitor was studied in 1M HCl using weight-loss method and potential measurement. The results show that the bark extract of *Euphorbia royleana* is an effective anti-corrosion inhibitor of mild steel in acidic media. The corrosion rate decreases with the time of immersion. Weight loss experiment shows that the loss in weight decreases with the time of immersion and inhibition efficiency increases with the concentration of extract. It was observed that maximum inhibition efficiency is 99.60% in 100% concentration of extract. Potential measurement study shows that bark extracts act as a mixed type of inhibitor i.e. inhibits both anodically as well as cathodically.

Keywords: Corrosion inhibitor, *Euphorbia royleana*, green corrosion inhibitors, inhibition efficiency, OCP

Introduction

Corrosion is an unavoidable natural phenomenon which is a serious issue and results in a huge impact on the economy [1]. In the UK, the corrosion cost is estimated to be 4-5% of the Gross National Products (GPS). For most industrialized nations; the average corrosion cost is 3.5-4.5% [2]. It is estimated that corrosion destroys one-quarter of the world's annual steel production, which corresponds to about 150 million tons per year in this sector [3]. It is estimated that with proper knowledge of corrosion prevention, about 25 to 30 % of this loss can be saved. Several methods can be applied to control corrosion. The use of inhibitors is one of the practical methods for protection against corrosion especially in acid media, to prevent unexpected dissolution and acid consumption [4,5]. Unfortunately, the uses of some chemical inhibitors have been limited because their synthesis is very often expensive and they can be toxic and hazardous for human beings environment as well [6]. This has encouraged the search for eco-friendly corrosion inhibitors as an alternative to replace inorganic and organic inhibitors to promote sustainable greenness to the environment. These non-toxic, benign, inexpensive, renewable and readily available alternative corrosion inhibitors have been found in different parts of plant extracts [7].

Natural products obtained from a plant containing alkaloids act as an inhibitor. They are environmentally friendly and economical. Nepal is rich in natural products. Herbs and shrubs are widely spread in nature [8]. As organic corrosion inhibitors are toxic so green inhibitors are of great interest which are biodegradable and do not contain heavy metal and other toxic compounds. Plant extracts can be used to effectively retard the corrosion rate, called the green corrosion inhibitor [9].

Green Inhibitors generally have hetero atoms. O, N and S are found to have higher basicity and electron density and thus act as corrosion inhibitors. O, N and S are the active centers for the process adsorption on the metal surface. The inhibition efficiency should follow the sequence O < N < S < P. The performance of a green inhibitor is related to the chemical structure and physicochemical properties of the compound like functional groups, electron density at donor atom, p-orbital character and electronic structure of molecule [1,10]. The inhibition could be due to adsorption of ions/molecules onto the metal surface, increasing or

decreasing anodic or cathodic reaction, decreasing the diffusion rate for reactants to the surface of the metal and formation of a protective barrier film [10,11].

Materials and Methods

Preparation of plant extract

The *Euphorbia royleana* (Siudi) plants were collected from Sanothimi, Bhaktapur. The barks of *Euphorbia royleana* plants were collected and dried in shadow for a month. After that dried barks were finely powdered in a grinder and stored in an air tight plastic jar. 100 g of dried powder barks of the plant were put into 400 mL 1 M HCl for about 3 days and then refluxed for about 3 hours. Then, the solution was filtered off and then diluted to 250 mL with 1 M HCl and marked as 100% or stock solution. The test media were prepared by diluting the required volume of extract in 1 M HCl. The extract of 10, 20, 30, 40 and 50% concentration were prepared and 1 M HCl without extract was taken as control.

Preparation of mild steel specimen

The mild steel sample was brought from the local market of Balaju, Kathmandu. The sample was cut into average dimensions of 30× 30 mm. The samples were polished with silicon carbide paper of 100, 400, 600, 800, 1000, 1200 and 1500 grits and thoroughly washed with distilled water and ethanol. It is then subjected to a weight loss experiment.

Weight loss experiment

Samples of size 30 × 30 mm were immersed in 50 mL of different concentration of extracts and in 1 M HCl as control. Weight loss was determined for one day. MS specimens were also immersed in 50 mL of 10% and 1 M HCl solution for 2, 5 and 7 days. The corrosion rates of the steel were calculated by the following expression.

Where,

Δw = weight loss in mg

D = Density of mild steel in g/cm^3

A = Area of sample in cm^2

T = Time of exposure in hours

The percentage inhibition efficiency (IE) was determined from

Where, W1 and W2 are weight loss of mild steel in without and with inhibitor solution

Potential measurement

The mounted and polished specimens were tested for potential measurements. They were immersed in different test media containing 10% and 100% concentration of the extracts. The potential was recorded at a day intervals for 2, 3, 4 days' interval for 23 days using a digital multimeter with respect to Saturated Calomel Electrode (SCE), as reference electrode and mild steel specimen as the working electrode. The plot of variation of potential (E) in volt versus SCE with exposure time was plotted.

Results and Discussion

Variation of weight loss with time of immersion and concentration of bark extract

The weight loss of the mild steel was calculated by the given equation,

Weight loss $\Delta w = W1\text{-}W2$

Where, W1 and W2 are weight loss of mild steel without and with inhibitor.

The results of the weight loss experiment for mild steel immersed in 1 M HCl with and without inhibitor were shown in Figure 1. The maximum loss in weight was found in 1 M HCl without *Euphorbia royleana* extract throughout the experiment. The addition of *Euphorbia royleana* extract to the test medium significantly reduced the weight loss. The addition of extract not only decreased the loss in weight but also delayed the action of the test medium. This was because plant extract had adsorbed on the surface of mild steel. It was also observed that loss in weight of mild steel was dependent on the concentration of *Euphorbia royleana* extract in the test medium. However, the weight loss was increased with increase in time. This may be due to the desorption of inhibitor when the mild steel was exposed for longer period.

It is observed clearly in Figure 2. that the weight loss of mild steel gradually decreases with an increase in

the concentration of plant extract due to adsorption of inhibitor on the mild steel surface.

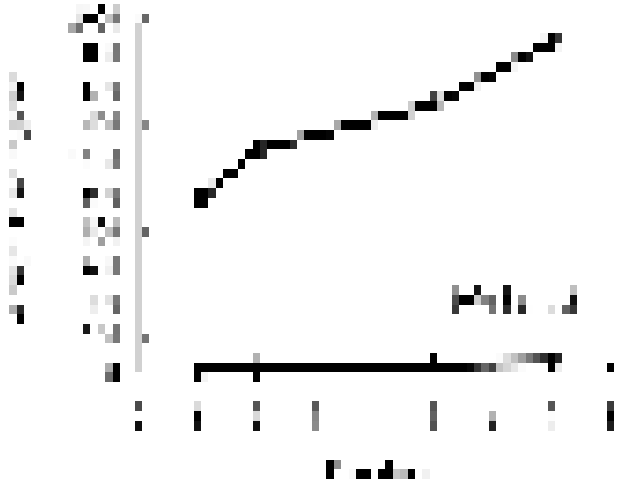

Figure 1: *Variation of weight loss with time of immersion*

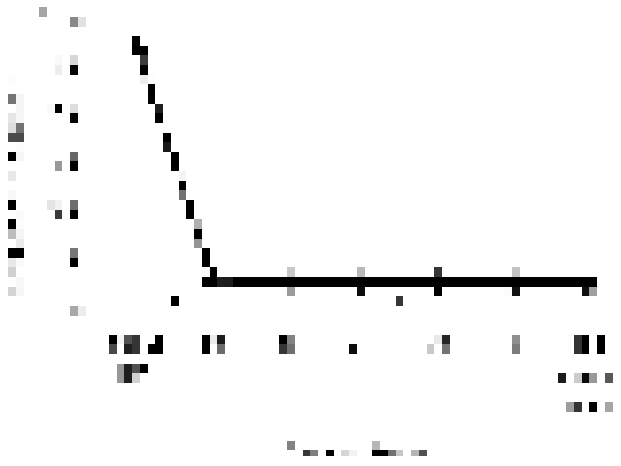

Figure 2: *Variation of weight loss with concentration*

Variation of inhibition efficiency with concentration of bark extract by weight loss method

Weight loss measurement was carried out for different concentrations of *Euphorbia royleana* bark extract to study the influence of concentration of extract on the inhibition efficiency for mild steel in 1M HCl. The inhibition efficiency of the extract on the mild steel increases with an increase in the concentration of the extract which is shown in Figure 3. This is because, as the concentration of the extract increases, the fraction of the surface covered by adsorbed molecule also increases which results in an increase in the inhibition efficiency increases progressively as the concentration of the extract increases up to about 100% (stock solution). The maximum inhibition efficiency of 99.60% was achieved.

Figure 3: *Variation of inhibition efficiency with concentration of extract*

Variation of corrosion rate with different concentration of extract and time of immersion

It is clearly seen that the corrosion rate decreases with the increasing concentration of extract as shown in Figure 4.

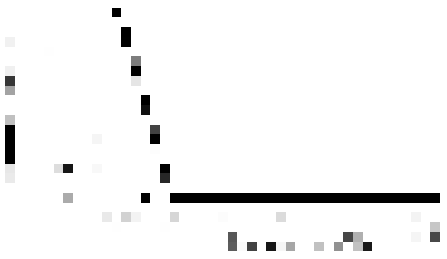

Figure 4: *Variation of corrosion rate with concentration of extract*

It is also seen that the corrosion rate is high initially which is decreased gradually with the time as shown in Figure 5.

Figure 5: *Variation of corrosion rate with time in days*

It may be due to the contamination of corrosion medium with corrosion products or may be due to the deposition of corrosion products on the surface of the steel sample.

These results confirm the good corrosion inhibition of extract towards the corrosion of mild steel in 1M HCl.

Potential measurement

OCP or corrosion potential (Ecorr) measurement was carried out using a digital multimeter in reference to Saturated Calomel Electrode (SCE) as a reference electrode. The graph plotted between the potential of mild steel versus time, as shown in fig.6. It was observed that potential shifted towards more positive sharply at first and then decreased slowly and became almost constant with the passage of time for HCl but for plant extract it was observed that potential shifted to more negative value than that of for HCl which reveals that sample was cathodically protected i.e. it is due to cathodic inhibition and later again potential shifted positively which shows that sample was anodically protected and then potential became almost constant. Therefore, it reveals that extract was the mixed type of inhibitor [1].

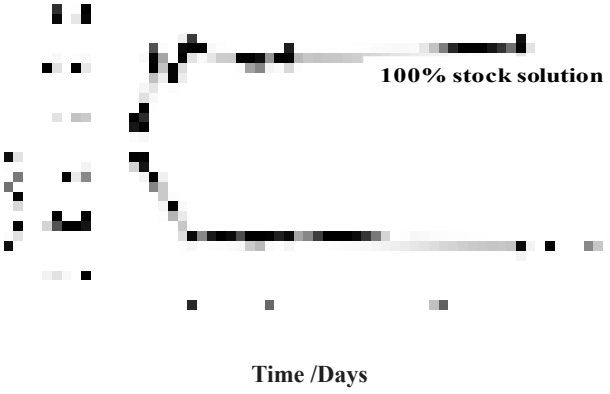

Figure 6: *Variation of corrosion potential with time in days*

FTIR spectroscopic analysis

The FTIR spectrum of *Euphorbia royleana* bark extract was analyzed which is shown in figure 7, the band at a frequency about (3500-3200) cm^{-1} is of O-H (3550-3200 cm^{-1}) or of N-H (3500-3300 cm^{-1}) functional group and band at the frequency (1700-1600) cm^{-1} is of C=O (1750-1680 cm^{-1}). Hence the FTIR studies reveal that the interaction of the inhibitor on the mild steel surface for adsorption in corrosion protection. Thus, the band indicates that there is a lone pair of electron in hetero atom which is responsible for adsorption on metal surfaces.

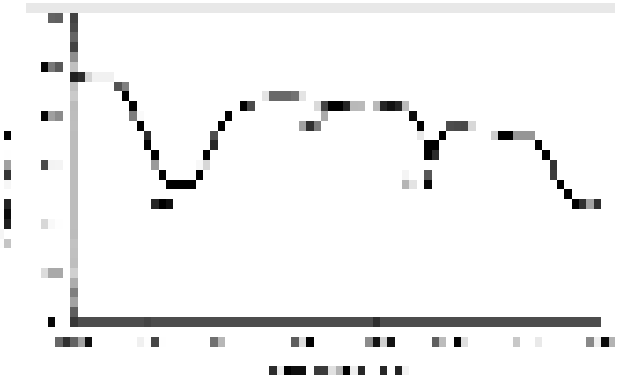

Figure 7: *FTIR Spectrum of Extract*

Conclusion

From the above results, the following conclusions can be made.

i. Inhibition efficiency is maximum (99.60%) when the mild steel was immersed in 100% stock solution for 24 hours. Effectiveness of extract towards corrosion is due to the presence of organic compounds that act as inhibiting film forming on the surface of mild steel.

ii. OCP measurement showed that the extract is of mixed inhibitor.

iii. FTIR analysis suggested that the adsorption takes place due to the presence of functional group O-H, C≡N and C=O group.

Acknowledgements

Department of Chemistry, Tri-Chandra Multiple Campus is acknowledged for providing necessary laboratory facilities for the experimental work and Central Department of Chemistry, Tribhuvan University, Kathmandu is acknowledged for providing FTIR spectra.

References

1. M. U. Rahman, S. Gul, M. Umair, A. Anwar and A. K. K. Achakzai, Anticorrosive activity of *Rosemarinus officinalis L.* leaves extract against mild steel in dilute hydrochloric acid, *International Journal Innovative Research in Advanced Engineering (IJIRAE)*, 2016, **3**(3), 38-43.

2. H. H. Uhliq, *Corrosion and Corrosion Control*, 3rd Ed., John Wiley and Sons, New York, 1985.

3. D. Landolt, *Corrosion and Surface Chemistry of Metals,* 1st Ed., EPFL press, New York, 2007. (DOI: 10.1201/9781439807880).

4. H. Ashassi-Sorkhabi, B. Shaabani, D. Seifzadeh, Corrosion inhibition of mild steel by some Schiff base compounds in hydrochloric acid, *Applied Surface Science,* 2005, **239,** 154-164. (DOI:10.1016/j.apsusc.2004.05.143).

5. A. K. Satapathy, G. Gunasekaran, S. C. Sahoo, A. Kumar and P. V. Rodrigues, Corrosion inhibition by *Justicia gendarussa* plant extract in hydrochloric acid solution, *Corrosion Science,* 2009, **51**(12) 2848-2856. (DOI:10.1016/j.corsci.2009.08.016).

6. J. Halambek, K. Berkovic, J. Vorkapic´-Furac, The influence of *Lavandula angustifolia L.* oil on corrosion of Al–3Mg alloy, *Corrosion Science*, 2010, **53**, 978–3983.

7. S. A. Umoren, U. M. Eduok, M. M. Solomon, and A. P. Udoh, Corrosion inhibition by leaves and stem extracts of *Sida acuta* for mild steel in 1 M H_2SO_4 solutions investigated by chemical and spectroscopic techniques, *Arabian Journal of Chemistry*, 2016, **9**, 209-224. (DOI:10.1016/j.arabjc.2011.03.008).

8. D. Rawal, J. Sijapati, N. Rana, P. Rana, A. Giri and S. Shrestha, Some high value medicinal plants of Khumbu region Nepal, *Nepal Journal of Science and Technology*, 2009, **10**, 73-82. (DOI:10.3126/njst.v10i0.2828).

9. P. R. Shrestha, H. B. Oli, B. Thapa, Y. Chaudhary, D. K. Gupta, A. K. Das, K. B. Nakarmi, S. Singh, N. Karki and A. P. Yadav, Bark extract of *Lantana camara* in 1M HCl as green corrosion inhibitor for mild steel, *Engineering Journal,* 2019, **23**(4), 205-211.(DOI:10.4186/ej.2019.23.4.205).

10. B. E. Amitha Rani and B. B. J. Bashu, Green inhibitors for corrosion protection of metals and alloys: an overview, *International Journal of Corrosion*, 2012, **2012**. (DOI:10.1155/2012/380217).

11. D. Ben Hmamou, R. Salghi, L. Bazzi, B. Hammouti, S. S. Al-Deyab, L. Bammoul, L. Bazzi and A. Bouyanzer, Prickly pear seed oil extract: A novel green inhibitor for mild steel corrosion in 1 M HCl solution, *International Journal of Electrochemical Science*, 2012, **7,** 1303-1318.

JNCS
Journal of Nepal Chemical Society December 2019, Vol. 40, 30-35
ISSN: 2091-0304 (print)
DOI: https://doi.org:10.3126/jncs.v40i0.27275
RESEARCH ARTICLE

Assessment of Total Phenolic, Flavonoid Content and Antioxidant Activity of *Ocimum sanctum Linn*

Ishwor Pathak[1*], Muna Niraula[2]

[1]*Department of Chemistry, Amrit Campus, Tribhuvan University, Kathmandu, Nepal*
[2]*Central Department of Chemistry, Tribhuvan University, Kathmandu, Nepal*
**Corresponding E-mail: pathakishwor14@gmail.com*

(Received: Sept. 30, 2019; Revised: Dec. 26, 2019 & Accepted: Dec. 28, 2019)

Abstract

Ocimum sanctum, commonly known as Tulasi in Nepal, is a pharmacologically important plant due to its active constituents. In this work, extraction was carried out in hexane, chloroform and methanol solvents and their phytochemical screening was performed. Total phenolic and flavonoid contents in the plant were measured by Folin-Ciocalteu colorimetric method and aluminum chloride colorimetric method respectively. Antioxidant activity of the extracts was evaluated using 1,1-diphenyl-2-picrylhydrazyl (DPPH) radical scavenging assay. Alkaloids, flavonoids, tannins, glycosides, polyphenols, terpenoids, tannins and steroids are mainly found in the extracts. Based on the result obtained, the plant posses a significant amount of total phenolic and total flavonoid content. Both phenolic and flavonoid contents were highest in methanol extract, followed by chloroform and hexane extract. Antioxidant activity of the extracts as ascorbic acid standard (IC_{50} value = 41.34 µg/mL) was in the order of methanol extract (IC_{50} value = 47.73µg/mL) > chloroform extract (IC_{50} value = 79.46 µg/mL) > hexane extract (IC_{50} value = 94.68 µg/mL). The extent of the antioxidant activity of the plant is following the number of total phenolics and flavonoids present in it.

Keywords: *Ocimum sanctum*, extract, phenolic content, flavonoid content, antioxidant activity

Introduction

Plants are primary sources of medicines since ancient times. Medicinally important plants contain the various bioactive secondary metabolites having several therapeutics importances [1]. Medicinal plants are advantageous for various treatments due to their fewer side effects, less expensive, efficacy and availability throughout the world. In Ayurveda, *Ocimum sanctum Linn*. has been used for its healing properties of the mind, body, and spirit [2]. *Ocimum sanctum,* commonly known as Tulasi or Tulsi in Nepali and Holy Basil in English, is the aromatic plant in the family Liliaceae [3]. It is a branched and erect herb having hair all over [4]. It is the most sacred plant among all the herbs found in Nepal. Different parts of *O. sanctum* (leaves, stems, flowers, roots, seeds and even whole plant) have been used for the treatment of bronchitis, arthritis, malaria, diarrhea, dysentery, skin disease, chronic fever, insect bite etc, [5,6]. Evidence shows that *O. sanctum* cures the physical, chemical, psychological, and metabolic stress of the human body by a unique combination of pharmacological actions [7]. It controls metabolic stress through normalization of blood glucose, blood pressure and lipid levels and psychological stress by enhancing positive effects on memory through anxiolytic and anti-depressant properties [8]. *O. santcum* also possesses anti-infertility, anticancer, antidiabetic, antifungal, antimicrobial, hepatoprotective, antispasmodic, analgesic and cardioprotective properties [9]. The plant is a rich source of essential oil and bioactive phytochemical constituents like alkaloids, flavonoids, terpenoids, phenolics, tannins and saponins [1,10]. Polyphenols and flavonoids present in this plant are largely responsible for imparting various therapeutic values including antioxidant potentiality. Antioxidants are the chemical compounds that can scavenge free radicals that are generated in the body due to various reasons. Free radicals are capable of attacking the healthy body cells which may lead to cellular damage, several diseases and disorders [11].

Materials and Methods

Plant materials

Fresh and matured leaves of *Ocimum sanctum* were collected from Dhading, Nepal, in the December month of 2018. The plant was authenticated at the Department of Botany, Amrit Campus, Kathmandu, Nepal. The collected leaves were cleaned, shade dried and powdered and stored in airtight bottles.

Extraction

The dried and powdered leaves of *Ocimum sanctum* were extracted separately with three different solvents hexane, chloroform and methanol by using soxhlet apparatus. Accurately weighed 50 g powdered leaves were filled in a thimble and placed in the central assembly of the soxhlet apparatus. Accurately measured 250 mL solvent such as hexane, chloroform, and methanol was added separately to a 500 mL round bottom flask. The extraction was done at 68 ºC, 61 ºC, and 64 ºC for six hours respectively. After that, the obtained liquid extracts were concentrated using a rotary evaporator (IKA RV 10 digital). The percentage yield (w/w) of the crude extracts was calculated and stored in the refrigerator at 5 ºC till required for analysis.

Phytochemical screening

The hexane, chloroform, and methanol extracts (1 gm) were completely dissolved in 100 mL of their mother solvents for the stock solution preparation. The obtained stock solutions were subjected to phytochemical screening by following standard protocols [12,13].

Determination of total phenolic content

Total phenolic content was determined by the modified Folin-Ciocalteu colorimetric method based on the oxidation-reduction reaction [14-16]. The stock solutions of hexane, chloroform, and methanol extracts were prepared by dissolving 100 mg in 1 mL of their mother solvents. Serial dilutions were carried out to get the concentrations of 0.125, 0.25, 0.5 and 1.0 mg/mL. 1.0 mL of each solution was taken in a test tube, and 5 mL of 10% Folin-Ciocalteu reagent was added on it. After five minutes, 4 mL of 7% Na_2CO_3 was added to the mixture. The mixture was shaken well and allowed to incubate for 30 minutes at 40 ºC for blue color development. The absorbance was measured at 760 nm against blank using a double beam UV/Visible spectrophotometer (UV professional double beam, Shimadzu made). Total phenolic content was determined as mg/g of gallic acid equivalent (mg of GAE/g of dry extract) by using the equation obtained from a standard gallic acid calibration curve y=0.014x, R^2=0.9951. Values are presented as the mean ±SE of each three replicates.

Gallic acid calibration curve

The Gallic acid calibration curve was prepared by the Folin-Ciocalteu reagent method with modification. Gallic acid (10 mg) was dissolved in methanol (1 mL). It was a concentration of 10mg/mL. It was diluted by adding methanol to prepare serial concentrations 10, 25, 50 and 100µg/mL. The above same procedure was followed for gallic acid standard. The absorbance was measured for all standard solutions by using UV-spectrophotometer (UV professional double beam, Shimadzu made) at a constant wavelength of 760 nm [17].

Determination of total flavonoid content

The total flavonoid content of extracts was estimated by the aluminum chloride colorimetric method by following standard protocol by Hossain *et al.* and Chandra *et al*. with some modifications [18-20]. Stock solutions of all three extracts were prepared by dissolving each extract (100mg) separately with their mother solvents. Serial dilutions were carried out to get the concentrations of 0.125, 0.25, 0.5 and 1.0 mg/mL. Different concentrations of different extracts (1 mL) were taken in different test tubes and added double distilled water (4.0 mL) and 5% sodium nitrate (0.3mL) then mixed. All the test tubes were kept in a dark place for 6 minutes. Then 10% aluminum chloride (0.3 mL) was added into the test tube and wait for 5 min in the dark for complete reaction. Finally, 2 mL of 1M NaOH was added to the mixture. Immediately, the volume of the mixture was made up to 10 mL by the addition of 2.4 mL double distilled water and mixed thoroughly. The absorbance of all samples was measured at a fixed wavelength of 510 nm using a UV/Visible spectrophotometer (UV professional double beam, Shimadzu made). Quercetin standard was used for the calibration curve. Total flavonoid content was determined as mg/g of quercetin equivalent (mg of QE/g of dry extract) by using the equation obtained from a standard quercetin calibration curve y=0.0081x, R^2=0.9744. All the

determinations were carried out in triplicate and the results were averaged.

Antioxidant activity test

The free radical scavenging activity was measured by using DPPH (1,1-diphenyl-2-picryl hydrazyl) radical scavenging assay as described by Hossain *et al.* and Sharma *et al.* with some modifications [18,21]. Different concentrations (10, 30, 50, 70, 90 &110 µg/mL) of extracts and ascorbic acid (positive control) were prepared. From each solution, 1 mL of each solution was taken in an Eppendorf tube and 1 mL of the 0.2 mM DPPH solution was added. The tubes were shaken and allowed to stand at 30 ºC for half an hour. The absorbance was taken on a UV-Visible spectrophotometer (UV professional double beam, Shimadzu made) at 517 nm. Lower the absorbance of the reaction mixture indicates higher free radical scavenging activity. Measurement was performed in triplicate and the percentage radical scavenging activity was calculated using the following equation:

The standard graph of concentration versus the percentage of free radical scavenging activity was plotted. Based on this graph, the IC_{50} value of each extract was calculated and these values were compared. The IC_{50} value closest to that of ascorbic acid is considered to have the best antioxidant property [22].

$$\% \text{ radical scavenging activity} = (Abs._{control} - Abs._{sample} / Abs._{control}) \times 100\%$$

Results and Discussion

Extraction and phytochemical analysis

The yields of hexane, chloroform, and methanol extracts of the leaves of *Ocimum sanctum* were 3.5%, 10.50%, 15.25% respectively. The percentage yield of extract increases with the increase of the polarity of the solvent. The qualitative analysis of the three different extracts (Table 1) showed the presence of different phytochemical constituents. Flavonoids and terpenoids were present in all extracts. Alkaloids, glycosides, polyphenols, tannins, and steroids were present in chloroform and methanol extract. Proteins were found in methanol extract only. The presence of these metabolites in the plant helps to show antioxidant potency and other biological properties [23].

Table 1: *Phytochemical screening of different extracts of leaves of Ocimum sanctum*

Phytochemicals	Hexane extract	Chloroform extract	Methanol extract
Alkaloids	-	+	+
Flavonoids	+	+	++
Cardiac glycosides	-	-	-
Glycosides	-	+	+
Polyphenols	-	+	++
Terpenoids	+	+	+
Steroids	-	+	+
Proteins	-	-	+
Quinones	+	-	-
Tannins	-	+	++
Reducing sugar	-	-	-

Key: + = Present - = Absent

Total phenolic content (TPC) and total flavonoid content (TFC)

In the present study, the total phenolic and flavonoid contents of three different extracts of *Ocimum sanctum* were determined. TPC and TFC were calculated by extrapolation from the calibration curve prepared from gallic acid and quercetin concentrations, respectively. Table 2 displays the TPC and TFC of three different extracts of *Ocimum sanctum.*

Table 2: *Total phenolic and total flavonoid contents of different extracts of Ocimum sanctum leaves*

Data expressed as mean ± SE of three replicates

Extract	Total phenolic content (mg GAE/g of dry extract)	Total flavonoid content (mg QE/g of dry extract)
Hexane	60.55 ± 0.25	16.91 ± 0.56
Chloroform	77.34 ± 0.76	38.47 ± 0.23
Methanol	180.21 ± 0.89	67.11 ± 0.43

The result showed significant total phenolic and flavonoid content in plant extracts. The number of total phenolic content was determined as quite high in methanol extract of *O. sanctum* (180.21 ± 0.89 mg GAE/g). It was found that total flavonoid content is also found highest in methanol extract (67.11 ± 0.43 mg QE/g) followed by chloroform and hexane extract. The polarity of the solvents may affect the concentration of TPC and TFC. The high concentration of phenolic and flavonoid components in the plant, may effectively eliminate free radicals and they directly contribute as antioxidants [23,24]. The sufficient amount of total phenolic and total flavonoid content in *O. sanctum* has been reported by

several authors also [25-29].

DPPH radical scavenging activity

DPPH assay was carried out to analyze the antioxidant activity of the plant by using ascorbic acid as standard. In this assay, different concentrations of different extract solutions and ascorbic acid solutions were incubated at room temperature and their absorbance was recorded by spectrophotometer. The percentage of free radical scavenging at different concentrations and IC_{50} values of each extract and ascorbic acid were calculated and the results are presented in table 3 and figure 1.

The figure above shows that percentage inhibition of DPPH free radical by extracts of *O. sanctum* was found to be near to ascorbic acid which was taken as standard. IC_{50} values of three extracts were also found to be close to the standard ascorbic acid taken. So, methanol extract of *O. sanctum* is more potent in terms of antioxidant activity. It also contains the highest amount of TPC (180.21 ± 0.89 mg GAE/g of dry extract) and TFC (67.11 ± 0.43 mg QE/g of dry extract). The high antioxidant activity of the methanol extract may be due to the presence of phytochemicals such as flavonoids, polyphenols, and tannins. This work is also supported by previous reports that flavonoids, polyphenols, and tannins found in plants have significant antioxidant activity [25,26]. This shows that *O. sanctum* leaves can act as a very good option in the field of medicine based on the antioxidant property of natural products chemistry. Previous studies from various researchers reported *O. Sanctum* as a protective antioxidant supplement [30,32]. Kelm *et al.* isolated six major compounds from *O. sanctum* which are responsible for exhibiting antioxidant activity by the plant [32].

Table 3: *DPPH free radical scavenging activity and IC_{50} values of O. sanctum extracts and standards*

Concentration (µg/mL)	**% free radical scavenging activity**			
	Hexane extract	Chloroform extract	Methanol extract	Ascorbic acid
0	0	0	0	0
10	5.71	24.28	44.28	48.57
30	18.57	31.42	52.85	57.14
50	30.0	42.85	60.0	62.85
70	40.0	50.0	65.71	67.14
90	48.57	54.28	68.57	74.28
110	54.0	57.14	71.42	77.14
IC_{50} value(µg/mL)	95.68	79.46	47.73	41.34

Values are expressed as mean ± SD (n=3)

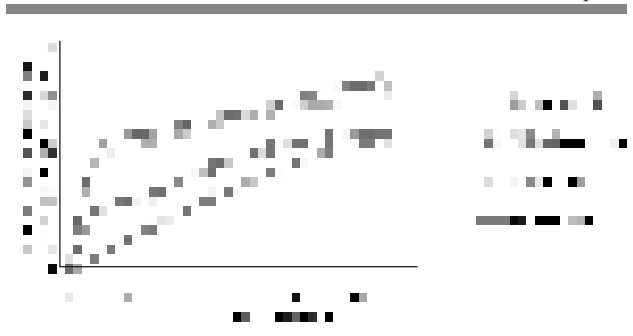

Figure 1: *Comparison of % radical scavenging between ascorbic acid and different extracts of O. sanctum*

Among the three different extracts, methanol extract was found to have the IC_{50} value of 47.73 µg/mL, very close to standard ascorbic acid (41.34 µg/mL).

Conclusion

In the present investigation, extractions from *Ocimum sanctum* leaves powder has been carried in hexane, chloroform and methanol solvents. Phytochemical screening of the extracts revealed the presence of alkaloids, flavonoids, tannins, glycosides, polyphenols, terpenoids, tannins and steroids. The plant possesses a high amount of total phenolic and total flavonoid contents. DPPH scavenging activity showed that the plant possesses high antioxidant properties. Among all three extracts, the IC_{50} value of methanol extract was the lowest and closest (47.73 µg/mL) to that of standard ascorbic acid (41.34 µg/mL). The significant potency of the extracts of *O.*

sanctum leaves as antioxidant agents may be due to the presence of high phenolic and flavonoid contents.

Acknowledgements

The authors are thankful to the Department of Chemistry, Amrit Campus, Tribhuvan University and Department of Forest and Soil Conservation, Babarmahal, Kathmandu for providing the laboratory facility.

References

1. K. Selvam, R. Rajinikanth, M. Govarthanan, A. Paul, T. Selvankumar and A. Sengottaiyan, Antioxidant potential and secondary metabolites in *Ocimum sanctum L*. at various habitats, *Journal of Medicinal Plants Research,* 2013, **7**(12), 706-712. (DOI: 10.5897/JMPR11.446).
2. S. I. Vidhani, V. G. Vyas, H. J. Parmar, V. M. Bhalani, M. M. Hossan, A. Gaber and B. A. Golakiya, Evaluation of some chemical composition, minerals fatty acid profiles, antioxidant and antimicrobial activities of Tulsi (*Ocimum sanctum*) from India, *American Journal of Food Science and Technology,* 2016, **4**(2), 52-57. (DOI: 10.12691/ajfst-4-2-5).
3. B. Joshi, G. P. Sah, B. B. Basnet, M. R. Bhatt, D. Sharma, K. Subedi, J. Pandey and R. Malla, Phytochemical extraction and antimicrobial properties of different medicinal plants: *Ocimum sanctum* (Tulsi), *Eugenia caryophyllata* (Clove), *Achyranthes bidentata* (Datiwan) and *Azadirachta indica* (Neem), *Journal of Microbiology and Antimicrobials,* 2011, **3**(1), 1-7.
4. G. Nahak, R. C. Mishra and R. K. Sahu, Phytochemical investigation and in vitro antioxidant evaluation of some *Ocimum species*, *Journal of Pharmacy Research*, 2011, **4**(7), 2340-2343.
5. P. Prakash and N. Gupta, Therapeutic uses of *Ocimum sanctum Linn* (Tulsi) with a note on eugenol and its pharmacological actions: a short review, *Indian Journal of Physiology and Pharmacology*, 2005, **49**(2), 125–131.
6. M. K. Khosla, Sacred tulsi (*Ocimum sanctum*) in traditional medicine and pharmacology, *Ancient Science of Life,* 1995, **5**(1), 53–61.
7. M. M. Cohen, Tulsi-*Ocimum sanctum*: A herb for all reasons, *Journal of Ayurveda Integrative Medicine,* 2014, **5**(4), 251-259.
8. V. Gradinariu, O. Cioanca, L. Hritcu, A. Trifan, E. Gille and M. Hancianu, Comparative efficacy of *Ocimum sanctum L.* and *Ocimum basilicum L.* essential oils against amyloid beta (1-42)-induced anxiety and depression in laboratory rats, *Phytochemistry,* 2015, **14**(4), 567-575.
9. P. Pattanayak, P. Behera, D. Das and S. K. Panda, *Ocimum sanctum Linn.* A reservoir plant for therapeutic applications: An overview, *Pharmacognosy Reviews,* 2010, **4**(7), 95-105. (DOI: 10.4103/0973-7847.65323).
10. B. Joseph and V. M. Nair, Ethanopharmacological and phytochemical aspects of *Ocimum sanctum Linn*-The Elixir of Life, *British Journal Pharmaceutical Research*, 2013, **3**(2), 273-292.
11. S. E. Lee, H. J. Hwang, J.-S. Ha, H.-S. Jeong and J. H. Kim, Screening of medicinal plant extracts for antioxidant activity, *Life Sciences*, 2003, **73**(2), 167-179.
12. A. J. Harborne, *Phytochemical methods a guide to modern techniques of plant analysis,* Springer Science & Business Media, UK, 1998.
13. B. Subba, A. Sharma and A. Budhathoki, Assessment of phytochemical content, antioxidant and antibacterial activities of three medicinal plants of Nepal, *Journal of Medicinal Plants Research,* 2016, **10**(45), 829-837. (DOI:10.5897/JMPR2016.6269).
14. F. L. Hakkim, G. Arivazhagan and R. Boopathy, Antioxidant property of selected *Ocimum species* and their secondary metabolite content, J*ournal of Medicinal Plants Research*, 2008, **2**(9), 250-257.
15. D. Gajula, M. Verghese, J. Boateng, L. T. Walker, L. Shackefold, S. R. Mentreddy and S. Cedric, Determination of total phenolics, flavonoids and antioxidant and chemopreventive potential of basil (*Ocimum basilicum L*. and *Ocimum tenuiflorum L*.), *International Journal of Cancer Research*, 2009, **5**(4), 130-143, (DOI: 10.3923/ijcr.2009.130.143).
16. H. Hossain, I. A. Jahan, H. S. Islam, D. S. Kanti, H. Arpona and A. Arif, Phytochemical screening and anti-nociceptive properties of the ethanolic

leaf extract of *Trema Cannabina Lour, Advanced Pharmaceutical Bulletin,* 2013, **3**(1), 103-108. (http://dx.doi.org/10.5681/apb.2013.017).

17. M. A. Hossain, K. A. S. AL-Raqmi, Z. H. AL-Mijizy, A. M. Weli and Q. Al-Riyami, Study of total phenol, flavonoids contents and phytochemical screening of various leaves crude extracts of locally grown *Thymus vulgaris*, A*sian Pacific Journal of Tropical Biomedicine,* 2013, **3**(9), 705–710. (DOI: 10.1016/S2221-1691(13)60142-2).

18. M. A. Hossain, M. D. Shah, C. Gnanaraj and M. Iqbal, In vitro total phenolics, flavonoids contents and antioxidant activity of essential oil, various organic extracts from the leaves of tropical medicinal plant *Tetrastigma* from Sabah, *Asian Pacific Journal of Tropical Medicine*, 2011, **4**(9), 717-721.

19. S. Sankhalkar and V. Vernekar, Quantitative and qualitative analysis of phenolic and flavonoid content in *Moringa oleifera Lam* and *Ocimum tenuiflorum L., Pharmacognosy Research,* 2016, **8**(1), 16-21. (DOI: 10.4103/0974-8490.171095).

20. S. Chandra, S. Khan, B. Avula, H. Lata, M. H. Yang, M. A. Elsohly and I. A. Khan, Assessment of total phenolic and flavonoid content, antioxidant properties, and yield of aeroponically and conventionally grown leafy vegetables and fruit crops: A comparative study, *Evidenced Based Complementary and Alternative Medicine*, 2014, **14**, 1-9. (DOI.org/10.1155/2014/253875).

21. K. R. Sharma, S. K. Kalauni and S. Awale, Antioxidant, phytotoxic and antimicrobial activities of methanolic extract of *Bauhinia variegata* barks, J*ournal of Institute of Science and Technology,* 2015, **20**(2), 37-41.

22. N. A. Khalaf, A. K. Shakya, A. Al-Othman, Z. El-Agbar and H. Farah, Antioxidant activity of some common plants, *Turkish Journal of Biology,* 2008, **32**(1), 51-55.

23. C. A. Rice-Evans, N. J. Miller and G. Paganga, Structure-antioxidant activity relationships of flavonoids and phenolic acids, *Free Radical Biology and Medicine*, 1996, **20**(7), 933–956.

24. E. J. Lien, S. Ren, H.-H. Bui and R. Wang, Quantitative structure-activity relationship analysis of phenolic antioxidants, *Free Radical Biology and Medicine*, 1999, **26**(3), 285-294. (DOI:285–294. 10.1016/S0891-5849(98)00190-7).

25. S. Kaur, Study of total phenolic and flavonoid content, antioxidant activity and antimicrobial properties of medicinal plants, *Journal of Microbiology and Experimentation,* 2014, **1**(1), 1-6.

26. S. Guleria, A. K. Tiku, G. Singh, A. Koul, S. Gupta and S. Rana, In-vitro antioxidant activity and phenolic contents in methanol extracts from medicinal plants, *Journal of Plant Biochemistry and Biotechnology,* 2013, **2**(1), 9-15. (DOI: 10.1007/s13562-012-0105-6).

27. B. Piyali, M. Poiyandarshini, M. Sayan and V. A. Swarup, Assessment of antioxidant, anti-inflammatory, anti-cholinesterase and cytotoxic activities of Tulsi leaves, *Advances in Pharmacology and Toxicology*, 2014, **15**(1), 19-29.

28. A. Bhattacharya, A. Agarwal, N. Sharma and J. Cheema, Evaluation of anti-oxidative constituents of three species of *Ocimum, International Journal of Life Sciences*, 2014, **8**(5), 14-17. (DOI: dx.doi.org/10.3126/ijls.v8i5.11858).

29. J. V. Vastrad, G. Goudav, S. A. Byadgi, R. D. Devi and R. Kotur, Identification of bioactive components in leaf extracts of *Aloe-vera* and tulasi, *Journal of Medicinal Plants Research,* 2015, **9**(28), 764-770.

30. E. Mitra, D. Ghosh, A. K. Ghosh, A. Basu and D. Bandyopadhay, Aqueous Tulsi leaf (*Ocimum sanctum*) extract possesses antioxidant properties and protects against Cadmium-induced oxidative stress in rat heart, *Journal of Pharmacy and Pharmaceutical Science*, 2014, **6**(1), 500-513.

31. J. Samson, R. Sheeladevi and R. Ravinandan, Oxidative stress in brain and antioxidant activity of *Ocimum sanctum* in noise exposure, *Neuro Toxicology,* 2007, **28**, 679-685.

32. M. A. Kelm, M. G. Nair, G. M. Strasburg and D. L. Dewitt, Antioxidant and cyclooxygenase inhibitory phenolic compounds from *Ocimum sanctum Linn*., *Phytomedicine*, 2000, **7**(1), 7-13.

JNCS
Journal of Nepal Chemical Society December 2019, Vol. 40, 36-43
ISSN: 2091-0304 (print)
DOI: https://doi.org:10.3126/jncs.v40i0.27276
RESEARCH ARTICLE

Physico-chemical Parameterization and Determination of Effect of Tributaries on Enhancement of Pollutants in Bagmati River

Mandira Pradhananga Adhikari*, Madhav Raj Neupane, Madan Kafle

Central Department of Chemistry, Tribhuvan University, Kirtipur, Nepal

*Corresponding E-mail:mandira43@hotmail.com

(Received: Sept. 18, 2019; Revised: Dec. 21, 2019 & Accepted: Dec. 22, 2019)

Abstract

Water quality parameterization is a great concern because chemical contaminants and microbiological impurities including pathogenic bacteria may pose a health risk and unfit for its domestic use. Alkalinity, pH, conductivity, chlorine demand, turbidity, and ammonia were measured to characterize the water quality of the Bagmati River. The effect of tributaries on Bagmati River was determined by sampling water from five different sites such as Pashupati (B-1), Shankhamul (B-2), Kupondol (B-1), Balkhu (B-4), and Jalbinayek (B-5) sites. The water samples B-2, B-3, B-4 and B-5 were less turbid but black in color while water sample B-1 was more turbid but grey in color. The pH of water samples ranged from 6.7 to 7.3. The alkalinity, conductivity and chlorine demand were 60 ppm, 95.7 μs and, 5.44 ppm, respectively for B-1 sample and increased almost continuously from B-2 to B-5 sample. The alkalinity was 360 ppm, conductivity was 862 μs and chlorine demand was 23.7 ppm for the last sample (B-5). The concentration of ammonia in the B-1 sample was only 0.0625 ppm whereas it was 3.32 ppm in the B-5 sample. The enhancement of chlorine demand and concentration of ammonia attributed that tributary and local effluent loaded extremely high levels of pollutants into the Bagmati River which might include pathogenic microorganisms. The random chance of some parameters like pH, conductivity, ammonia, turbidity along the Bagmati River indicates the impacts of different tributaries on Bagmati River. The chorine demand showed a positive correlation with conductivity, alkalinity and ammonia while the negative correlation with turbidity. This revealed that the conductive alkaline pollutants consumed more chlorine than colloidal particles. From the study it is considered that the Bagmati River water contains natural as well as anthropogenic pollutants which is extremely hazardous not only to the people using river water but also for the living organism rely on the river.

Keywords: Alkalinity, chlorine demand, river water, turbidity, water pollution.

Introduction

The Bagmati originates from the Shivapuri Hills and flows through the Kathmandu valley. It is enormous important culturally, historically, biologically, and geologically. It is one of the holy rivers of Hindu. The river passes by the holy Pashupatinath and many other culturally important small temples. Culturally and historically, there are no alternatives to river water for the people in Kathmandu and other places of Nepal. People take bath, take water in their hands for paying gods and homage to their ancestors and bring small quantities of water to their home for use in rituals. It provides habitat and food for many living organisms. In addition, some people living near the bank are still using Bagmati River water for bathing, washing vegetables, utensils and clothing, in agriculture, industry and irrigation [1-3].

Such an immense important Bagmati River is suffering from an enormously high level of pollutants [4]. Many residents in Kathmandu valley are discharging untreated sewage, personal garbage and industrial waste into the river. The degradation of water quality and ecology of Bagmati River threaten not only human, but also living organisms rely on the river. The consumption of contaminated water causes a variety of water-borne diseases like cholera, dysentery, diarrhea, typhoid etc [1,2,5]. WHO estimates that about 3.4 million people die every year as a result of water-

related diseases in developing countries [6]. In Nepal, many children up to 4 years die from water-borne diseases [7,8]. Although numerous campaigns were conducted to clean the Bagmati River, the stinking smell and blackish color of the Bagmati River water still increasing. This indicates that the determination of source of pollutants and the measurement of pollutants level along the Bagmati River is decidedly important to rectify the problem and implement the action effectively. The measurement of pollutant levels of water after mixing the tributaries will be the one step to rectify the role of tributaries on Bagmati River water pollution.

Water quality can be characterized by physico-chemically and biologically [9]. Some of the commonly used Physico-chemical parameters are pH, alkalinity, conductivity, ammonia, turbidity, dissolved oxygen (DO), biological oxygen demand (BOD), chemical oxygen demand (COD) etc. The measurement and comparison of these parameters with water quality standards can determine the quality and usability of water. High pH of river water is not suitable for life whereas low pH is especially harmful to immature fish and insects and also responsible for corrosion [5]. The highly alkaline water is usually unpalatable [10-12]. Conductivity relates to the salinity (total dissolved salt) and total dissolved solids, both of which affect water quality and aquatic life [11]. The decomposition of organic waste matter, gas exchange with the atmosphere, forest fires, animal and human waste and nitrogen fixation processes are the natural sources of ammonia. Ammonia is an important nutrient for plants and algae that reside in river water. However, the elevated concentration of ammonia is toxic to aquatic life. The concentrations ranging from 0.53 to 22.8 mg/L are toxic to freshwater organisms [9].

Materials and Methods

Samples were collected from five different sampling sites along the Bagmati River in September. This is the last month of the rainy season. Therefore, water level and velocity of water flow were high during the sampling time. The sampling sites were selected to determine the effect of the tributaries on the enhancement of the pollutant level including pathogen in the Bagmati River. The pretreated plastic bottles were used to collect samples from about 1 feet depth in each sampling site. The samples were collected randomly on different days. Therefore, the temporal variation of the water quality parameter of Bagmati river water was not considered in this study. The temperature and pH of water samples were measured directly on the spot using thermometer and pH meter (CE, pH600), respectively. The collected samples were brought into the laboratory and stored in a cool place and analyzed as soon as possible. Each sample was analyzed at least three times for each parameter.

Physico-chemical parameters were analyzed by using the standard method and using the instrument. The alkalinity, hardness were determined by titrimetric methods. Chlorine demand is measured by implementing the starch-iodine method. The concentration of ammonia was determined by the using Phenate method. The turbidity and conductivity of water samples were measured using Nephelometer and conductivity meter, respectively.

Results and Discussion

The present study was focused to measure the water quality parameter along the river to determine the effect of tributaries on the enhancement of contaminants on the Bagmati River inside the Kathmandu valley. As shown in Figure 1, water flows from Pashupati, Shankhmul, Kupondol, Balkhu sites to the Jalbinayak site. Along with the flow of water, it collects water from the Manahara, Dhobikhola, Bishnumati, and Balkhukhola rivers. The sampling covered about 12 kilometers length of the Bagmati River ranging from Pashupati to Jalbinayak. The sampling sites (5 sites) were selected in such a way that the effect of tributaries on the water quality of the Bagmati River could be determined. The sampling sites of Bagmati River were represented by the black spot in the Figure 1. The water samples were represented as B-1, B-2, B-3, B-4 and B-5 for Pashupati, Shankhamul, Kupondol, Balkhu and Jalbinayak water samples respectively. The B-1 was considering as the water sample before loading pollutants from the tributaries of Kathmandu valley. The samples B-2, B-3, B-4 and B-5 determine the effects of Monohara, Dhobikhola, Bishnumati and Balkhukhola rivers on Bagmati River, respectively. Three samples were collected from B-1 and B-2 at different times. The analytical results showed the almost same value for different parameters. Therefore, the influence of time on the water quality parameter of Bagmati River water was not considered in this study. The samples were collected randomly at different

sampling sites on different days.

Figure1: *Sampling sites of Bagmati River*

Physico-chemical parameterizations of river water sample

The physical parameters such as temperature, color, pH, and conductivity of five different samples were shown in Table 1. Temperature was 19 ˚C in the case of B-1, B-2, and B-3 samples, and it was 18 ˚C in the case of B-4 and B-5. Some of the water quality parameters are influenced by the temperature of the water. High temperature decreases the oxygen level in the water which is favorable for the growth of bacteria at the anaerobic condition. This may enhance the chlorine demand. Similarly, the temperature also effects on physical properties such as pH, conductivity, alkalinity etc. [6]. In this study, the samples were collected randomly from different observation sites. The observed temperatures of all samples were almost equal. Therefore it was considered that all samples had a similar environmental condition and the temperature difference had a negligible effect on the measured parameters of the samples. The color of water indicates the quality of water. It is greatly influenced by the suspended and dissolved particles as well as ambient conditions in which water is present. From the color of water, the physical, chemical and bacteriological conditions can be determined. The color of water sample the B-1 was grey in color while all other samples were black (Table 1) although the color of the B-3 sample was greyish black. The black color of river water is an indication of the presence of anthropogenic pollutants.

Bagmati River water flows continuously along with the sampling sites from B-1, to B-2, B-3, B-4 and B-5. During its flow it collects water from different tributaries, hence, the water quality of Bagmati River water is influenced by the water quality of tributaries. Figure 2 shows photographs of water samples. The photograph shows that the B-1 sample was turbid and purely grey in color but the other samples were appeared black, dirty and unhealthy in nature. Figure 2 shows that the color and transparency were different for the different water samples. The sample B-2 was transparent and black in color. The sample B-3 was more turbid and black color was less pronounced as compared to sample B-2. Similarly sample B-4 appeared to be transparent but suspended particles were clearly observed in this sample. The sample B-5 was blackish in color. The photograph showed that B-1 sample mostly contains fine particles of clay and the sample B-3 contains clay particles with pollutants. However, other samples might contain pollutants such as dissolved organic matter, decaying sewage, nasty debris, etc.rather than clay particles [9]. The variation of color and transparency of sample water from upstream (Pashupati) to downstream (Jalbinayak)

Table 1: *Physical parameterization of water samples*

Water sample	Temperature (˚C)	Color	pH	Conductivity (µS/cm)
B-1	19	Grey	7.3	95.7
B-2	19	Black	7.5	522
B-3	19	Greyish Black	7.1	582
B-4	18	Black	6.9	507
B-5	18	Black	6.7	862

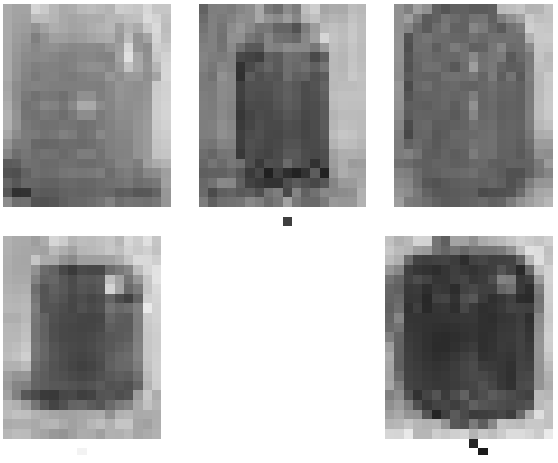

Figure 2*: Photograph of water sample of (a) Pashupati (B-1), (b) Shankhamul (B-2), (c) Kupondol (B-3), (d) Balkhu (B-4), and (e) Jalbinayak (B-5).*

revealed that there was a great influence of tributaries on water quality parameters of Bagmati River.

The concentration of hydrogen ion [H^+] in water is represented by pH. The water with a low pH (<6.5) could be soft and corrosive while water with a high pH (> 8.5) could be hard and corrosive in nature [13,14]. The pH of different water samples was tabulated in Table 1. The pH was ranged from 6.7 to 7.5 which falls within the range of natural water (6.5 to 8.5) [14]. The samples B-4 and B-5 were slightly acidic while other samples were slightly basic in nature. The pH revealed that water samples might contain weak electrolytes. Conductivity is related to the concentration of ions present in the water. The observed conductivity was 95.7, 522, 582, 507 and 862µS/cm for the samples B-1, B-2, B-3, B-4 and the B-5, respectively. The highest conductivity was observed in the case of B-5.The conductivity of water samples (B-2, B-3 and B-4) were five times and B-5 sample was almost nine times higher than that of B-1 samples. The drastic enhancement of conductivity attributed that the tributaries and/or local outlet loaded conducting pollutants in the Bagmati River.

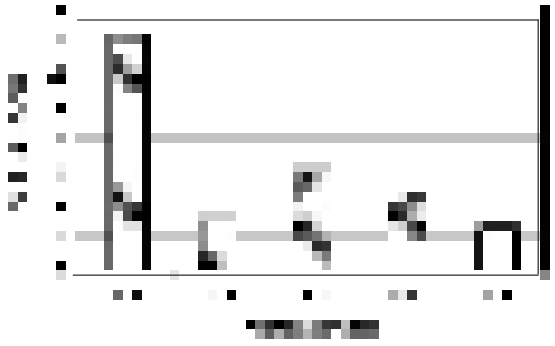

Figure 3: *Turbidity of different water samples of Bagmati River*

Turbidity is another important parameter that indicates the presence of insoluble particulate matter. Turbidity in natural water is caused by clay, silt, industrial wastes, organic matter, sewage, phytoplankton and other microscopic organisms. Excessive turbidity in river water is harmful to fish and aquatic animals however, it is suitable for food and shelter for pathogens which enhances the growth of pathogens [15]. The turbidity was 14.2, 3.2, 6.2, 4.48 and 2.64 NTU for sample B-1, B-2, B-3, B-4 and B-5, respectively (Figure 3). The maximum turbidity was observed in the case of a water sample from the Pashupati site (B-1) i.e., before mixing of tributaries of Kathmandu valley. The measured turbidity of different sample water was comparable to the transparency revealed by the photograph (Figure 2). The photograph shows that the water samples B-2, B-4 and B-5 were more transparent that the water samples B-1 and B-3. The data attributed that the dark polluted water samples contains soluble pollutants whereas grey water samples contain insoluble suspended particles. From the results, it is considered that the less polluted grey water contains clay, silt etc. but polluted black water contain soluble conductive pollutants especially B-5.

Alkalinity protects water to become acidic. Hence, it is important for fish and aquatic life. The pH of the water will change when the buffering capacity of water is decreased. Water with low levels of alkalinity (<155 ppm) has the low buffering capacity, hence, is more likely to be corrosive. The alkalinity of natural water is determined by dissolving the soil, limestone or dolomite minerals in the water [12,14]. Figure 4 shows that the alkalinity of water samples B-1 was low (50 ppm) but that of B-5 was more than 7 times higher (360 ppm). It was also found that alkalinity was increased continuously down flow from B-1 to B-5 sampling sites. Alkalinity mainly determines the concentration of carbonate, bicarbonate and hydroxyl ion in water. The alkalinity of the water sample reveals that water sample B-1 contains a less amount of carbonate and bicarbonate ions whereas concentrations of these ions were increased continuously by the tributaries in other samples. The alkalinity observed in this study was lower than that reported by previous studies (875 ppm [16] and 494 ppm [4]). The sample was collected in September. During this time the water level and flow velocity of Bagmati River were high. The lower value of alkalinity in this study may be due to the dilution of river water by continuous rainfall or due to the presence of anthropogenic pollutants rather than natural soil and minerals.

Ammonia gas is extremely soluble in water. It is found either as ammonium hydroxide or ammonium ion in the water. When the pH of the water is less than 7 the ammonia is present as the ammonium ion and as the pH of the water is higher than 7 it is present as the ammonium hydroxide [10]. Whatever may be the form of the presence of ammonia in natural water is considered as indicative of sanitary pollution. Although, it is widely used and common in

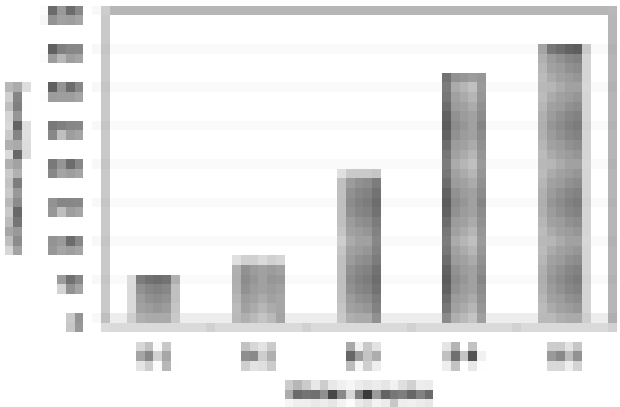

Figure 4: *Alkalinity of different water samples of Bagmati River*

our society, it can be both hazardous and caustic. It can block the transfer of oxygen in the gills of fish. The safe level of ammonia is between 0.02 and 0.4 in marine environments [7,17]. The concentration of ammonia observed for the different water samples was plotted in Figure 5. The ammonia concentration was only 0.0632 ppm in the case of the B-1 sample which was within the limit (0.2 ppm) for the surface water as recommended by WHO [17]. However, the concentration of ammonia was extremely high for the other samples. It was 2.3, 1.84, 1.63 and 3.32 ppm for B-2, B-3, B-4 and B-5, respectively. The concentration of ammonia in B-2 and B-3 was very high as compared to that in the case of sample B-1but it was lower than that of the sample of B-2. The photograph (Figure 2) and turbidity (Figure3) of water samples B-3 indicated that the sample contains clay particles in addition to another pollutant. The decrease in the concentration of ammonia in this sample may be due to the mixing of the tributaries such as Dhobikhola and Bishnumati containing less amount of municipal waste (sanitary pollution). Kafle (2016) reported that the Bagmati River water at Balkhu sites was more polluted than the Dhobikhola and Bishnumati river water [16]. Milner et.al. (2015) reported that the municipal waste and sewage entering the river drastically enhances the concentration of ammonia in Kathmandu valley especially near the Chovar (nearby B-5 sites of this study) [1]. The concentration of ammonia in the B-5 sample was highest and it was nearly two times that in the B-4 sample. It reveals that Blkhukhola loaded a high concentration of ammonia in the Bagmati River.

The difference between the amount of chlorine added and chlorine remaining (residual chlorine) after a certain time in the water sample is called chlorine demand. It depends on the chlorine dosage, contact time, temperature, pH, nature, and amount of impurities in water. Chlorine demand was measured by maintaining a chlorine dose of 40 ppm, contact time of 35 minutes, the temperature at 18-19 and pH of 6-7.

Figure 5: *Ammonia concentration of different water samples*

Figure 6 showed that the chlorine demand of B-1sample was low (5.44 ppm) and continuously increased from B-2 (11 ppm) to B-5 (23.7 ppm) samples. The chlorine demand attributes the presence of inorganic and organic contaminants with pathogenic microorganisms in the water [4,13]. Adhikari and Sah (2017) observed the chlorine demand as high as 12 ppm, 20 ppm and 22 ppm for the Bagmati River (Pashupati site), Dhobikhola and Bishnumati, respectively. Increasing the chlorine demand along the Bagmati River revealed that tributaries and local effluent enhanced the pathogenic microorganism excessively in addition to chemical pollutants.

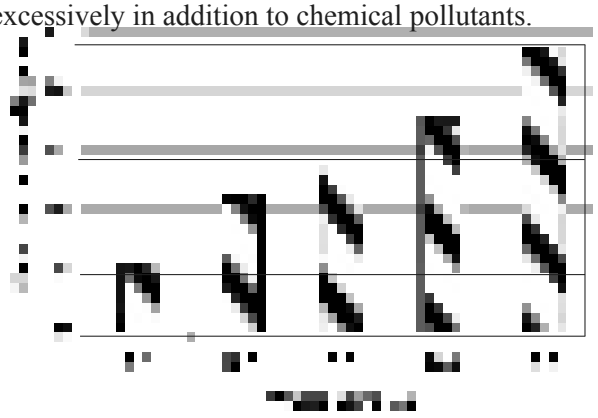

Figure 6: *Chlorine demand of different water samples of the Bagmati River*

Correlation curves

Correlation is a statistical measure that indicates the extent to which two or more variables fluctuate together. A positive correlation indicates the extent to which those variables increase or decrease in parallel; a negative correlation indicates the extent to which one variable increases as the other decreases. The dependency of chlorine demand on different parameters such as ammonia, turbidity, alkalinity, and conductivity was shown below in Figure 7, 8, 9 and 10 respectively. Figure 7 shows the positive correlation between chlorine demand and concentration of ammonia on Bagmati River water. The correlation coefficient (r^2=0.74) revealed the positive impact of ammonia concentration on chlorine demand for a given sample of water. The results attribute that the tributaries containing municipal waste loaded ammonia and pathogenic microorganism in the Bagmati River that excessively enhanced the chlorine demand.

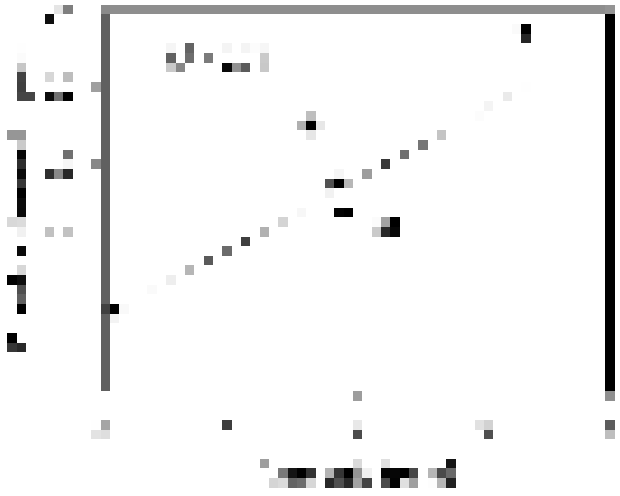

Figure 7: *Correlation curve between chlorine demand and ammonia*

Figure 8 shows the dependency of chlorine demand on the turbidity of different water samples in the Bagmati River. It evinced that there was a negative correlation between these variables i.e., the dependency of turbidity on chlorine demands for a given sample of Bagmati River was poor. The results attribute that the high consumption of chlorine by water sample was due to the presence of soluble impurities rather than the colloidal particles in the river water.

Figure 9 shows the dependency of chlorine demand on the alkalinity of different samples of water in the Bagmati River. There was a positive correlation (r^2=0.86) between the variables and the correlation coefficient close to the proximity of unity.

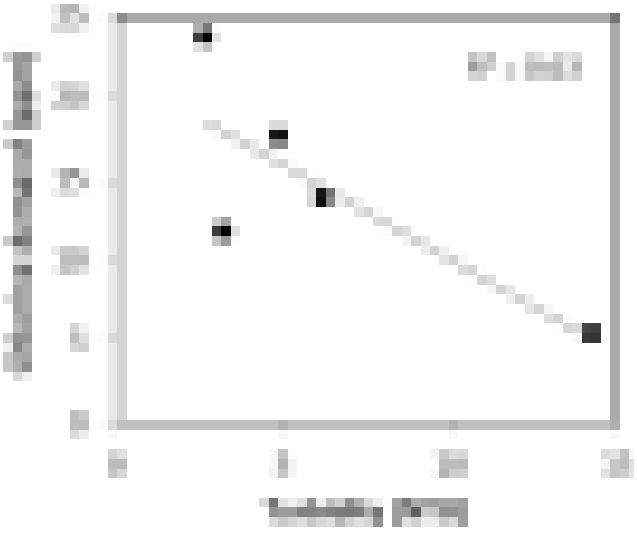

Figure 8: *Correlation curve between chlorine demand and turbidity*

Both these parameters were found to be increasing along the Bagmati River going down from Pashupati to Jalbinayak sites. It attributes that in addition to ammonia the alkalinity includes other pollutants that also consumed chlorine.

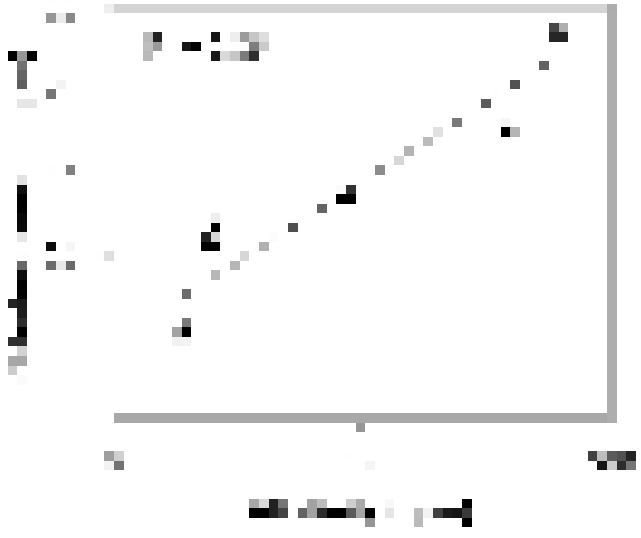

Figure 9: *Correlation curve between chlorine demand and alkalinity*

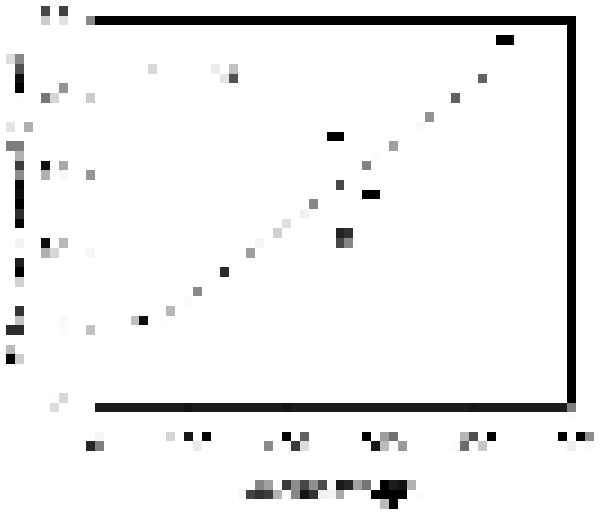

Figure 10: *Correlation curve between chlorine demand and conductivity*

Figure 10 shows the correlation between chlorine demand and conductivity of Bagmati River water. It showed that there was a positive correlation between the variables with a better correlation coefficient (r^2=0.84) which was more close to the proximity of unity. Both these parameters were found to be increasing in all sampling sites going down from the Pashupati site to Jalbinayak. It inferred that in additions to pathogenic microorganism the conductive ions like ammonia, chlorides, sulfides, carbonates, bicarbonates present in the river water were responsible for high chlorine demand.

Conclusion

The water samples were collected from five different sites of the Bagmati River to understand the effect of tributaries on the Bagmati River water system. As expected all measured parameters such as pH, alkalinity, conductivity, ammonia and chlorine demands were very low at the Pashupati site and very high at Jalbinayak site. The alkalinity and chlorine demand were continuously enhanced along the Bagmati River from Pashupati to Jalbinayak sites. The conductivity and ammonia were very low at Pashupati site and they were enhanced randomly along the downstream from Shankhamul to Jalbinayak. In addition to these parameters, pH, color and turbidity of water samples attribute that the different tributaries had different impacts on the water quality of Bagmati River. All the measured parameters indicated that the B-5 sample contained an extremely high level of pollutants as compared to the B-1 sample. The extremely high concentration of ammonia and chlorine demand and color of the water samples attributed that effluent from Balkhukhola loaded extremely high levels of pathogenic microorganism in addition to chemical pollutants. The correlation curves attributed that the contribution of ammonia and alkalinity on chlorine demand was positive while that of turbidity was negative. It showed that the municipal waste containing soluble salt including ammonia consumed more chlorine than solid particles including clay, soil etc. Hence, it is considered that the tributaries are highly responsible for enhancement of precarious pollutants in river water, which is extremely hazardous for all living organisms, relies on the Bagmati River. A more detail study is necessary to understand the contribution of different tributaries in the enhancement of types and amount of pollutants in the Bagmati River.

References

1. C. Milner, H. Basnet, S. Gurung, R. Maharjan, T. Neupane, D. N. Shah, B. M. Shakya, R. Tachamo, R. D. Shah, and S. Vaidya, Bagmati River Expedition 2015: A baseline study along the length of the Bagmati River in Nepal to gather data on physical, chemical, and biological indicators of water quality and pollution; and document human-river interaction, *Nepal River Conservation Trust and Biosphere Association, Kathmandu, Nepal*, 2015.
2. A. N. C Wolfe, Microbial contamination in the Kathmandu valley drinking water supply and Bagmati river. *Master of Engineering Thesis*. Civil and Environmental Engineering Department, Massachusetis Institute of Technology, USA, 2000.
3. M. Sagara and R. Lipscomb, *Study of filtration for point-of-use drinking water treatment in Nepal,* Veirginia Polytechnic Institute and State University, Falls Church, Virginia, 2003.
4. M. P. Adhikari and M. K. Sah, Chlorine demand and water pollutants of pond and river water, *Journal of Nepal Chemical Society*, 2017, **36**, 39-48.
5. M. S. Khadka, The groundwater quality situation in alluvial aquifers of the Kathmandu valley, Nepal, *AGSO Journal of Australian Geology &*

Geophysics, 1993, **14**, 207-211.

6. WHO, *Guidelines for Drinking Water Quality*, 3rd Ed, World Health Organization, 2004, Geneva.
7. S. Sharma, R. M. Bajracharya, B. K. Sitaula and J. Merz, Water quality in the central Himalaya, *Current Science,* 2005, **89**(5), 774-786.
8. C. K. Sharma, Chemical pollution of the soil and groundwater in the Kingdom of Nepal, *Ground Monit Manage*, 1990, **173,** 391-397.
9. M. O. Ben-Coker, Effect of Slaughter house discharge on Water Quality of Ikpoda River, Nigeria, *Bioscience Technology,* 2012, **2**(1), 1-4.
10. M. K. Ladipo, V. O. Ajibola and S. J. Oniye, Seasonal variations in physicohemical properties of water in some selected locations of the Lagos lagoon, *Science World Journal*, 2011, **6**(4), 5-11.
11. Ch. Leelavathi, U. K. Sainath, and A. K. Rabbni, Physicochemical characterization of ground water of Autonagar, Vijayawada, Krishna district, *International Journal of Engineering Development and Research (IJEDR),* 2016, **4**(2), 1324-1328.
12. N. K. Koju, T. Prasai, S. Shrestha and P. Raut, Drinking water quality of Kathmandu valley, *Nepal Journal of Science and Technology,* 2014, **15**(1), 115-120.
13. O. C. Modoi, C. Roba, Z. Torok and A. Ozunu, Environmental risks due to heavy metal pollution of water resulted from mining wastes in NW Romania, *Environmental Engineering and Management Journal,* 2014, **13**(9), 2325-2336.
14. World Health Organization, *International Standard for Drinking Water*, 1999, **5**, 3-6.
15. K. Cinque, M. A. Stevens, D. J. Roser, N. J. Ashbolt and R. Leeming, Assessing the health implications of turbidity and suspended particles in protected catchments, *Water Science Technology*, 2004, **50**(1), 205-210.
16. M. Kafle, Chemical characterization of water from different sources at different places, *M.Sc. Thesis,* Central Department of Chemistry, Tribhuvan University, Nepal, 2016, 41-47.
17. World Health Organization "*Guidelines for Drinking-Water Quality* 4th Ed, World Health Organization, 2011, 20 Avenue Appia, 1211 Geneva 27, Switzerland.

JNCS
Journal of Nepal Chemical Society December 2019, Vol. 40, 44-51
ISSN: 2091-0304 (print)
DOI: https://doi.org:10.3126/jncs.v40i0.27281
REVIEW ARTICLE

Removal of Fluoride from Aqueous Solution Using Biomass-Based Adsorbents: A Review

Ram Lochan Aryal[1], Bhoj Raj Poudel[1], Surendra K Gautam[2], Hari Paudyal[1], Megh Raj Pokhrel[1], Kedar Nath Ghimire[1*]

[1]*Central Department of Chemistry, Tribhuvan University, Kirtipur, Kathmandu, Nepal*

[2]*Department of Chemistry, Tri-Chandra Multiple Campus, Tribhuvan University, Kathmandu, Nepal*

[*]*Corresponding E- mail: knghimire@gmail.com*

(Received: Sept. 30, 2019; Revised: Dec. 23, 2019 & Accepted: Dec. 24, 2019)

Abstract

Various separation techniques have been successful for the removal of fluoride from aqueous solution. In this review, an extensive list of various biomass-based adsorbents from literature has been explored and their adsorption capacities under different conditions for the removal of fluoride available in the literature to date are presented. Several adsorbents have shown good adsorption capacities, however, modified biomass had shown excellent adsorption capacities compared to commercial materials. This paper reviews the fluoride uptake capacities of biomass materials and their modified forms as adsorbents against different experimental limits.

Keywords: Fluoride removal, aqueous solution, adsorption, treatment techniques

Introduction

In recent years, fluoride and fluorosis are globally common issues. Many developing countries have been facing problems with fluorosis. Due to natural and anthropogenic activities, the ground water becomes infected by fluorides [1,2]. Fluorine is one such pollutant that threatens living organisms especially humans [3]. Fluoride in drinking water has both merits and demerits to human health. Fluorides in trace amounts are essential for living beings for improvement of bone and dental enamel but higher concentration than 1.5 mg/L causes skeletal and dental fluorosis [4,5]. Industries such as glass and ceramic production, electroplating, brick and ironworks, semiconductor manufacturer and aluminum smelters produce fluoride contaminants that are discharged into water resources [6,7]. The effluents of these industries have higher fluoride concentration than natural waters, ranging from ten to thousands of mg/L [8]. According to the World Health Organization guidelines (WHO), the fluoride concentration in drinking water should not exceed 1.5 mg/L [9]. According to the Environmental Protection Agency (EPA) the maximum contaminant level of fluoride ions in drinking water is 4.0 ppm [10-12]. Excess fluoride is toxic but limited fluoride is necessary for calcification of dental enamel and bone formation. Excess intake of fluoride would lead to various diseases such as osteoporosis, arthritis, brittle bones, cancer, infertility in women, male sterility, brain damage, Alzheimer's syndrome, thyroid disorder and even death in severe cases [13,14]. About 40% of ingested fluoride is absorbed in the stomach as HF in aqueous solution. Prolonged and excessive intake of fluoride may result in serious health problems, fluorosis, which is characterized by mottling of teeth in mild cases and even the softening of bones and neurological damage in extreme cases [15]. It has been reported by several research groups that fluoride can interfere with DNA synthesis, carbohydrates, lipids, proteins, vitamins and mineral metabolism [16,17]. Besides, on short exposure, a high dose of fluoride affects kidney in both humans and animals [18]. Due to the toxic effects of fluoride on human health, tremendous research and development efforts are being put all over the developing countries for the removal of excess fluoride from drinking water. The removal of fluoride from aqueous solution is of prime concern. The methods for the removal of fluorides include chemical precipitation, ion exchange, membrane filtration, coagulation, electrochemical

treatments, and adsorption using activated carbon, carbon nanotubes, activated alumina and other natural and synthetic materials [19-24]. Most of these methods have high operational and maintenance costs, low fluoride removal capacities, lack of selectivity for fluoride, low selectivity in presence of other competing ions, generation of large volumes of sludge and complicated procedures in the treatment process. The widely used adsorption methods are activated carbon (AC), activated alumina and other synthetic materials. These techniques cannot work effectively due to the short service life of adsorbent, blockage problem, more cost, and sensitivity to the pH of the solution [25]. However, the adsorption method has been reported as one of the most effective, economical and eco-friendly of the various defluoridation techniques [26-30].

The biosorption process using biomass waste is an eco-friendly and easy method. It is the promising alternative adsorbent over the conventional adsorbents in the adsorption process.

Table 1: *The maximum Fluoride adsorption capacity of various raw adsorbents*

Adsorbents	Adsorption capacity Q_{max}(mg/g)	References
Citrus limonium leaf	1.4	[37]
Sweet lemon peel	0.744	[38]
Citrus limetta peel	1.915	[39]
Ultrafine Tea powder	1.26	[40]
Sandalwood leaf powder	4.66	[41]
Banana peel	8.15	[42]
Neem leaf powder	4.70	[43]
Tamarind fruit shell	1.53	[44]
Pipal leaves	0.80	[45]
Chitosan	1.39	[46]

The improved selectivity and sorption capacities of low-cost adsorbents derived from waste bio-mass loaded with metal ions have drawn the attention of many researchers in this field. There is an increasing trend of using biomass-based fluoride adsorbents, very few studies show that raw biomass has the ability of the adsorption of fluorides. But raw biomass can show very low adsorption capacity as compared to the commercial anion exchangers. The adsorption capacities of fluoride by some raw biomass and various commercial adsorbents are shown in Table 1 and Table 2 respectively.

Table 2: *The maximum fluoride adsorption capacity of various commercial adsorbents*

Adsorbents	Adsorption Capacity (mg/g)	References
La – loaded 200CT resin	25.46	[46]
Commercial READF resin	39.9	[47]
READF-(PG)	41.04	[47]
READF-(HG)	44.65	[47]
Amberlite 200 CT	9.5	[47]
Hydroxyapatite	28.57	[48]
Hardened alumina cement (ALC)	34.36	[49]

The low fluoride removal efficiency of raw biomass adsorbent compared to commercial adsorbents (as shown in Table 1 and Table 2) can be described due to the presence of negatively charged functional groups like amino, carboxyl, alcohols and esterson the surface of lignocellulosic materials of bio-mass, while positively charged functional group is limited[31-36].

Table 3: *The maximum fluoride adsorption capacity of various agricultural waste adsorbents*

Adsorbents	Modifying agent	Adsorption Capacity (mg/g)	References
Seaweed(M - CSW)	Zr(IV) – CSW La(III) – CSW	18.05 11.02	[20]
Tea powder	UTP –Zr	12.43	[40]
Orange waste gel	Saponification by loading Zr (IV)	22.8	[47]
Azollafiliculoides	HCl	11.2	[50]
Orange waste	Conc. Sulphuric acid, Zr(IV)	13.49	[51]
Porous corn starch	PS-Zr	25.41	[52]
Rice husk	$Al(OH)_3$ Coated	14.82	[53]
Rice straw	$KMnO_4$ Modified	15.77	[54]
Cotton cellulose	Iron loaded	18.43	[55]
Orange waste	La-SOJR	20.33	[56]
Orange waste	Sc – SOJR	11.4	[56]

Due to the lack of anion binding sites on the polymeric backbone, raw biomass-based adsorbents are found to be less effective in the removal of fluoride. In addition, the polymeric organic compounds (cellulose, lignocellulose and lignin) can leach into the aqueous solution so raw biomass-based adsorbent retards the adsorption capacity of fluoride anion. Thus, in order to increase the adsorption capacity of raw biomass, it is modified depending on the nature of pollutants, which is depicted in Table 3. The adsorption capacity of modified metal loaded adsorbents is found to be excellent due to its high binding sites, selectivity towards fluoride, large surface area and chemical stability.

Mechanism of fluoride adsorption

Bio waste consists of cellulose, hemicellulose, pectin, lignin, and polyoses. Pectin contains carboxyl groups as well as its methyl ester groups. The methyl ester portion of pectin can be converted into a carboxyl group by saponification reaction using $Ca(OH)_2$ or NaOH.

ions that enhances the ligand exchange mechanism with fluoride ions. The equilibrium pH of the solution is found to be increased after the adsorption of fluoride indicating that hydroxyl ions are released during adsorption, which further supports the mechanism mentioned below [56].

Figure 1: *Adapted mechanism of saponification followed by metal ion loading*

Thus, obtained saponified waste is further treated with rare earth metal ions. The carboxyl group and oxygen atom of the pyranose ring of pectic acid in the bio-waste form a stable five-membered chelate with the loaded metal ion. Due to hydroxyl ions as well as water molecules present in the coordination sphere of metal ions, it exhibits the ligand exchange mechanism with fluoride ions. Due to the steric hindrance of pectic acid, it is difficult to neutralize all the positive charges of the loaded metal ions with carboxyl groups. So, one or two positive charges of the loaded metal ion can be neutralized by carboxyl groups while other positive charges are neutralized by hydroxyl ions in the solution. The increase in the oxidation state of loaded metal ions increases the number of hydroxyl ions on the coordination spheres of the loaded metal

Factors affecting adsorption

Effect of pH

The pH of an aqueous solution is an important parameter for the adsorption at a solution adsorbent interface. The adsorption of fluoride increases with increasing pH and it is in the pH range of 2-4, because of the presence of more protonated sites in the ion exchange with F^-, then decreased with further increase in pH. The low adsorption at low pH (pH<2) may be due to the formation of weakly ionizable hydrofluoric acid (pK_a of HF = 3.2) or more than 95% of fluoride remains in the non-ionic form which is difficult to be adsorbed onto the anion exchange site of the adsorbent. The maximum fluoride adsorption was found to occur at pH 2-4. The decrease in fluoride adsorption at pH above 5 is due to the competition

Figure 2*: Adapted Mechanism on the adsorption and desorption of fluoride ion [56]*

of hydroxide ions for the adsorption sites because hydroxide ion concentration increases with the rise of pH of the solution [20,56,57].

Effect of initial fluoride concentration and adsorbent dose

The fluoride adsorption was found to be affected by both the adsorbent dose and the initial fluoride concentration. It was found that for a fixed fluoride concentration, the percentage of adsorption gradually increases with increasing adsorbent dose from 1.0mg/g to 5.0mg/g at 303 K. It might be due to the increased surface area and availability of more adsorption sites for fluoride adsorption. But for a constant dose, total available adsorption sites were limited so due to limited available adsorption sites, at higher concentrations of fluoride solution, there would be extreme competition among fluoride ions for the adsorption sites resulting in the decrease or constancy in adsorption [41]. Dehghani *et al.* [57] studied that fluoride adsorption increases with increasing adsorbent dose due to a greater extent of adsorption sites and more surface area.

Effect of contact time and kinetic study

The contact time of fluoride and adsorbent during adsorption is important in determining the kinetics of the process. The adsorption of fluoride depends on the contact time of the adsorbent and solution. Rapid uptake of fluoride and establishment of equilibrium in a short period of time denotes the efficiency of the adsorbents. In physical adsorption, most of the fluoride is adsorbed within a short interval of contact time. However, strong chemical bonding of the fluoride with adsorbents needs a longer contact time to reach equilibrium. In the beginning, the adsorption of fluoride increases rapidly with an increase in contact time then slows down and reaches equilibrium [57]. Khound *et al.* [41] studied the adsorption of fluoride with Sandalwood leaf powder (SLP) and the amount of adsorption increased with time upto 120 min. The rapid removal of fluoride at initial stages might be due to the vacant adsorption sites and it can adsorb more fluoride ions from the solution. The time-dependent adsorption data have been analyzed using three kinetic models, pseudo-first-order, pseudo-second-order and intraparticle diffusion model.

Adsorption isotherms

The adsorption isotherm determines how the fluoride molecules distribute between the liquid and solid phase during the adsorption process at an equilibrium state. Adsorption isotherm provides information about the effectiveness of the biomass for the removal of fluoride from contaminated water. The adsorption data were analyzed using Langmuir, Freundlich, Temkin, Redlich-Peterson and Sips isotherm [58]. Cai *et al.* [40] studied the Zr-loaded tea powder which is best fitted with the Langmuir isotherm model based on monolayer adsorption of adsorbate onto the adsorbent surface with the limited number of binding sites. Abu Bakar *et al*. [58] studied modified Palm Kernel Shell which is fitted with Freundlich, Redlich-Peterson and Sips isotherm.

Thermodynamic study

The thermodynamic feasibility and the spontaneity can be predicted by observing the effect of change of temperature upon the adsorption process and hence evaluating thermodynamic parameters; Gibb's free energy of adsorption (ΔG^0), enthalpy of adsorption (ΔH^0) & entropy of adsorption (ΔS^0). An adsorption process is generally considered as physical if $\Delta H^0 <$ 84 KJ/mol and the chemical if ΔH^0 lies between 84 – 420 kJ/mol [59]. With the rise in temperature, fluoride adsorption increases if adsorption is endothermic and decreases for the exothermic process.

Effect of co-existing anions

Various anions in the solution can interfere with fluoride removal in the adsorption process. The percentage of fluoride removal decreases in the presence of PO^{4-} -, SO^{4-} -, NO^{3-} and Cl^- anions. The uptake capacity depends on ionic radii. Ionic radii of fluoride, chloride and nitrate ions are 0.133, 0.181 and 0.179 nm which is quite similar. The ionic radii and surface charge densities of phosphate (0.238 nm) and sulphate (0.230 nm) anions are larger than of fluoride ions and interfere with the adsorption of fluoride at the active site. Sometimes, the addition of competitor anions in water causes an increase in pH. This increases in pH value results in the decrease of fluoride adsorption [57].

Conclusion

This review has attempted to cover a wide range of adsorbents and treatment techniques which have been used for the removal of fluoride from aqueous solution. The capacity of treatment techniques and

their merits and limitations were highlighted. In addition to this, different types of adsorbent and their adsorption capacities were presented. It showed that chemically modified metal loaded biomass for the removal of pollutants has attracted the attention of more researchers. Chemically modified adsorbents enhance the adsorption capacity of fluoride due to a higher number of active binding sites, selective metal ion adsorption, rapid adsorption kinetics, improve structural stability and ion exchange capacity. These adsorbents were found to be efficient for fluoride removal, not only from the industries but also from the living organisms and the surrounding environment. The use of biomass adsorbents may contribute to the sustainability of the environment and water resources. Undoubtedly, biomass adsorbents provide a lot of promising benefits for commercial purposes in the future. More studies should be carried out for low-cost adsorption processes to enhance large scale use of biomass adsorbents. Low-cost adsorbents should be used to minimize cost and maximize heavy metal removal efficiency.

References

1. N. Sivarajasekar, T. Paramasivan, S. Muthusaravanan, P. Muthukumaran and S. Sivamani, Defluoridation of water using adsorbents – A concise review, *Journal of Environment and Biotechnology Research*, 2017, **6**, 186 – 198.
2. V. Sivasankar, S. Murugesh, S. Raj Kumar and A. Darchen, Cerium dispersed in carbon (CeDC) and its adsorption behaviour: A first example of tailored adsorbent for fluoride removal from drinking water, *Chemical Engineering Journal,* 2013, **214**, 45-54.
3. K. N. Ghimire, Effective removal of fluoride onto metal ions loaded orange waste, *Journal of Nepal Chemical Society,* 2011, **27**, 61-66. (https://doi.org/10.3126/ jncsv27i1.6660).
4. E. J. Reardon and Y. Wang, A limestone reactor for fluoride removal from waste waters, *Environmental Science &Technology*, 2000, **34**, 3247-3253.
5. P. Koilraj and S. Kannan, Aqueous fluoride removal using Zn-Cr layered double hydroxides and their polymeric composites: Batch and column studies, *Chemical Engineering Journal*, 2013, **234**, 406-415.
6. F. Shen, X. Chen, P. Gao, and G. Chen, Electrochemical removal of fluoride ions from industrial waste water, *Chemical Engineering Science*, 2003, **58,** 987-993.
7. D. L. Adhikari, R. L. Aryal, S. Bhattarai, S. K. Gautam and B. R. Poudel, Removal of chromium (VI) from aqueous solution using chemically modified sweet lime (*Citrus limetta*) peels as adsorbent, *Journal Nepal Chemical Society,* 2017, **36**, 82-95.
8. K. A. Krishnan and A. Haridas, Removal of phosphate from aqueous solutions and sewage using natural and surface modified coir pith, *Journal of Hazardous Materials*, 2008, **152** (2), 527-535.
9. K. N. Ghimire, K. Inoue, K. Makino and R. P. Dhakal, Adsorptive removal of arsenic and fluoride by using orange juice residue, *Electrometallurgy and Environmental Hydrometallurgy*, 2003, **2,** 1937-1950.
10. S. Ayoob, A. K. Gupta and V.T. Bhat, A conceptual overview on sustainable technologies for the defluoridation of drinking water, *Critical Reviews in Environmental Science and Technology*, 2008, **38**, 401-470.
11. N. Kawashima, R. Wadachi, H. Suda, T. Yeng and P. Parashes, Root canal medicaments, *International Dental Journal,* 2009, **59**, 5-11.
12. J M. Kauffman, Water fluoridation: A review of recent research and actions, *Journal of American Physicians and Surgeons,* 2005, **10**(2), 38.
13. R. Lavecchia, F. Medici, L. Piga, G. Rinaldi and A. Zuorro, Fluoride removal from water by adsorption on a high alumina content bauxite, *Chemical Engineering Transactions*, 2012, **26**, 225-230.
14. K. Abu Zeid and L. Elhatow, *Impact of fluoride content in drinking water*, In Arab Water Healthy Conference Egypt: Cairo, 2007.
15. R. C. Meenakshi Maheshwari, Fluoride in drinking water and its removal, *Journal of Hazardous Materials,* 2006, **137**, 456-463.
16. S. K. Jha, R. K. Singh, T. Damodaran, V. K. Mishra, D. K. Sharma, D. Rai, Fluoride in groundwater: toxicological exposure and remedies, *Journal of*

Toxicology and Environmental Health, Part B, 2013, **16**(1), 52-66.

17. X. Fan, D. J. Parker and M. D. Smith, Adsorption kinetics of fluoride on low cost materials, *Water Resources*, 2003, **37**, 4929-4937.

18. Y. Zhou, C. Yu and Y. Shan, Adsorption of fluoride from aqueous solution on La^{3+} impregnated cross-linked gelatin, *Separation and purification Technology*, 2004, **36**, 89-94.

19. M. Islam and R.K. Patel, Thermal activation of basic oxygen furnace slag and evaluation of its fluoride removal efficiency, *Chemical Engineering Journal*, 2011, **169**, 68-77.

20. H. Paudyal, B. Pangeni, K. Inoue, H. Kawakita, K. Ohto, K. N. Ghimire and S. Alam, Preparation of novel alginate based anion exchanger from *Ulva japonica* and its application for the removal of trace concentrations of fluoride from water, *Bioresource Technology*, 2013, **148**, 221-227.

21. N. Meunier, J. F. Blais and R. D. Tyagi, Selection of a natural sorbent to remove toxic metal from acidic leachate produced during soil decontamination, *Hydrometallurgy,* 2002, **67**, 19-30.

22. V. K. Gupta and T. A. Saleh, Sorption of pollutants by porous carbon, carbon nanotubes and fullerene– An overview, *Environmental Science & Pollution Research*, 2013, **20**, 2828-2843.

23. A. Shrestha, B. R. Poudel, M. Silwal and M. R. Pokhrel, Adsorptive removal of phosphate onto Iron loaded Litchi chinesis, *Journal of Institute of Science and Technology,* 2018, **23**, 81-87.

24. P. R. Bhatt, R. L. Aryal, B. R. Poudel, S. Bhattarai and S. K. Gautam, Adsorptive removal of Cr (VI) from aqueous solution onto charred sugarcane bagasse, *Journal Nepal Chemical Society*, 2018, **39**,62-69.

25. M. A. Barakat. New trends in removing heavy metals from industrial waste water, *Arabian Journal of Chemistry*, 2011, **4**(4), 361-77.

26. Z. Song, C. Z. Williams and R. G. Edyvean, Treatment of tannery waste water by chemical coagulation, *Desalination*, 2004, **164**(3), 249-59.

27. D. Rajkumar and K. Palanivelu, Electrochemical treatment of industrial Wastewater, *Journal of Hazardous Materials*, 2004, **113**, 123-129.

28. C. Namasivayam and D. Kavitha, Removal of Congo red from water by adsorption onto activated carbon prepared from coir pith, an agricultural solid waste, *Dyes and Pigments,* 2002, **54,** 47-58.

29. V. K. Gupta, T. A. Saleh, Sorption of pollutants by porous carbon, carbon nanotubes and fullerene-an overview, *Environmental Science and Pollution Research*, 2013, **20**(5), 2828-2843.

30. I. Ali, New generation adsorbents for water treatment, *Chemical Reviews,* 2012, **112**, 5073-5091.

31. K. Biswas, K. Gupta and U. C. Ghosh, Adsorption of fluoride by hydrous iron(III)-Tin(IV) bimetal mixed oxide from the aqueous solutions, *Chemical Engineering Journal*, 2009, **149**, 196-206.

32. F. Fu and Q. Wang. Removal of heavy metal ions from wastewaters: a review, *Journal of Environmental Management*, 2011, **92**(3), 407-18.

33. S. Kagne, S. Jagtap, P. Ddhawade, S. P. Kamble, S. Devotta and S. S. Rayalu, Hydrated cement: A promising adsorbent for the removal of fluoride from aqueous solution, *Journal of Hazardous Materials*, 2008, **154**, 88-95.

34. Y. Deng, D. K. Nordstrom and R. B. McCleskey, Fluoride geochemistry of thermal waters in Yellowstone National Park: I. Aqueous fluoride speciation, *Geochimica et Cosmochimica Acta*, 2011, **75**, 4476-4489.

35. M. R. Pokhrel, B. R. Poudel, R. L. Aryal, H. Paudyal and K. N. Ghimire, Removal and recovery of phosphate from water and wastewater using metal-loaded agricultural waste-based adsorbents: a review, *Journal of Institute of Science and Technology*, 2019, **24**(1), 77-89.

36. S. Karki, R. L. Aryal, S. R. Bhattrai, S. K. Gautam and B. R. Poudel, Adsorptive removal of Arsenic (III) from aqueous solution using chemically modified sweet lime (*Citrus limetta*) peels, *Journal of Nepal Chemical Society*, 2017, **37**,11-19.

37. V. Tomar, S. Prasad and D. Kumar, Adsorptive removal of fluoride from aqueous media using *Citrus limonum* (lemon) leaf, *Microchemical Journal*, 2014, **112**, 97-103.

38. A. Mohammad and C. B. Majumder, Removal of fluoride from synthetic waste water by using bio-adsorbents, *International Journal of Research in Engineering and Technology*, 2014, **3**, 776-784.

39. T. Singhand and C. B. Majumder, Kinetics for removal of fluoride from aqueous solution through adsorption from mousambi peel, ground nut shell and neem leaves, *International Journal of Science Engineering Technology*, 2015, **3**(4), 879-883.

40. H. Cai, L. Xu, G. Chen, C. Peng, F. Ke, Z. Liu, D. Li, Z. Zhang and X. Wan, Removal of fluoride from drinking water using modified ultrafine tea powder processed using a ball–mill, *Applied Surface Science*, 2016, **375**, 74-84.

41. N. J. Khound and R. K. Bharali, Biosorption of fluoride from aqueous medium by Indian sandalwood (*Santalum Album*) leaf powder, *Journal of Environmental Chemical Engineering,* 2018, **6**, 1726-1735.

42. N. K Mondal and A. Roy, Potentiality of a fruit peel (banana peel) toward abatement of fluoride from synthetic and underground water samples collected from fluoride affected villages of Birbhum district, *Applied Water Science*, 2018, **8**(3), 90.

43. R. K. Bharali and K. G. Bhattacharyya, Biosorption of fluoride on Neem (*Azadirachta indica*) leaf powder, *Journal of Environmental Chemical Engineering*, 2015, **3,** 662-669.

44. V. Ramanjaneyulu, M. Jaipal, N. Yasovardhan and S. Sharada, Kinetic studies on removal of fluoride from drinking water by using tamarind shell and pipal leaf powder, *International Journal of Emerging Trends in Engineering and Development*, 2013, **5**, 146-155.

45. M. A. M. Sahli, S. Annouar, M. Tahaikt, M. Mountadar, A. Soufiane and A. Elmidaoui, Fluoride removal for underground brackish water by adsorption on the natural chitosan and by electrodialysis, *Desalination*, 2007, **21**, 37-45.

46. L. Fang, K. N. Ghimire, M. Kuriyama and K. Inoue. Removal of fluoride using some lanthanum (III) loaded adsorbents with different functional groups and polymer matrices, *Journal of Chemical Technology and Biotechnology*, 2003, **78**, 1038-1047.

47. H. Paudyal, B. Pangeni, K. Inoue, M. Matsueda, R. Suzuki, H. Kawakita, K. Ohto, B. K. Biswas and S. Alam, Adsorption behaviour of fluoride ions on Zirconium (IV)-loaded orange waste gel from aqueous solution, *Separation Science and Technology*, 2012, **47**, 96-103.

48. A. Samant, B. Nayak and P. K. Mishra, Kinetics and mechanistic interpretation of fluoride removal by nanocrystalline hydroxyapatite derived from Limacine artica shells, *Journal of Environmental Chemical Engineering*, 2017, **5,** 5429-5438.

49. S. Ayoob and A. K. Gupta, Insights into isotherm making in the sorptive removal of fluoride from drinking water, *Journal of Hazardous Materials*, 2008, **152**, 976 – 958.

50. M. A. Zazouli, A. H. Mahvi, S. Dobaradaran, M. Barafrashtehpour, Y. Mahdavi and D. Balarak, Adsorption of fluoride from aqueous solution by modified *Azolla filiculoides, Adsorption*, 2014, **47**(4), 349-358.

51. H. Paudyal, B. Pangeni, K. Inoue, H. Harada, H. Kawakita, K. Ohto and S. Alam, Adsorptive removal of trace concentration of fluoride using orange waste treated using concentrated sulfuric acid, *International Journal of Materials Science and Applications*, 2017, **6**, 212-222.

52. L. Xu, G. Chen, C. Peng, H. Qiao, F. Ke, R. Hou and X. Wan, Adsorptive removal of fluoride from drinking water using porous starch loaded with common metal ions, *Carbohydrate Polymers,* 2017, **160**, 82-89.

53. V. Ganvirand K. Das, Removal of fluoride from drinking water using aluminum hydroxide coated rice husk ash, *Journal of hazardous materials*, 2012, **185**(2-3), 1287-1294.

54. A. A. M. Daifullah, S. M. Yakout and S. A. Elreefy, Adsorption of fluoride in aqueous solutions using $KMnO_4$-modified activated carbon derived from steam pyrolysis of rice straw, *Journal of Hazardous Materials*, 2007, **147**(1-2), 633-643.

55. Y. Zhao, X. Li, L. Liu and F. Chen, Fluoride removal by Fe(III)-loaded ligand exchange cotton cellulose adsorbent from drinking water, *Carbohydrate Polymers*, 2008, **72**(1), 144-150.

56. H. Paudyal, B. Pangeni, K. Inoue, H. Kawakita, K. Ohto, H. Harada and S. Alam, Adsorptive removal of fluoride from aqueous solution using orange waste loaded with multi-valent metal ions, *Journal of Hazardous Materials*, 2011, **192**, 676-682.

57. M. H. Dehghani, M. Farhang, M. Alimohammadi, M. Afsharnia and G. Mckay, Adsorptive removal of fluoride from water by activated carbon derived from $CaCl_2$–modified *Crocus sativus* leaves: Equilibrium adsorption isotherms, optimization, and influence of anions, *Chemical Engineering Communications*, 2018, **205**, 955-965.

58. A. H. B. A. Bakar, Y. S. Koay, Y. C. Ching, L. C. Abdullah, T. S. Y. Choong, M. Alkhatib, M. N. Mobarekeh and N. A. M. Zahri, Removal of fluoride using quaternized palm kernel shell as adsorbents: equilibrium isotherms and kinetics studies, *BioResources*, 2016, **11**, 4485-4511.

59. M. Horsfall Jnr, and A. I. Spiff, Effects of temperature on the sorption of Pb^{2+} and Cd^{2+} from aqueous solution by caladium bicolor (*Wild cocoyam*) biomass, *Electronic Journal of Biotechnology*, 2005, **8**, 43-50.

JNCS
Journal of Nepal Chemical Society December 2019, Vol. 40, 52-56
ISSN: 2091-0304 (print)
DOI: https://doi.org:10.3126/jncs.v40i0.27282
RESEARCH ARTICLE

Electrospun Spider-net Structured Nanofibers Membrane from Homogeneous Solution of Nylon-6 and Poly (Ethylene oxide)

Manoj Kumar Jha[1], Dinesh Shah[1], Khuma Sharma Dhital[2], Lok Ranjan Bhatta[3], Sahira Joshi[1], Ram Kumar Sharma[1], Hem Raj Pant[1]*

[1]Nano-Materials Lab, Department of Applied Sciences and Chemical Engineering, Pulchowk Campus, IOE, Tribhuvan University, Kathmandu, Nepal

[2]Department of Chemistry, Patan Multiple Campus, Tribhuvan University, Kathmandu, Nepal

[3]Biological Resources Unit, Faculty of Science, Nepal Academy of Science & Technology, Khumaltar, Lalitpur, Nepal

**Corresponding E-mail: hempant@ioe.edu.np*
(Received: Sept. 30, 2019; Revised: Dec. 23, 2019 & Accepted: Dec. 24, 2019)

Abstract

Membrane development encompasses wide range of technology areas including process and product design, materials engineering, chemical engineering, as well as interaction phenomenon. Advances in membrane technology can solve most of the global concerns related to water, air, energy, healthcare and global warming. In this study, a simple electrospinning technique was applied to prepare composite nanofibers from Nylon-6 and polyethylene oxide (PEO) blend solutions. The effect of PEO on the morphology of the fiber was investigated. It was observed that the addition of PEO in the Nylon-6 solution resulted in the formation of ultrafine nanofibers along with the main fiber, which can be considered as a spider-net-like morphology. The nano/sub-nano arrangement of the fiber resembling a three-dimensional (3D) spider-net structure enhances the mechanical strength of the resulting nanofibers as compared to the pristine Nylon-6 nanofibers.

Keywords: Electrospinning, nylon-6/PEO composite, nanofiber, spider-net morphology

Introduction

In recent years, the development of electrospinning techniques has been increasingly investigated [1]. Electrospinning is considered as a simple and easy technique to fabricate the ultrafine continuous nanofibers morphology. Pure polymers, as well as the blending of a given polymer with other polymers/ oligomers, have been successfully electrospun into micro/ nanofiber matrices for various applications [2,3]. The fibers produced by this method have shown amazing characteristics, such as a very large surface-to-volume ratio and a high porosity with a small pore size [4,5]. These characteristics make the electrospun fibers suitable for various potential applications such as filtration, protective clothing, tissue scaffold, wound dressing, drug delivery system, sensor, and optical materials [1,6-8].

The hybrid mats produced by electrospinning possess unique physical and chemical properties and therefore, research interest in the formation of polymer hybrid mats has been increased in the past decades. Despite the ease of nanofiber fabrication, it is yet challenging to fabricate electrospun nanofibers with a diameter of less than 10 nm. After the successful preparation of nano-net like fibers via electrospinning process by Ding's group [9], benefits from the nano/sub-nano fibers have been realized and several research activities have been directed towards the development of nano-net like structures for various applications [2,5,6,10]. An important property of a polymer blend is the miscibility of its components because it affects the mechanical properties, the morphology, and the permeability and degradation [2]. Consequently, in this study, we report the preparation of a hybrid spider-web like a mat of polymer and oligomer using a simple electrospinning technique with the diameter of fibers ranging from nanometer to sub-nanometer

scale. Nylon-6 is a biodegradable semi-crystalline polymeric material with good thermal, chemical, and mechanical properties [3,11]. Electrospinning of the blend solution of Nylon-6 and polyethylene oxide (PEO) may exhibit properties shown by both individual polymers and oligomer, thereby resulting in a material with improved properties. The choice of PEO is motivated by its wide variety of applications such as biomaterials including scaffolds, drug delivery [1], tissue engineering [12], wound healing, and conductive fibers.

Materials and Methods

Nylon-6 (medium molecular weight of KN 120 grade) was obtained from Kolon, Korea. Formic acid and acetic acid were purchased from Showa, Chemicals, Japan. Poly (ethylene oxide) oligomer was obtained from Sigma-Aldrich, USA. All the chemicals were used without any purification.

Nylon-6/PEO blend solutions were prepared by mixing at different content of PEO (0.5%, 1%, 2%, and 4% PEO with respect to the weight of Nylon-6) in Nylon-6 at 20% final concentration. Formic acid and acetic acid (4:1) were used as the solvent. After stirring continuously to get a perfect blended solution, electrospinning was carried out. A high voltage power supply (CPS-60 K02 V1, Chungpa EMT, South Korea) of 22 kV to the syringe micro-tip was supplied to electrospun the nanofibers. The tip-to-collector distance was kept at 16 cm. The as-obtained nylon-6/PEO nanofiber mats were vacuum dried in an oven at 30 ^{o}C for 12 h to remove the residual solvent and the samples were used for characterizations. The nanofiber mats containing 0.5, 1, 2, and 4% PEO in Nylon-6 were denoted as NP0.5, NP1, NP2, and NP4, respectively. For comparison, pristine Nylon-6 nanofiber mat without using PEO is also prepared by the aforementioned process.

Characterizations

The morphology of the electrospun mats was investigated using FE-SEM (S-4700, Hitachi, Japan). Structural characterization was carried out by X-ray diffractometer (XRD, Rigaku, Japan) with Cu K_{α} (λ = 1.540 Å) radiation over Bragg angles ranging from 10 to 80˚. The bonding configurations of the samples were characterized by means of Fourier-transform infrared (FT-IR). Mechanical properties were measured with a universal testing machine (AG-5000G, Shimadzu, Japan), under a crosshead speed of 10 mm/min. The samples were prepared in the form of a standard dumbbell-shaped according to ASTM Standard 638 via die-cutting from the mat and tested in the machine direction. Five samples were tested for each mat.

Results and Discussion

Figure 1 depicts the FE-SEM images of the as-synthesized pristine Nylon-6 NFs and Nylon-6/PEO composite NFs. As in figure 1A, the pristine Nylon-6 nanofibers exhibited a smooth, bead free, and continuous nanofibrous morphology throughout their lengths. The average diameter of the pristine Nylon-6 NFs was recorded as 213 nm. In the case of composite nanofibers, a clear arrangement of spider-web-like morphology due to the ultrafine nanofiber network was observed. It can be seen that the ultrafine nanofibers are connected to the main fiber. This type of spider-net-like arrangement of nanofibers provides a large surface area to volume ratio, thereby widening the applications of nanofibers. The average diameters of ultrafine in Mats NP0.5, NP1, NP2, and NP4 were found to be 21, 28, 32, 40 nm, respectively.

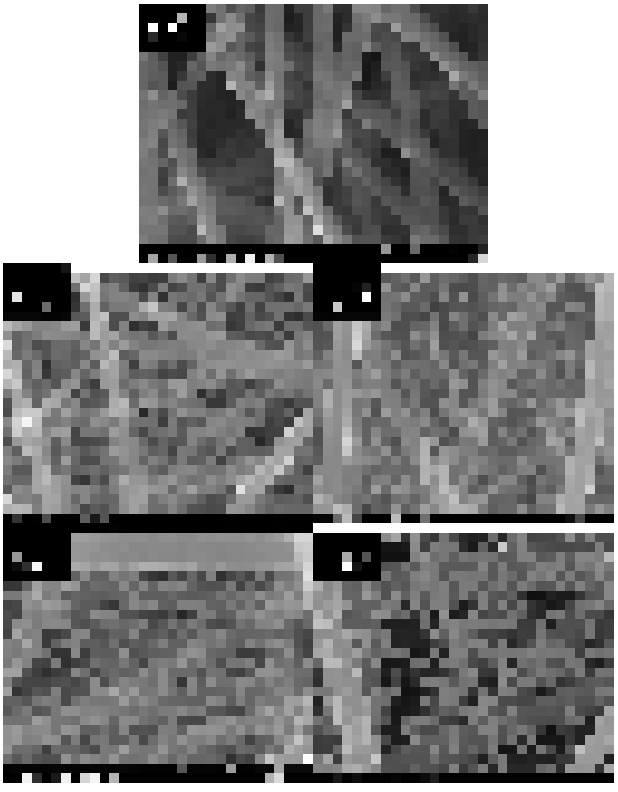

Figure 1: *High magnification FESEM images of nanofibers: Nylon-6 (A), NP0.5 (B), NP1 (C), NP2 (D) and NP4 (E).*

Besides the variation in diameter, the arrangement of ultrafine nanofibers in the mats is different. The nanofibers in mat N2 show a three dimensional (3D) arrangement with multiple layers connecting to the main fiber body. At the lower content of PEO, the ultrafine nanofibers start to form, therefore they are distributed to the limited area (Figure 1B). With the increase in PEO content, a clear distribution of ultrafine fibers were observed; however, the pattern of arrangement is different. Among the four different samples, the best arrangement of spider-net fibers was observed in the NP2 sample (Figure 1C). Therefore, it can be concluded that 1% is the optimum content of PEO in the Nylon-6 solution for getting the nano/sub-nano fibrous arrangement. The partial phase separation of homogeneously mixed higher molecular nylon and lower molecular PEO portion should be started from the stable jet region, and becomes more pronounced during vibrating and whipping of the jet during electrospinning [13]. During jet whipping, PEO forms a surface layer whereas nylon forms the core of the jet. From the surface PEO layer, sub-nano fibers (fiber diameter < 50nm) are formed whereas from core nylon, nanofibers (fiber diameter>200nm) are formed.

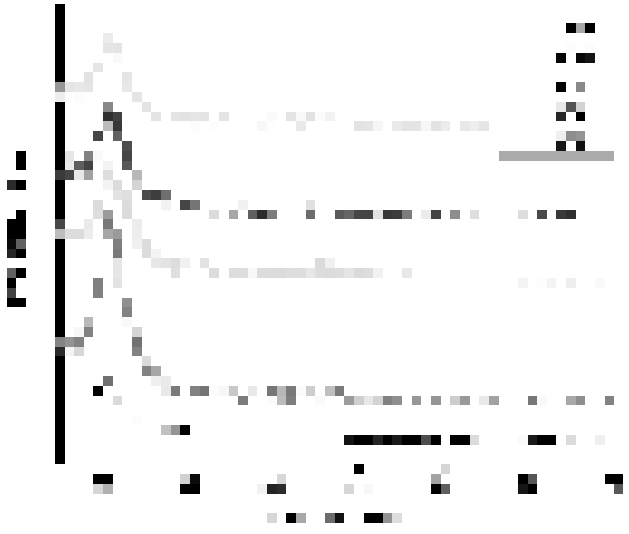

Figure 2: *XRD spectra of different formulations.*

XRD analysis was carried out in order to examine the crystal structure of the prepared samples. Nylon-6 nanofiber exhibited a characteristic peak at approximately 2θ values of 20.5 °, which can be termed as α crystalline phase [13]. After blending with PEO, the diffraction peak was observed at approximately 2θ values of 21.2°. This shifting towards the higher values of 2θ° indicated a conversion from α to γ phase [13].

Figure 3: *IR spectra of Nylon-6 and Nylon-6/PEO composite nanofibers.*

Figure 3 depicts the characteristic FTIR peaks of pristine nylon-6 and nylon-6/PEO blend nanofiber composites. In pristine Nylon-6 nanofibers, the bands appeared at 3300 and 3085 cm^{-1} correspond to the NH stretching vibrations [14]. The peaks at 2860 and 2930 cm^{-1} belong to the C-H stretching vibrations. The bands at 1640 and 1445 cm^{-1} are associated with (C=O) amide I and (C-N) amide II, respectively [14,15]. These bands were observed to be decreased

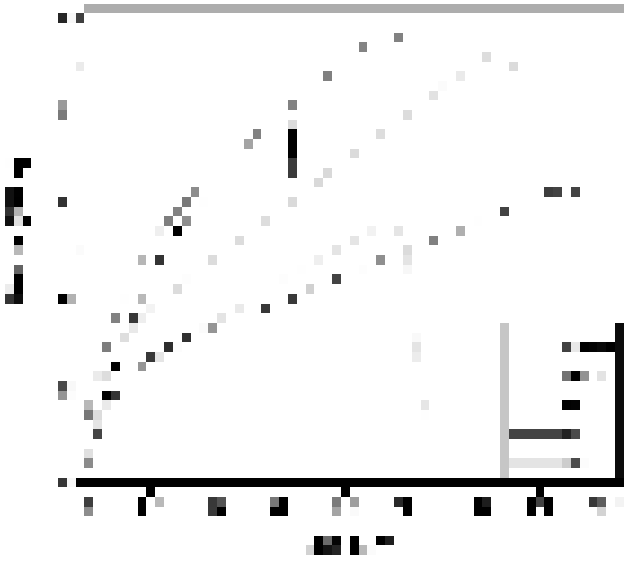

Figure 4: *Stress-strain curves of various formulations of nanofiber mats.*

in the case of composite nanofibers, which may be due to the hydrogen bonding with PEO. We studied the mechanical properties of the as-synthesized mats by the UTM machine. The study revealed that at the lower content of PEO, the mechanical property of the Nylon-6 is increased, whereas with further increasing PEO content, the mechanical strength decreased. The highest mechanical performance in the case of the NP1 sample is attributed to the well-formed 3D spider-net like morphology. As compared to the other samples, the sub-nano fibers are highly interconnected with the main fibers in NP1. The FESEM morphologies (Figure 1) also support the mechanical strength data.

Conclusion

Nylon-6 and PEO polymers are properly blended with each other to produce composite bimodal electrospun nanofibrous membranes. 3D spider-net morphology of Nylon-6/PEO composite nanofibers was successfully prepared by the electrospinning technique. The interconnected fibrous morphology improved the mechanical property of the hybrid fibers. Thus prepared high aspect ratio Nylon-6/PEO composite nanofibers can be used in different fields such as filtration, wound healing, etc.

Acknowledgments

The research work was supported by the World Academy of Science, Trieste, Italy (TWAS)/Swedish International Development Corporation Agency (Sida) (project number; 18-168RG/ CHE/AS_G-FR3240303651) and University Grant Commission, Nepal (project number; -CRG-74/74Engg-02). We are thankful to Chonbuk National University, the Republic of Korea for characterizing the samples.

References

1. B. Pant, M. Park and S-J. Park, Drug delivery applications of core-sheath nanofibers prepared by coaxial electrospinning: a review, *Pharmaceutics* 2019, **11**, 305.
2. H. R. Pant, M. P. Bajgai, K. T. Nam, K. H. Chu, K. H. Park and H. Y. Park, Formation of electrospun nylon-6/methoxy poly(ethyleneglycol) oligomer spider-wave nanofibers, *Materials Letters*, 2010, **64**, 2087-2090. (doi:doi.10.1016/j.matlet.2010.06.047).
3. B. Pant, H. R. Pant, D. R. Pandeya, G. Panthi, K. T. Nam, S. T. Hong, C. S. Kim and H. Y. Kim, Characterization and antibacterial properties of Ag NPs loaded nylon-6 nanocomposite prepared by one-step electrospinning process, *Colloids and Surfaces A: Physicochemical and Engineering Aspects,* 2012, **395**, 94-99. (doi:doi.10.1016/j.colsurfa.2011.12.011).
4. B. Pant, M. Park, S-J. Park and H. Y. Kim, High strength electrospun nanofiber mats via CNT reinforcement: A review, *Composites Research,* 2016, **29**, 186-193. (doi:10.7234/composres.2016.29.4.186).
5. X. Wang, B. Ding, G. Sun, M. Wang and J. Yu, Electro-spinning/netting: A strategy for the fabrication of three-dimensional polymer nano-fiber/nets, *Progress in Materials Science*, 2013, **58**, 1173-1243. (doi:doi.10.1016/j.pmatsci.2013.05.001).
6. B. Pant, M. Park and S-J. Park, One-step synthesis of silver nanoparticles embedded polyurethane nano-fiber/net structured membrane as an effective antibacterial medium, *Polymers* 2019, **11**, 1185.
7. L. Ping and D. Bin, Applications of electrospun fibers, *Recent Patents on Nanotechnology* 2008, **2**, 169-182. (doi:doi.10.2174/187221008786369688).
8. H. R. Pant, B. Pant, P. Pokharel, H. J. Kim, L. D. Tijing, C. H. Park, D. S. Lee, H. Y. Kim and C. S. Kim, Photocatalytic TiO_2–RGO/nylon-6 spider-wave-like nano-nets via electrospinning and hydrothermal treatment, *Journal of Membrane Science*, 2013, **429**, 225-234. (doi:doi.10.1016/j.memsci.2012.11.025).
9 B. Ding, Li. C. Y. Miyauchi, O. Kuwaki and S. Shiratori, Formation of novel 2D polymer nanowebs *via* electrospinning, *Nanotechnolog,* 2006, **17**, 3685-3691. (doi:10.1088/0957-4484/17/15/011).
10. H. R. Pant, H. J. Kim, M. K. Joshi, B. Pant, C. H. Park, J. I. Kim, K. S. Hui and C. S. Kim, One-step fabrication of multifunctional composite polyurethane spider-web-like nanofibrous membrane for water purification, *Journal of Hazardous Materials*, 2014, **264**, 25-33. (doi:doi.10.1016/j.jhazmat.2013.10.066).

11. H. R. Pant, P. Risal, C. H. Park , L. D. Tijing, Y. J. Jeong and C. S. Kim, Core–shell structured electrospun biomimetic composite nanofibers of calcium lactate/nylon-6 for tissue engineering, *Chemical Engineering Journal*, 2013, **221**, 90-98. (doi:doi.10.1016/j.cej.2013.01.072).

12. P. Basu, A. Repanas, A. Chatterjee, B. Glasmacher, U. N. Kumar and I. Manjubala, PEO–CMC blend nanofibers fabrication by electrospinning for soft tissue engineering applications, *Materials Letters*, 2017, **195**, 10-13. (doi:doi.10.1016/j.matlet.2017.02.065).

13. Y. C. Tseng and S-P. Rwei, Synthesis and characterization of the feed ratio of polyethylene oxide (0 10 wt % PEO) in the nylon-6/PEO copolymer system, *Journal of Applied Polymer Science*, 2012, **123**, 796-806. (doi:10.1002/app.34653).

14. K-H. Lee, K-W. Kim, A. Pesapane, H-Y. Kim and J. F. Rabolt, Polarized FT-IR study of macroscopically oriented electrospun nylon-6 nanofibers, *Macromolecules*, 2008, **41**, 1494-1498. (doi:10.1021/ma701927w).

~

JNCS
Journal of Nepal Chemical Society December 2019, Vol. 40, 57-66
ISSN: 2091-0304 (print)
DOI: https://doi.org:10.3126/jncs.v40i0.27283
RESEARCH ARTICLE

Fabrication and Characterization of Starch-Based Biodegradable Polymer with Polyvinyl Alcohol

Shanta Pokhrel*, Lalita Sundari Rai
Department of Chemistry, Tri-Chandra Multiple Campus, Tribhuvan University, Kathmandu, Nepal

Corresponding E-mail: shantabhattarai2014@gmail.com
(Received: Sept. 18, 2019; Revised: Dec. 24, 2019 & Accepted: Dec. 26, 2019)

Abstract

Starch is a renewable, biodegradable and low-cost natural biopolymer with high availability. Starch was extracted from *Solanum tuberosum* (potatoes) and its preliminary properties were studied. The structure of extracted starch was characterized by Fourier Transform Infrared Spectroscopy (FTIR) and Scanning Electron Microscopy (SEM). A series of starch-based biodegradable blends, with polyvinyl alcohol (PVA) were prepared by using glycerol as a plasticizer and citric acid as a crosslinking agent, through solution casting method and their biodegradable properties were studied. The structure of the blend was characterized by Fourier Transform Infrared Spectroscopy (FTIR) and Differential Scanning Calorimeter (DSC). The morphology of starch shows the potato starch has oval or ellipsoid in the structure having a size of 20-35 μm. The compatibility of the two components can be improved by the hydroxyl group present on both starch and PVA. As compared to pure polyvinyl, the melting point of the blend was decreased. The blends were found degradable within a weak.

Keywords: Biodegradable, DSC, starch, polyvinyl alcohol, PVA/starch blend.

Introduction

The plastic we used in our daily life is easy to use, inexpensive, flexible as well as durable. But they are chemically synthesized from petrochemical industries and produced with huge toxic additives. They are non-renewable, non-degradable and lack of infrastructure [1,2]. Being non-degradable they cause white pollution and reduce the resources. The preparation of biodegradable plastic is a wise thought to overcome these problems, which can be prepared from agricultural products [3].

Solanum tuberosum is the third major source of starch [4]. It is naturally occurring agricultural residue and renewable which can be used to produce degradable plastic [5]. Pure starch has low water resistibility, processability, thermal stability, and strength. To overcome these fallacies starch is often blended with other degradable polymers such as polylactic acid (PLA), poly--caprolactone (PCL), polyvinyl alcohol (PVA) [2,3,6]. PVA is semicrystalline, non-toxic, water-soluble, having excellent optical and physical properties [7]. The blend of PVA and starch still lacks some mechanical and thermal properties [2]. So, glycerol and citric acid (CA) can be used as a plasticizer and crosslinking agent respectively [8,9].

Several kinds of research have been conducted on the biodegradation of starch, PVA and starch –blends. Starch can be readily metabolized by a range of microorganisms to fermentation products such as ethanol [10,11], hydrogen [12,13] and methane [14]. PVA is also susceptible to biological degradation, however, the process was slow [15]. Furthermore, the overall number of PVA degrading microorganisms was rather limited in comparison to the widespread species able to degrade aliphatic polyesters, such as polyhydroxyalkanoate (PHA) and PLA [16].

Chen *et al*., observed that the rates of biodegradation in starch–PVA cast films were degraded much faster than pure PVA [17]. Mao *et al*. in his work reported that the addition of PVA slowed the degradation process in the samples [9]. Russo *et al.* investigated the degradability of thermoplastic starch and PVA blends under anaerobic conditions and concluded that predominantly PVA remained at the end and that

starch was almost entirely degraded [18]. Chai *et al*. evaluated the biodegradability of modified starch–PVA blends with bio-reactivity kinetic models. And conclude, the degradability of PVA was enhanced with the addition of the starch [19]. Cinelli *et al.* characterized the biodegradability with or without a cross-linking agent of PVA, starch, and lignocellulosic films. Results were in favor of biodegradation [20].

Tang; Zou *et al.* done their studied the biodegradability of nano-SiO_2 reinforced starch/PVA nanocomposite films. Results showed that nanoparticles had no significant influence on the biodegradability of films [21]. Popescu *et al.* researched the degradation of clay–starch–PVA nanocomposite films and concluded that the biodegradation of films depended on both type and content of nanoparticles and the nanoparticles hindered the rate of biodegradation [22].

Starch–PVA films can be chosen for the biomedical and clinical field (such as drug control release carrier and biomembrane) [23], while chemically bonded composites can be taken as recyclable sizing agents [24]. PVA/starch has been considered for the replacement of polystyrene foams for expanded foams as loose-fill packaging materials.

According to Vilpoux and Avérous, the commercial alternative to polystyrene (PS) is a blend with 95% of hydroxyl propylated high amylose starch and 5% of PVA [25]. PVA/starch blends are sensitive to moisture but they are good in providing barriers to oxygen and carbon dioxide. So they can act as flavor and aroma barriers, having good resistance to most organic compounds and solvents can be used in food technology [2]. Although there are several kinds of research have done on fabrication and characterization of PVA/starch film with the mechanical test, still there is a lack of research on thermal properties and complete biodegradation. Hence this work is a step further to study thermal behavior and biodegradation of PVA/starch blends.

Materials and Methods

Materials

Solanum tuberosum were collected from National Potato Research Project (NPRP), Khumaltar, Lalitpur in the month of June 2018, they were cultivated in Parwanipur, Bara district and harvested in March and stored in cold store of NPRP, Lalitpur. Polyvinyl alcohol, glycerol, citric acid were brought from Thermo Fisher Scientific India Pvt. Ltd. (India). The water used in the whole thesis work was de-ionized water brought from the local shop of Kathmandu.

Extraction of starch from *Solanum tuberosum*

The process of extraction of starch from *Solanum tuberosum* was done according to Singh and Singh [26]. The tubers of *Solanum tuberosum* was cleaned properly, peeled off and cut into small pieces and were dipped in water containing a small amount of potassium metabisulfite ($K_2S_2O_5$). Then grinned and filtered, the residue was washed with distilled water and left for decantation. After complete decantation, the starch cake was collected and dried at a temperature of 40 ^{0}C in a hot-air cabinet drier.

Preparation of PVA/starch blends

The fabrication of starch with PVA was done by following the protocol mentioned by Shi *et al. via* the solution casting process [23]. The solution was prepared by dissolving the PVA, starch, and glycerol in hot water at 95 ^{0}C to form a homogeneous gel-like solution then citric acid was added into the mixture with a mechanical stirrer for 10 minutes at 30 ^{0}C. Bubbles were removed with an aspirator. The prepared solution was poured on a pre-warmed glass Petri-plate and evaporated from the molds at 25 ^{0}C for one week. The dried films were sealed in polyethylene bags and were stored at 20 ^{0}C to characterize them.

Characterization

Characterization of extracted starch

Moisture content

The determination of moisture content of starch follows the AOAC process [27]. The crucible and lid were dried in the oven at 105 ^{0}C for 3 hours and transferred to desiccator to cool. Weighed it out. Weighed 3 g starch sample was spread uniformly in the crucible. Then the crucible was placed in an oven for 3 hours at 105 ^{0}C. After that, it was transferred to desiccator with the partially covered lid to cool. Reweighted the dish and starch sample. For this, three concurrent data was taken and the mean value was found then moisture content was calculated by the following equation (i).

$$\text{Moisture (\%)} = \frac{(W_1 - W_2)}{W_1} \times 100\ \% \text{ ----------(i)}$$

Where, W_1 = weight of sample before drying in gram.

W_2 = weight of sample after drying in gram.

Ash content

To determine the ash content of the starch AOAC method was followed [27]. The crucible and lid were placed in the furnace at 550 ^{0}C overnight. The crucible was cooled in a desiccator for 20 minutes. The crucible and lid were weighed to decimal places. The starch sample was weighed and put into the crucible. The crucible was heated over low Bunsen flame with half covered. When flames were no longer produced, crucible with lid was placed in the furnace. It was heated at 550 ^{0}C overnight. During heating, the crucible was not covered by a lid. The lid was placed on crucible after complete heating, to prevent loss of fluffy ash. Then it was placed in desiccator to cool down. The ash with crucible and lid was weighed. And the ash content was calculated by the following equation (ii).

$$\text{Ash (\%)} = \frac{\text{weight of ash}}{\text{weight of sample}} \times 100\ \% \text{ ----------(ii)}$$

Amylose content

A starch sample of 0.10 g was weighed into 100 cm^3 volumetric flask and 1 cm^3 of 99% ethanol and 9 cm^3 of 1 M sodium hydroxide (NaOH) solution were carefully added. The contents were mixed thoroughly and the sample solution was heated for 10 mins in boiling water to gelatinize the starch. After cooling the solution was made up to the mark with distilled water and shaken thoroughly. 5 cm^3 of starch solution in a 100 cm^3 volumetric flask was treated with 1.0 cm^3 of 1M acetic acid and 2.0 cm^3 of iodine solution. The solution was diluted to the mark with distilled water and absorption was read using a spectrophotometer at 620 nm. The absorbance of a blank solution prepared accordingly was subtracted from that of the sample and amylose and amylopectin contents were calculated using equations (iii) respectively.

$$\text{Amylose content (\%)} = 3.06 \times \text{absorbance} \times 20\% \ldots\ldots \text{(iii)}$$

Fourier transform infrared (FTIR) spectroscopy

The FTIR analysis for starch samples was done in the Nepal Academy of Science and Technology (NAST), Khumaltar, Lalitpur by using SHIMADZU spectrophotometer (IR Prestige-21) Nepal. The spectra were obtained at a resolution range of 400 cm^{-1} to 4000 cm^{-1}.

Scanning electron micrograph (SEM)

For surface morphology, starch samples were dehydrated in 99.8% ethanol and sprinkled on carbon tape mounted on an aluminum stub. Then they were coated with a thin gold film using a sputter coater and observed in a FEGSEMMAIA3 (model 2016) microscope (Tescan, Czech Republic) at an accelerating potential of 2 kV.

Characterization of PVA/starch blends

Fourier transform infrared (FTIR) spectroscopy

FTIR analysis for PVA/starch blends was done by IRTracer-100, SHIMADZU in the Central Department of Chemistry, Tribhuvan University, Kritipur, Kathmandu, Nepal. The sample was prepared by mixing the fine powder with KBr and pressing. The spectra were obtained at a resolution range of 400 cm^{-1} to 4000 cm^{-1}.

Differential scanning calorimeter (DSC)

Differential scanning calorimetry thermograms were recorded by NETZSCH DSC 204 F1 phoenix (India) instrument. Sample pieces of about 10 g were placed in an aluminum pan and were first cooled to room temperature and held there for 5 min. After that, a heating scan was conducted from 25 ^{0}C to 250 ^{0}C at a heating rate 10 K/min.

Biodegradation test of PVA/starch blends

Here the process of Azahari *et al.* was performed for the process of biodegradation test of PVA/starch blends [28]. The biodegradation test was performed under compost burial conditions. One vase of the approximate capacity of 5 L was filled with cow's dung compost. The composites were cut into 2 cm × 2 cm in square shape and each sample was enclosed in tea bags individually and made. The samples were buried in the compost at a depth of 10 cm and the moisture of the compost was maintained by sprinkling water at regular intervals of time.

The degradation of the samples was determined at regular intervals of 7 days by carefully removing the sample from the compost and washing it gently with

ethanol to remove the trace of compost from the film and dried in an oven at 60 ^{0}C for 4 hours and weight of the samples were taken on a digital balance.

Results and Discussion

Yield of starch

The yield of starch from the tuber of *Solanum tuberosum* was calculated using the standard equation, on the basis of the mass of raw *Solanum tuberosum* sample of starting material. Using raw *Solanum tuberosum* sample as reference the yield of starch was found to be 3.82 % in Khumal Rato (KR).

The yield of starch was found affected by various artificial factors including wet storage [29], genetic variation [30,31], the drying conditions of the raw materials (oven-dried chips and flour have higher yield than sun-dried ones) [32], harvesting time and root storage (root storage decreased starch content) [33,34], the form of the roots used for extraction (fresh root gave better extraction efficiency and purer starch than dried chips and pellets) [35], and the environmental conditions for growing the crop (e.g., two growth locations gave significant difference in the starch yield of the same variety) [30]. Thus for high starch yield, varieties with high dry matter content and thin peel thickness are suitable [36]. All these factors can be controlled, and careful selection of the parameters would lead to a maximum of starch yield. It should be noted that high yield does not necessarily mean the starch would have the desired quality for any specific application.

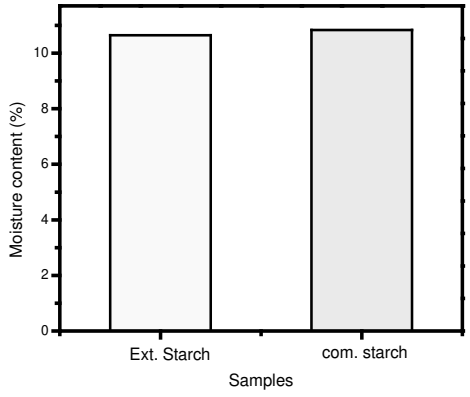

Figure 1: *Moisture content of extracted starch and commercial starch.*

The moisture content of extracted starch from Khumal Rato and commercial starch is represented in Figure 1.

The result showed that the moisture content of Khumal Rato was 10.65% and commercial starch was 10.84%. The relatively low moisture content of the starches makes them easy to store at room temperature and less prone to colonization by organism degradation as shown for root, tuber and cereal starches [37,38] making them suitable for utilization in industries like the filler in biodegradable plastic and pharmaceutical industry that make use of low moisture content. The range of moisture contents in these starches varied from 7.54 to 9.37%. Tapioca starch showed slightly lower moisture content (7.54%) than corn starch (7.74%) and similar to the results of on mango starch [39]. Potato starch had a significantly higher moisture level (9.37%) than other starches.

Ash content of extracted starch and commercial starch is shown in Figure 2. From the graph, the ash content of the starch from the Khumal Rato was 0.7% and commercial starch was 0.8. However, the ash content of the potato was significantly higher than 0.20 to 0.22% for Oat starches [40]. The ash content is an estimate of the total mineral content of the starch. The low ash content is an indication of the good quality of the starches, because high mineral content is sometimes used to retard the growth of certain microorganisms [36].

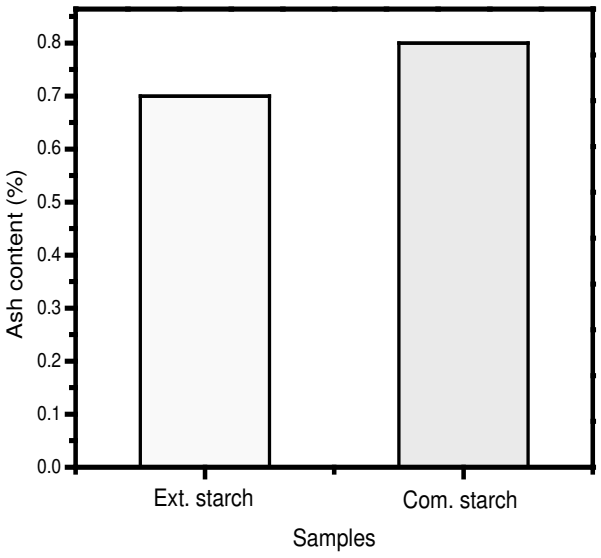

Figure 2: *Ash content of extracted starch and commercial starch.*

The amylose content of starch determines its properties (such as water-binding capacity, thickening, gelling, etc.) and as a result dictates most of its uses. The

results obtained showed significant variations. The amylose contents (in terms of amylose equivalent) for extracted starches from Khumal Rato was found to be 23.26%, higher than values reported for mango [39] and corn starches 16.9–25.3 % [41] and also higher than that of oat [40] and of tapioca (16.27%). These values were slightly higher than those reported by Glicksman and Rapaille and Vanhemelrijck for potato (22%) starch, but comparable to that for corn (26%) and tapioca (17%) starches. Thus, the starch could be applied in industries that produce, fillers, thickeners, binders, etc.[42].

Xia *et al.,* reported that the structure of amylose is sensitive to physical and chemical treatments. When slight applied of heat change the amount of content.

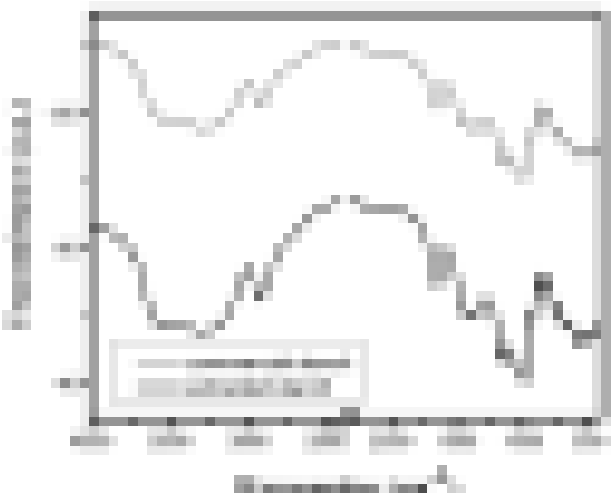

Figure 3: *FTIR spectra of extracted starch and commercial starch.*

The FTIR spectra of extracted starch and commercial starch are presented in Figure 3, whereas the interpretation of each peak is given in Table 1.

As shown in the graph, the presence of an absorption band at around 3600-3300 cm^{-1} for both starch is due to the vibration of the hydroxyl groups (-OH). The band at 2927 cm^{-1} is the characteristic peak of the C-H stretching vibration of the amylase and amylopectin, present in starch. The peak occurred for extracted starch at 1645 cm^{-1} is due to the tightly bound water molecules. The changes in the crystallinity of the starch are reflected around this band. The band at 1157 cm^{-1} of extracted starch and commercial starch is assigned as a complex mode involving the CH_2OH side chain in amylase.

In addition, the characteristic C-O-C ring vibration on starch leads to an absorbance peak at around 700-900 cm^{-1}. The C-O bending associated with the OH group would cause an absorbance peak at around 1648 cm^{-1}. Furthermore, the absorbance peak at 1419 cm^{-1} implied the presence of C-H symmetrical scissoring of CH_2OH moiety. The uncommon CO_2 peak in starch (2358 cm^{-1}) was observed in the potato starch IR spectrum. It might result from measuring conditions [43].

SEM is used to investigate the granule morphology of the potato starch. The morphology of starch was shown in Figures 4 and 5.

Table 1: *Band assignment of potato starch.*

S. No.	Functional group	Wave number cm^{-1}	Potato starch cm^{-1}
1	O-H stretching	3600 – 3300	3569-3170
2	C-H stretching	2931	2931
3	C-O bending associated with OH group	1637	1645
4	CH_2 symmetric deformation	1458	1437
5	CH_2 symmetric scissoring	1415	1419
6	C-H symmetric bending	1385-1375	1381
7	C-O-C asymmetric stretching	1149	1157
8	C-O stretching	1200-800	993
9	C-O-C ring vibration of carbohydrate	920,856; 758	929, 858,763

The starch image has 20 and 50 resolutions. The image revealed that the potato starch granules exits in smooth granule form have oval and ellipsoid shapes with sizes ranging from 5 to 35 µm in width and 15 to 60 µm in height.

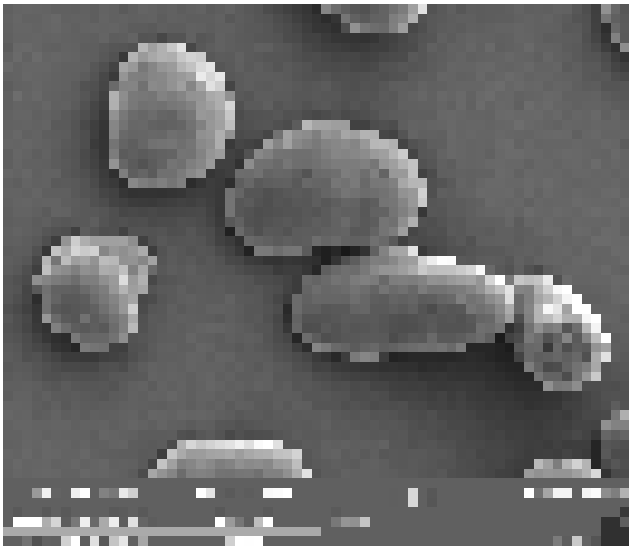

Figure 4: *SEM image of potato starch having 20 µm resolution.*

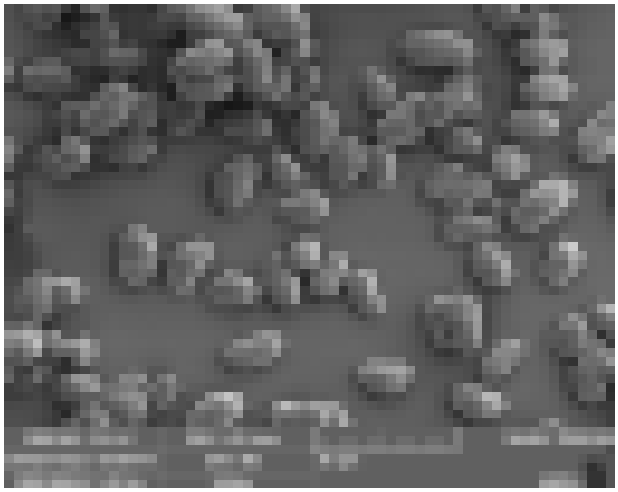

Figure 5: *SEM image of the potato starch powder having 50 μm resolution.*

Wang reported in his work, the sizes of small and large granules ranged from 0.4 to 3μm and from 6 to 40 μm in maize starch, from 0.6 μm and from 10 to100 μm in potato starch, and from 0.6 to 6μm and from 10 to 70 μm in pea starch, respectively. Fannon et al. mentioned that SEM has been used to relate granule morphology to starch genotype. Svegmark and Hermanson reported that the variation in size and shape of starch granules is due to the biological origin. Singh and Singh claimed that the morphology of granules depends on the biochemistry of chloroplast or amyloplast and physiology of plants [44].

Characterization of PVA/starch blends

The fabricated starch/PVA blends were transparent, flexible, are characterized via FTIR, DSC and biodegradation test.

The FTIR spectra of PVA/starch blends with different content of PVA shown in Figure 6 and band assignment is shown in Table 2.

Broad and strong absorption band from 3200-3600 cm^{-1} is the cause of the stretching vibration of -OH present in starch. The absorption band 2931 cm^{-1} is due to an aliphatic saturated C-H stretching vibration of starch.

Another absorption band at 1640 cm^{-1} is because of the stretching vibration of C=O and at 1651cm^{-1} is due to the bending mode of the absorbed water and some contribution from the carboxylate group. The vibration of the CH_2 group produces an absorption

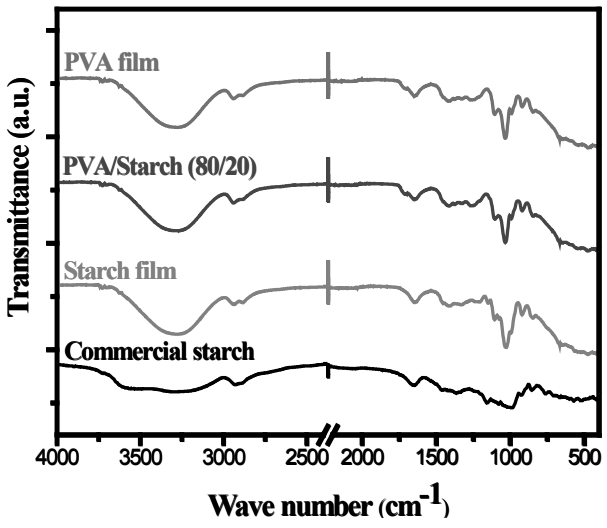

Figure 6: *FTIR spectra of commercial starch and PVA/ starch blends*

band at 1409 cm^{-1}. Due to the cause of C-O stretching an absorption band at 1035 cm^{-1} was produced.

Blout *et al.,* reported that a peak at 2361 cm^{-1} is due to atmospheric carbon dioxide. Peaks due to water in the films occur at 1652 cm^{-1} and around 3240 cm^{-1}. The later peak overlaps the peak due to the -OH stretching of hydroxyl groups.

Table 2: *Characteristics FTIR bands starch/PVA blend.*

S.N.	Functional group [3,8]	Wave number (cm^{-1}) [3,8]	Blends
1	-OH stretching	3600-3200	3285
2	C-H	3000-2850	2931
5	C-C	1636	1640
6	CH_2	1461-1417	1409
8	C-O	1141-1093	1035
9	C-O-H	669	652

Another research by Finch *et al.*, mention that peaks at 2912, 1324 and 843 and 1084 cm^{-1} are attributed to the C–H stretching, C–H bending and C–O stretching of PVA, respectively. The broad high absorption peak at 3237 cm^{-1} is assumed to arise from the -OH stretching frequencies of PVA and water hydroxyl groups. The band at 1708 cm^{-1} was attributed to the carbonyl functional groups due to residual acetate groups remaining after the manufacture of PVA from hydrolysis of polyvinyl acetate or oxidation during manufacturing and processing [44].

Differential Scanning Calorimeter (DSC) provides information about thermal changes that do not involve a change in sample mass change in sample mass. Now it is a more commonly used technique than TGA. The results of the thermal behavior of PVA and starch with glycerol and citric acid, was shown in Figure 7. From the DSC curve, the melting point (T_m) of PVA blend without starch was found 198 ^{0}C, and the melting point for PVA/S 5%, PVA/S 20%, PVA/S 40% were found 141 ^{0}C , 137 ^{0}C and 131 ^{0}C respectively.

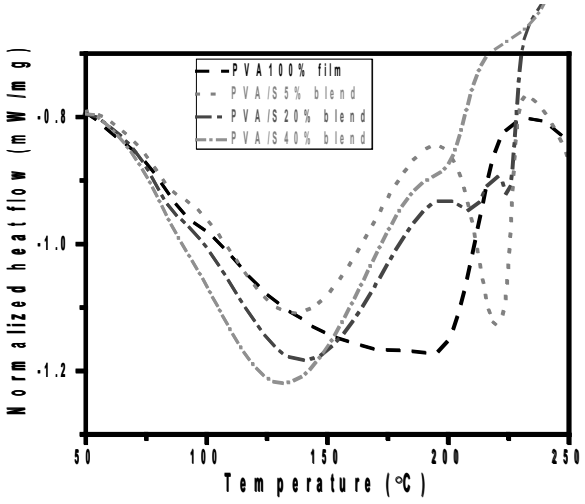

Figure 7: *DSC curve of PVA/starch blends with glycerol and citric acid.*

The observed T_m is lower than that of reported one which is 230 ^{0}C for pure PVA. This is because the PVA film had already contained some water as the plasticizer. When glycerol was added, the T_m decreased. The reduction in T_m was attributed to the reduction in the cohesive forces of attraction between the polymer chains. The plasticizer molecules penetrated the polymer matrix because they were smaller than the polymer molecule. As a result, polar attractive forces were established between the plasticizer and chain segments, which were responsible for the reduction of the cohesive forces and, therefore, a reduction of T_m. Shi *et al.* and Shreedhar *et al.* also reported the decreased of T_m in their work [23].

The biodegradation result showed that the buried blends were found completely degraded after taken out from the vase. So the calculation of weight loss couldn't perform. There is the various possible reason behind the degradation. Lucas *et al.* mentioned that in the process of biodegradation, the resistance and durability of polymeric materials are made weak by the action of microorganisms or/and environmental abiotic factors. Another suitable possible reason was given by Bonhomme *et al.* and Leja *et al.* according to them, the growth of microorganisms adhering to the polymer surface can provoke the formation of cracks, increase the size of pores and others defects, that may lead to the disintegration of a material into small fragments [45].

Conclusion

Starch was successfully extracted from locally cultivated tubers' potatoes (*Solanum tuberosum*). It is white, an amorphous in nature, tasteless, odorless, insoluble in cold water, alcohol, and ether. The preliminary results indicate the quality of extracted starch is good and they are as reliable as commercial starch. The FTIR peak at 2919 cm^{-1} indicates the presence of amylose and amylopectin. Morphology of starch shows, smooth granule, oval and ellipsoid in shape of 5-35 μm in size.

The film of starch and PVA was successfully fabricated by solution casting methods with the use of glycerol as a plasticizer and citric acid as the crosslinking agent. The fabricated blends were transparent, flexible and smooth. The blend was physically bonded. The plasticizer and crosslinking agent help blend to increase flexibility. The physically bonded blend is easily affected by moisture, temperature and air. -OH groups on starch and PVA formed hydrogen bonding interactions, which could improve the compatibility of the two components. As compared to pure polyvinyl, the melting point of the blend was decreased and the blend was found degradable in nature.

Acknowledgements

I am very much thankful to the National Potato Research Project (NPRP) of Nepal Agricultural Research Council (NARC), Khumaltar, Lalitpur, Nepal for their assistance with the collection of samples. I would like to express my sincere thanks to Dr. Khaga Raj Sharma (Central Department of Chemistry, Tribhuvan University, Kirtipur, Nepal for his assistance with FTIR. I would like to express my gratitude to Associate Professor Dr. Mirsolav Slouf (Institute of Macromolecular Chemistry, Czech Academy of Sciences, Czech Republic) and Dr. Jakub Sirc, (Institute of Polymer Networks and Gels, Czech Republic) for their great help in scanning electron microscope (SEM). I am greatly thankful to Dr. Vimal

Katiyar and Ms. Neha Mulchandani (Indian Institute of Technology, Guwahati, India) for the Differential Scanning Calorimetry (DSC). I would also like to acknowledge Dr. Rajesh Pandit, Department of Chemistry, Tri-Chandra Multiple Campus, Kathmandu for the data interpretation of DSC.

References

1. B. Ghanbarzadeh, H. Almasi and A. A. Entezami, Improving the barrier and mechanical properties of corn starch-based edible films: Effect of citric acid and carboxymethyl cellulose, *Industrial Crops and Products*, 2011, **33**, 229-235. (DOI: org/10.1016/j.indcrop.2010.10.016).
2. X. Tang and S. Alavi, Recent advances in starch, polyvinyl alcohol based polymer blends, nanocomposites and their biodegradability, *Carbohydrate Polymer*, 2011, **85**, 7-16. (DOI: org/10.1016/j.carbpol.2011.01.030).
3. H. Tian, J. Yan, A. V. Rajulu, A. Xiang and X. Luo, Fabrication and properties of polyvinyl alcohol/starch blend films: Effect of composition and humidity, *Journal of Biological Macromolecules*, 2017, **96**, 518-523. (DOI: 10.1016/j.ijbiomac.2016.12.067).
4. Z. Zhu and W. Guo, Frequency, moisture content, and temperature dependent dielectric properties of potato starch related to drying with radio-frequency/microwave energy, *Scientific Reports,* 2017, **17**, 1-11. (DOI:10.1038/s41598-017-09197-y).
5. C. Menzel, E. Olsson, T. S. Plivelic, R. Andersson, C. Johansson, R. Kuktaite, L. Jarnstrom and K. Koch, Molecular structure of citric acid cross-linked starch films, *Carbohydrate Polymer,* 2013, **96**, 270-276. (DOI: 10.1016/j.carbpol.2013.03.044).
6. P. A. Sreekumar, M. A. Al-Harthi and S. K. De, Effect of glycerol on thermal and mechanical properties of polyvinyl alcohol/starch blends, *Journal of Applied Polymer Science*, 2012, **123**(1): 135-142. (DOI: 10.1002/app.34465).
7. R. Nagarkar and J. Patel, Polyvinyl alcohol: A comprehensive study, *Acta Scientific Pharmaceutical Sciences*, 2019, **3**(4), 34-44.
8. L. T. Sin, W. A Rahman, A. R. Rahmat and A. A. Samad, Computational modeling and experimental infrared spectroscopy of hydrogen bonding interactions in polyvinyl alcohol-starch blends, *Journal of Polymer*, 2010, **51**, 1206-1211. (DOI: 10.1016/j.polymer.2010.01.021).
9. L. J. Mao, S. Imam, S. Gordon, P. Cinelli and E. Chiellini, Extruded cornstarch-glycerol-polyvinyl alcohol blends: mechanical properties, morphology, and biodegradability, *Journal of Polymers and the Environment*, 2000, **8**(4), 205–211.
10. F. W. Bai, W. A. Anderson and M. Moo-Young, Research review paper: Ethanol fermentation technologies from sugar and starch feed stocks, *Biotechnology Advances*, 2008, **26**, 89– 105. (DOI: 10.1016/j.biotechadv.2007.09.002).
11. L. Jamai, K. Ettayebi, E. J. Yamani and M. Ettayebi, Production of ethanol from starch by free and immobilized *Candida tropicalis* in the presence of α-amylase, *Bioresource Technology*, 2007, **98**(14), 2765–2770. (DOI: 10.1016/j.biortech.2006.09.057).
12. K. Tadasa and K. Takeda, Anaerobic digestion of raw starch by *Bacillus species, Journal of Fermentation Technology*, 1986, **64**(1), 81-85. (DOI: 10.1016/0385-6380(86)90062-2).
13. H. Yang and J. Shen, Effect of ferrous iron concentration on anaerobic bio-hydrogen production from soluble starch, *International Journal of Hydrogen Energy*, 2006, **31**(15), 2137-2146. (DOI: 10.1016/j.ijhydene.2006.02.00).
14. T. Amon, B. Amson, V. Karyvoruchko, A. Machmuller, K. Hopfner-Sixt and V. Bodiroza, W. Zollitsch, Methane production through anaerobic digestion of various energy crops grown in sustainable crop rotations, *Bioresource Technology*, 2007, **98**(17), 3204-3212. (DOI: 10.1016/j.biortech.2006.07.007).
15. E. Grinzato, G. Cadelano and P. Bison, Moisture map by IR thermography, *Journal of Modern Optics*, 2010, **57**, 1770-1778. (DOI: 10.1080/09500341003731597).
16. E. Chiellini, A. Corti and R. Solaro, Biodegradation of poly(vinyl alcohol) based blown films under different environmental conditions, *Polymer Degradation and Stability,* 1999, **64**, 305–312.

(DOI: 10.1016/S0141-3910(98)00206-7).

17. L. Chen, S. H. Iman, T. M. Stein, S. H. Gordon, C. T. Hou and R. V. Greene, Starch-polyvinyl alcohol cast film-performance and biodegradation, *Polymer Preprints,* 1997, **37**, 461–462.
18. M. A. Russo, C. O'Sullivan, B. Rounsefell, P. J. Halley, R. Truss and W. P. Clarke, The anaerobic degradability of thermoplastic starch: Polyvinyl alcohol blends: Potential biodegradable food packaging materials, *Bioresource Technology,* 2009, **100**, 1705-1710. (DOI: 10.1016/j. biortech.2008.09.026).
19. W. L. Chai, J. D. Chow, C. C. Chen, F. S. Chuang and W. C. Lu, Evolution of biodegradability polyvinylalcohol/starch blends: A methodological comparison of environmentally friendly materials, *Journal of the Polymers and the Environment*, 2009, **17**, 71–82. (DOI: 10.1007/s10924-009-0123-1).
20. P. Cinelli, E. Chiellini, S. H. Gordon and S. H. Imam, Characteristics and degradation of hybrid composite films prepared from PVA, starch and lignocellulosics, *Macromolecular Symposia*, 2003, **197**, 143–155. (DOI: 10.1002/ masy.200350714).
21. S. Tang, P. Zou, H. Xiong and H. Tang, Effect of nano-SiO_2 on the performance of starch/ polyvinyl alcohol blend films, *Carbohydrate Polymers,* 2008, **72**, 521–526. (DOI: 10.1016/j. carbpol.2007.09.019).
22. M. C. Pascu, M. C. Popescu and C. Vasile, Surface modification of some nanocomposites containing starch, *Journal of Physics D: Applied Physics,* 2008, **41**, 1–12. (DOI: 10.1088/0022-3727/41/17/175407/meta).
23. R. Shi, J. Bi, Z. Zhang, A. Zhu, D. Chen, X. Zhou, L. Zhang and W. Tian, Ageing of soft thermoplastic starch with high glycerol content, *Carbohydrate Polymer,* 2008, **72**, 763-770. (DOI: 10.1002/app.25193).
24. M. M. Hashem, W. Kesting, A. A. Hebeish, N. Y. Abou-Zeid and E. Schollmeyer, Characterization and application of poly(vinyl alcohol)/starch composite as a sizing agent, *Die Angewandte Makromolekularechemie,* 1996, **241**, 149–163. (DOI: 10.1002/apmc.1996.052410112).
25. O. Vilpoux and L. Avérous. Starch-based plastics. In M. P. Cereda, and O. Vilpoux (Eds.), Technology, use and potentialities of Latin American starchy tubers, *NGO Raízes and Cargill Foundation, São Paolo – Brazil*, 2004, **18,** 521–553.
26. J. Singh and N. Singh, Studies on the morphological, thermal and rheological properties of starch separated from some Indian potato cultivars, *Food Chemistry,* 2001, **75**, 67-77. (DOI: 10.1016/S0308-8146(01)00189-3).
27. AOAC, *Official Methods of Analysis*, Association of official analytical chemist (AOAC), Washington, DC, 2000.
28. N. A. Azahari, N. Ohtman and H. Ismail, Biodegradation studies of poly(vinylalcohol)/ corn starch blend films in solid and solution media, *Journal of Physiological Science*, 2011, **22**, 15-31.
29. A. N. Jyothi, K. S. Kiran, B. Wilson, S. N. Moorthy and B. Nambisan, Wet storage of cassava starch: use of sodium metabisulphite and acetic acid and the effect on starch properties, *Starch–Stärke,* 2007, **59**, 141–148. (DOI: 10.1002/ star.200600583).
30. I. R. M. Benesi, M. T. Labuschagne, A. G. O. Dixon and N. M. Mahungu, Stability of native starch quality parameters, starch extraction and root dry matter of cassava genotypes in different environments, *Journal of the Science of Food and Agriculture*, 2004, **84**, 1381–1388. (DOI: 10.1002/jsfa.1734).
31. R. Joseph, H. H. Yeoh and C. S. Loh, Induced mutations in cassava using somatic embryos and the identification of mutant plants with altered starch yield and composition, *Plant Cell Reports*, 2004, **23**, 91-98. (DOI: 10.1007/s00299-004-0798-7).
32. V. Olomo and O. Ajibola, Processing factors affecting the yield and physicochemical properties of starch from cassava chips and flour, *Starch–Stärke*, 2003, **55**, 476–481. (DOI: 10.1002/ star.200300201).
33. I. R. M. Benesi, M. T. Labuschagne, L. Herselman, N. M. Mahungu and J. K. Saka, The effect of genotype, location and season on cassava starch

extraction, *Euphytica,* 2008, **160**, 59–74. (DOI: 10.1007/s10681-007-9589-x).

34. A. T. Osunsami, J. O Akingbala and G. B. Oguntimein, Effect of storage on starch content and modification of cassava starch, *Starch–Stärke,* 1989, **41**, 54–57. (DOI: 10.1002/star.19890410205).
35. F. Meuser, H. D. Smolnik, C. Rajani and H. G. Giesemann, Comparison of starch extraction from tapioca chips, pellets and roots, *Starch–Stärke*, 1978, **30,** 299–306. (DOI: 10.1002/star.19780300904).
36. J. C. Pérez, J. I. Lenis, F. Calle, N. Morante, T. Sánchez, D. Debouck and H. Ceballos, Genetic variability of root peel thickness and its influence in extractable starch from cassava (*Manihot esculenta Crantz)* roots, *Plant Breeding,* 2011, **130**, 688–693. (DOI: 10.1111/j.1439-0523.2011.01873.x).
37. S. S. Nielsen, *Food Analysis*, 2nd Ed. Aspon Publication, Maryland, 1998, 40-250.
38. E. Nuwamanya, Y. Baguna, E. Wembabazi and P. Rubaihayo, A comparative study of the physicochemical properties of starches from root, tuber and cereal crops, *African Journal of Biotechnology*, 2011, **10**(56), 12018–12030. (DOI: 10.5897/AJB10.2310).
39. A. Uba, T. Izuagie, L. G. Hassan, M. Achor and D. M. Sahabi, Charaterization of starch isolated from Mangifera indica seeds, *Nigerian Journal of Basic and Applied Science*, 2011a, **19**(2), 224-230.
40. R. Hoover, T. Hughes, H. J. Chung and Q. Liu, Composition, molecular structure, properties, and modification of pulse starches: A review, *Food Research International,* 2010, **43**, 399–413. (DOI: 0.1016/j.foodres.2009.09.001).
41. K. S. Sandhu and N. Singh, Some properties of corn starches II: Physicochemical, gelatinization, retrogradation, pasting and gel textural properties, *Food Chemistry,* 2007, **101**, 1499-1507. (DOI: 10.1016/j.foodchem.2006.01.060).
42. Y. Yuan, L. Zhang, Y. Dai and J. Yu, Physicochemical properties of starch obtained from *Dioscorea nipponica* Makino comparison with other tuber starches, *Journal of Food Engineering*, 2007, **82**, 436-442. (DOI: 10.1016/j.jfoodeng.2007.02.055).
43. A. H. D. Abdullah, S. Chalimah, I. Primadona and M. H. G. Hanantyo, Physical and chemical properties of corn, cassava, and potato starchs, *Earth Environmental Science*, 2018, **160**, 012003. (DOI: 10.1088/1755-1315/160/1/012003).
44. J. Wang, K. Guo, X. Fan, G. Feng and C. Wei, Physicochemical properties of C-type starch from root tuber of Apios fortunei in comparison with maize, potato, and pea starches, *Molecules*, 2018, **23**, 2132. (DOI: 10.3390/molecules23092132).
45. S. Pokhrel, R. Adhikari and P. N. Yadav, Fabrication and characterization of biodegradable poly(vinyl alcohol)/chitosan blends, *Asian Journal of Chemistry,* 2017, **29**, 1602-1606. (DOI: 10.14233/ajchem.2017.20612).

JNCS
Journal of Nepal Chemical Society December 2019, Vol. 40, 67-72
ISSN: 2091-0304 (print)
DOI: https://doi.org:10.3126/jncs.v40i0.27285
RESEARCH ARTICLE

Extraction of Silica Nanoparticles from Rice Husk Ash (RHA) and Study of Its Application in Making Composites

Bimal Kumar Raut, Khim Prasad Panthi*

Department of Chemistry, Tri-Chandra Multiple Campus, Tribhuvan University, Kathmandu, Nepal

Corresponding E-mail: khimcdc@gmail.com

(Received: Sept. 30, 2019; Revised: Dec. 24, 2019 & Accepted: Dec. 29, 2019)

Abstract

Nanotechnology is the most emerging field in the area of different scientific research. Various methods of synthesis of nanoparticles are available. The wet chemical synthesis method is applicable in the extraction of silica nanoparticles from Rice Husk Ash (RHA). Rice husk is a form of waste product from the rice milling industries which is produced in an abundance amount in and around the country. Rice husk which is generally left on the field as a waste contains 60% silica content and can be economically viable raw materials for the extraction of silica [1-2]. Initially, Rice husk was burnt to obtain its ash. Then, a simple bottom-up approach, the sol-gel method was applied, and fine powder silica in the nanoscopic range was extracted. After extraction of it, internal arrangement and average particle size were recognized by XRD while molecular components and structure present in silica were identified by FTIR. The obtained silica was then used in making of ceramics matrix nanocomposites (particularly silica-sand cement block), and its mechanical properties were identified by compressive strength test using Instron testing machine which was found to be increased in comparing with the compressive strength of ceramics composite (Sand cement block) prepared in the same ratio and same size of mold as that of ceramics matrix nanocomposites. The ceramics matrix nanocomposites acquiring higher mechanical strength than Ceramics composite occurred due to the incorporation of Silica nanoparticles.

Keywords: Rice husk, sol-gel method, ceramics matrix nanocomposites, ceramics, composite, silica nanoparticles

Introduction

The project work was carried out with an objective to extract silica nanoparticles from rice husk ash (RHA), the silica content in rice husk ash and to prepare composite using extracted silica nanoparticles to find out whether nanoparticles affect in mechanical properties of composite or not. Nanoparticles are nanomaterials having all three dimensions in the range of 1-100 nm [3]. All nanoparticles are nanomaterials but not all nanomaterials are nanoparticles. Nanomaterials are materials having at least one of their dimensions in the range of 1-100 nm. This range is called nanoscale.

Rice is the second most widely consumed food item globally, with rice paddy production registering about 758 million metric tons in 2070, a number that will increase gradually due to the projected demand of the world population [4]. The RHA is an agricultural waste, which is generally used as ameliorants to break up clay soils and improved soil structure but is also used for the production of silica. The properties of RHA depend on the ecological circumstances of its origin as well as the process applied for burning the husk [5]. Silica which is the constituents of silicon and oxygen has the molecular formula SiO_2. Silica has been widely used in vegetable oil refining, pharmaceutical products, detergents, adhesive, chromatograph column planning and ceramics [6-8]. Not only this, silica is also found to be used in water purification, vulcanizing rubber, control of insect pests, in stored food stuffs, manufacturing refractory bricks, and as admixture in low cost concrete block manufacturing [9].

Abundantly available waste RHA has been widely used as raw materials for the preparation of silica gel

and powder following (Kamath and Protocor, 1998) [1].

Nanoparticles exhibit attractive properties such as low thermal expansion, high mp, high thermal stability, high thermal resistance and chemical stability [10,11]. The interfacial area that creates a significant volume fraction of the interfacial polymer with the properties different from bulk polymer even at low filter loadings [12,13]. Several researchers have studied the effect of particle size and volume fraction on the mechanical response of composite [14-18]. However, among the numerous polymer composites; silica polymer nanocomposites are most commonly reported in the literature and are also employed in variety of applications, such as electronics, automotive and aerospace industries as well as used in many industrial products due to their good mechanical characteristics [19].

Ceramics is defined as the solid materials that are not metal, plastic, or derived from plants or animals [20]. Ceramics have some distinctive properties including good chemical inertness, high temperature stability brittleness, high mp and an electrical insulation capability [21]. Furthermore, Chemical bonding (both covalent and non covalent) between filler and a polymer improves materials compatibly, and thus enhances certain properties of matrix above and beyond what is accomplished by single doping with filler [22-24]. Using similarly sized dopant and matrix elementary building blocks may have certain distinctive advantages [25].

Materials and Methods

Chemicals used: Distilled water, 1N NaOH, 1N HCl

Apparatus used: Beaker, conical flask, burner, wire gauze, magnetic stirrer, filter paper (Whatmann 41), hot air oven

Preparation of chemical reagents

Preparation of 1N NaOH

Mass of NaOH required (w) = NEV/1000

Where, N= Normality, E= Equivalent wt.,

V=Volume required in mL

For 600 mL, mass of 1N NaOH required was 24 g. It was taken in a volumetric flask and little amount of distilled water was added to dissolve it. After it got fully dissolved, distilled water was added upto the mark of 600 mL.

Preparation of 1N HCl

As concentrated HCl has approximately strength of 36%, its normality calculated to be 11.6 N by using the following formula:

$$\text{Normality} = \frac{(\%\text{ by mass x specific gravity x } 10)}{\text{Equivalent weight}}$$

Where, % by mass = 36
Specific gravity = 1.1789
Equivalent weight = 36.5

For 200 mL of 1 N dilute HCl, 17.24 mL of concentrated HCl was added up to 200 mL of distilled water. It was calculated by the following way:

$$\underset{\text{(Conc. HCl)}}{V_1N_1} = \underset{\text{(1 N Dil. Hcl)}}{V_2N_2}$$

Where, V_1 = Volume of concentrated HCl to be calculated

N_1 = Normality of Concentrated HCl (11.6 N)

V_2 = Volume of dilute HCl to be prepared (200 mL)

N_2 = Normality of dilute HCl (1 N)

Preparation of rice husk ash from rice husk

Rice Husk was collected from the nearest Rice milling industry, which was then burnt and converted into ash. The ash converted was then made into fine powder.

Extraction of silica from rice husk ash

This was done by Sol-gel method. In this method, 50 g RHA was weighed and dispersed in 300 mL of distilled water in a beaker. The pH of solution maintained at 7 by testing with litmus paper. The solution was then stirred by magnetic stirrer for 2 hours.

It was then filtered by Whatmann 41 filter paper and the residue was washed with 500 mL of water.

The residue was then dispersed in 300 mL 1N NaOH and boiled with constant stirring for 1 hour. It was then filtered through whatmann 41 filter paper. The residue was then washed with 500 mL boiling water. The filtrate was collected and allowed to cool. Then, the filtrate was titrated with 1N HCl till the pH of filtrate became neutral.

When pH of filtrate became 7, gel obtained. The gel was allowed to age for 18 hours. After 18 hours, 500 mL of distilled water was added into volumetric flask containing gel and crushed the gel. After crushing the

gel, the solution was left for some time, later which two layers were seen. Upper layer comprised of water called supernatant and lower layers consisted of gel.

The supernatant was discarded by the help of dropper and the washing process was repeated for 3 more times. The gel obtained after removing supernatant was kept in an oven for 18 hours at 80 degree Celsius. The gel produced called xerogels, which was then kept in air tight plastic bottle.

The method applied following (Kamath and Protocor, 1998) [1] can be explained step wise as:

Preparation of ceramics matrix nanocomposites (CMNs)

The CMNs, silica-sand cement block was prepared. For this purpose, the extracted silica from RHA was mixed to the sand cement mixture, which is believed to increase the mechanical property. Firstly extracted silica, sand and cement were mixed in the porcelain basin in the ratio of 1:4:1. Then, distilled water (generally 26-33% of the total weight of mixtures) was added on it till the required texture was obtained. After then, it was framed in a 2 cm cube mold and the curing process was done by immersing the block in distilled water. As 3 days strength test was followed, the blocks were removed from distilled water after low-cost days and allowed it to dry, free from any moisture. The compressive test of the block was then done.

Ceramics composites

The preparation method was the same as that of CMNs, silica-sand cement block. The only difference is that silica nanoparticles were not added to cement and sand.

In this process, sand and cement were taken in the porcelain basin in the ratio of 4:1 and mixed properly. Then distilled water was added till the required texture was obtained. After then, framing was done in 2 cm cube mold. Like the preparation of the ceramics matrix nanocomposite block, the curing process and strength testing procedure of the ceramics composite block was done by the same method.

The main purpose behind the preparation of ceramics composite was to find the difference between mechanical strength of ceramics matrix nanocomposite block containing nanoparticles (silica-sand cement block) and the ceramics composite block without nanoparticles (sand cement block).

Results and Discussion

FTIR analysis

The FTIR of silica nanoparticles shows various peaks as a result of the absorption of light of a wavelength in infra red region. From the graph of Transmittance% vs. wave number per cm, it is cleared that rocking vibration occurs at 800cm-1. Similarly; Si-O asymmetrical stretching vibration occurs at 1068 $cm^{-1.}$

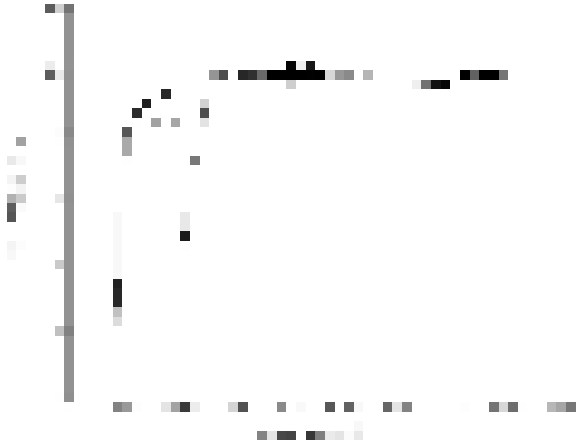

Figure 1: *FTIR of silica nanoparticles*

Some very small peaks are due to instrumental error but chemists found it as a result of carbon dioxide.

Table 1: *FTIR data sample containing silica nanoparticles*

S. N.	Wave number cm^{-1}	Description
1.	800	Rocking vibration
2.	1068	Si-O-Si asymmetrical stretching vibration

XRD analysis

Confirmation of the effectiveness and the size of silica nanoparticles were provided by X-ray studies (XRD). The center of peak and the value of FWHM required to calculate the size of nanoparticles was determined by using origin software.

On the basis of X-ray curves, Lorentzian fitting was done. It is intended to a one-mode system and believes to describe a decaying system over time. The data of XRD (two theta degree value vs. intensity) was copied into origin software. Then, two strong peaks were selected efficiently and analyzed in multi-peaks fitting. As mentioned above, Lorentzian fitting was done which then by double-clicking on the center of peaks gave the value of angle of the center of peak (2θ) and the FWHM value.

The center of peak and FWHM value on using origin software found to be 32.10910 and 0.37580. The value of θ calculated by dividing the center of the peak by 2 and FWHM value was then converted into radian which found to be 6.55×10-3. The wavelength used was 1.5406Å and Scheerer's constant value (κ) used was 0.94. Thus, by using Scheerer's formula, the size of the particle was determined.

$$D = K\lambda / \beta Cos\theta$$

Thus, putting all the values, the particle size was found to be 23 nm.

Figure 2: *XRD of silica nanoparticles*

Compressive test

At first, the cross-sectional area and the breaking load of both the blocks, ceramics matrix nanocomposite (containing silica nanoparticles), and another ceramics composite (without silica nanoparticles) were measured and their value was found to be:

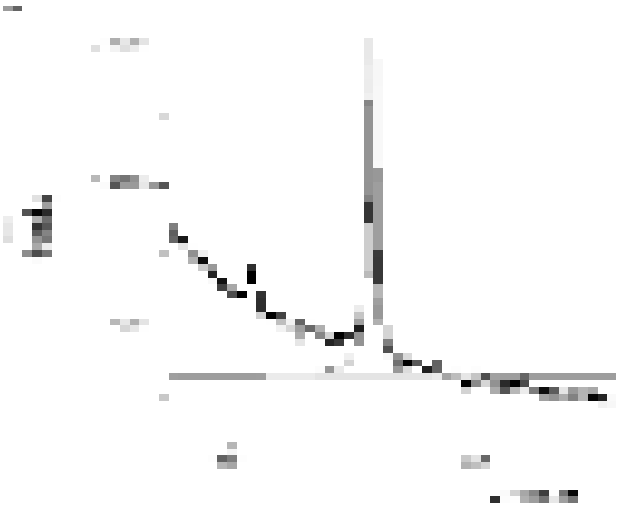

Figure 3: *Lorentzian fitting for prominent peak of silica nanoparticles*

Table 2: *Cross-sectional area and breaking load of blocks*

Block	Cross-sectional Area(cm^2)	Breaking load(N)
Ceramics Matrix Nanocomposite block	4	40
Ceramics Composite block	4	24

Thus, by putting the value in a formula,

$$\text{Compressive strength} = \frac{\text{Breaking load}}{\text{Cross-sectional area}}$$

It was found that the compressive strength of block containing silica nanoparticles (ceramics matrix nanocomposite) was 10N/cm^2 and 6 N/cm^2 for the block having no silica (ceramics composite).

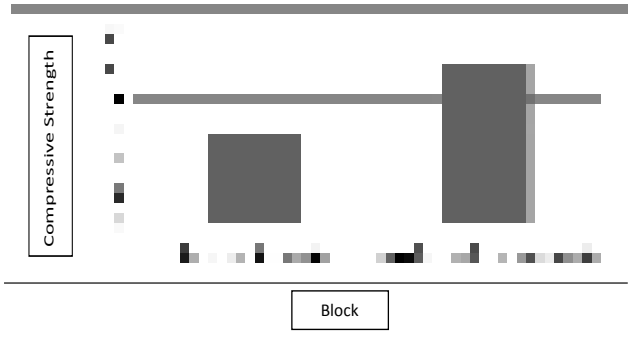

Figure 4: *Bar Diagram showing the result of compressive test*

Conclusion

Silica nanoparticles were synthesized from Rice Husk Ash (RHA) by using the sol-gel method. The synthesized silica nanoparticles found to be 26 g (52%), which is almost equal to 60% and seems to follow the citation [1,2]. The Silica nanoparticles were characterized by spectroscopic techniques like FTIR and XRD. As per the result of XRD, the particle size was found to be 23 nm. By analyzing the data of FTIR, rocking vibration, and Si-O-Si asymmetrical stretching vibration was found. Similarly, synthesized silica nanoparticles were then incorporated in sand cement mixture in 1:4:1 ratio to prepare ceramics matrix nanocomposite block. In the same way, ceramics composite block was also prepared where silica nanoprticles were not incorporated in the sand-cement mixture. The mechanical property of prepared blocks was characterized by compressive strength test using the Instron testing machine. As per the result of compressive test, the ceramics matrix nanocomposite block containing the silica nanoparticles found to have almost 1.67 times greater strength than the ceramics composite block containing no silica. This proves that silica nanoparticles enhances the mechanical strength and hence it can be used in several construction materials.

Acknowledgements

I would like to thank my friend Dipa Aryal, Krishna G. C. and Hemraj Upadhyay. I am very thankful to Dr. Suresh Dhungel, Senior Scientist at NAST, Assoc. Prof. Dr. Surendra Kumar Gautam, Department of Chemistry, Tri-Chandra Multiple Campus and Asst. Prof. Achyut Adhikari, Central Department of Chemistry, Tribhuvan University. This work was carried out at the lab of Tri-Chandra Multiple Campus, Ghantaghar, Kathmandu. XRD was carried out at NAST, Satdobato. FTIR was carried out in the Central Department of Chemistry, Kirtipur. The mechanical property was tested in the Soil Lab of Pulchowk Engineering Campus. I am thankful to all of them.

References

1. S. R. Kamath and A. Proctor, Silica gel from rice husk ash: preparation and characterization, *Cereal Chemistry*, 1998, **75**, 484-487.
2. A. Chakraverty and S. Kalemullah, Conversion of rice husk into amorphous silica and combustible gas, *Energy Consers. Mgmt*., 1991, **32**, 565-570.
3. S. K. Murthy, Nanoparticles in modern medicine: State of the art and future challenges, *International Journal of Nanomedicine,* 2007, **2**(2), 129-141.
4. K. S. Lokare, Rising from the ashes: renewable silica from rice husk ash, *Advanced BioFuels USA*, 2017.
5. M. R. F. Gonzlaves and C. P. Bergmann, Thermal insulators made with rice husk ashes: production and correlation between properties and microstructure, *Constr. Build Materials*, 2007, **21**(12), 2059-2065.
6. C. J. Brinker and G. W. Scherer, *Applications. in: sol-gel science, the physics and chemistry of sol-gel processing*, Academic Press, San Diego, CA, 1990, 839-880.
7. R. K. Iler, S*ilica gels and powders, The Chemistry of Silica,* 1979, 462-599.
8. A. Proctor, P. K. Clark and C. A. Parker, Rice hull ash adsorbent performance under commercial soy soil bleaching conditions, *Journal of the American Oil Chemists' Society*, 1995, **72**, 459-462.
9. U. Kalapathy, A. Proctor and J. Shultz, A simple method for production of pure silica from rice hull ash, *Bioresource Technology,* 2000, **73**, 257-262.
10. W. K. Kriven, J. F. Siah, M. Schmucker et al., High temperature microhardness of single crystal, *Journal of the American Ceramic Society*, 2004, **87**(5), 970-972.
11. R. R. Tumalla, Development of high performance interfill material for system chip technology, *Journal of the American Ceramic Society*, 1991, **74**(2), 895-899.
12. A. C. Balazas, T. Emrick and T. P. Russel, Nanoparticle polymer composites, Where two small world meet, *Science*, 2006, **314**, 1107-1110.
13. R. Krishnamoorti and R. A. Vaia, Polymer nanocomposites, *Journal of Polymer Science Part B-Polymer Physics*, 2007, **45**, 3252-3256.

14. A. C. Moloney, H. H. Kausch and H. R. Stieger, The fracture of particulate filled epoxide-resins. *Journal of Material Science*, 1984, **19**, 1125-1130.

15. M. Frounchi, T. A. Westgate, R. P. Chaplin and R. P. Burford, Fracture of polymer networks based on diethylene glycol bis(allyl carbonate), *Polymer*, 1994, **35**, 5041-5045.

16. F. Stricker, Y. Thomann and R. Mulhaput, Influence of rubber particle size on mechanical properties of polypropylene-SEBS blends, *Journal of Applied Polymer Science*, 1998, **68**, 1891-1901.

17. R. T. Quazi, S. N. Bhattacharya and E. Kosior, The effect of dispersed paint particles on the mechanical properties of rubber toughened polypropylene composites, *Journal of Material Science*, 1999, **34**, 607-614.

18. A. Boonyapookana, K. Nagata and Y. Mutoh, Fatigue crack growth behavior of silica particulate reinforced epoxy resin composite, *Composite Science and Technology,* 2011, **71**, 1124-1131.

19. A. Moisala, Q. Li, I. A. Kinloch and A. H. Windle, Thermal and electrical conductivity of single and muti-walled carbon nanotube epoxy composites, *Composites Science and Technology*, 2006, **66**, 1285-1288.

20. D. W. Richerson, The Magic of Ceramics, *American Ceramic Society,* Wiley 2012, 2nd Ed.

21. M. N. Rahaman, *Ceramic Processing and Sintering*. Marcel Dekker, New York, 2003, 2nd Ed., 1-2.

22. Y. Chen and J. O. Iroh, *Chemistry of Materials,* 1999, **11**, 1218.

23. Z. Ahmad and, J. E. Mark, *Chemistry of Materials*, 2001, **13**, 3320.

24. S. Campbell and D. Scheiman, *High Performance Polymers*, 2002, **14,** 17.

25. C. A. Mitchell, J. L. Bahr, S. Arepalli, J. M. Tour and R. Krishnamoorti, *Macromolecules*, 2002, **35**, 8825.

26. D. Rolison, *Science*, 2003, **299,** 1698.

JNCS
Journal of Nepal Chemical Society December 2019, Vol. 40, 73-77
ISSN: 2091-0304 (print)
DOI: https://doi.org:10.3126/jncs.v40i0.27286
RESEARCH ARTICLE

Dielectric Phase Transition Behaviour Study of Dry Route Derived $(Ba_{0.5}\ Sn_{0.5})\ TiO_3$ Ceramics

Bhojraj Bhandari[1*], Bhadra Prasad Pokheral[2]

[1]Department of Physics, Goldengate International College, Kathmandu, Nepal

[2] Pulchowk Engineering Campus, Institute of Engineering, Tribhuvan University, Pulchowk, Lalitpur, Nepal

**Corresponding E-mail: boydbhandari@gmail.com*

(Received: Sept. 21, 2019; Revised: Dec. 13, 2019 & Accepted: Dec. 15, 2019)

Abstract

Ceramic materials display a wide range of properties that facilitate their use in many different product areas. Currently, there has been keen interest in the field of ceramic materials due to their excellent mechanical and physical properties. Barium Stannate Titanate (BST) is a binary solid solution system composed of ferroelectric Barium titanate and non-ferroelectric barium titanate. In this study, the phase transition behavior of $(Ba_{1-x}Sn_x)$ TiO_3 (x = 0.5) (BST) ceramics was obtained by the dry-route method. The previous studies were based on Sn^{2+} on the Ti site with varying values of x. The powders after calcination are compacted in the form of pellets using a hydraulic press at an optimized load above 70 KN. The experimental density of our sample measured by liquid displacement method with glycerin was lower than theoretical density, giving the shape is highly dense with low porosity. The structure shows that on increasing the Sn^{2+} content volume decreases due to the size of Sn^{2+}, which is smaller than that of Ba^{2+}, in comparison to $BaTiO_3$. As the demand of lead-free environment-friendly sensor is increasing, thus obtained BST has great applications as a sensor material in modern electronic devices.

Keywords: Porosity measurement, phase transitions, dielectric property, Curie-Wiess law

Introduction

The development of Science & technology unified people all over the world like a single-family. While discussing with research and innovation, scientists as well as researchers have been attracted to those materials which are convenient, economical and more applicable. During the last few decades, people are being attracted to other materials rather than metals, like ceramic, polymer glass etc.

The word ceramics derived from the Greek word keramikos [1]. A ceramic is an inorganic, non-metallic solid prepared by the action of heat and subsequent cooling. Ceramic materials may have a crystalline or partly crystalline structure, or may be amorphous (e.g., a glass). Because most common ceramics are crystalline, the definition of ceramic is often restricted to inorganic crystalline materials, as opposed to the non-crystalline glasses. The earliest ceramics were pottery objects made from clay, either by itself or mixed with other materials. This clay is often times fired in a kiln and then glazed and re-fired to create a colored, smooth surface. Ceramics now include domestic, industrial and building products and art objects etc. In the 20th century, new ceramic materials were developed for use in advanced ceramic engineering; for example, in semiconductors, superconductors etc.

Ceramic materials display a wide range of properties that facilitate their use in many different product areas. They are harder and stiffer than steel, more heat and corrosion resistant than metals or polymer's, less dense than most metals and their alloys; and their raw materials are both plentiful and inexpensive. Therefore, ceramics materials display a wide range of properties, which facilitate their use in many different product areas.

Everyday new and different applications have been discovered. Currently, there has been keen interest in the field of ceramic materials due to their excellent

mechanical and physical properties [2]. Electronic ceramics are very useful in device fabrication. The electronic ceramics, such as, barium titanate ($BaTiO_3$), lead titanate ($PbTiO_3$), lead zirconate ($PbZrO_3$) with ABO_3 perovskite structure show ferroelectric and anti-ferroelectric behaviors which are being used in many applications in electronics and optics. A large number of applications of these ceramic materials is the consequences of ferroelectric and anti-ferroelectric properties such as dielectric, piezoelectric, pyroelectric and electro-optic properties. Such properties can be improved and modified by chemical substitutions at A or B site of ABO_3 compounds [3].

Phase transitions of these materials involve a change in atomic as well as spin or electronic configuration and can change their physical properties quite drastically [2]. More commonly, phase transition can be brought about by a change in the temperature of a system. The ferroelectric and anti-ferroelectric phase transition in perovskite has been considerable interest due to their wide range of technological applications.

Barium stannate titanate (BST) is a binary solid solution system composed of ferroelectric barium titanate and non-ferroelectric barium titanate. Both of them are of perovskite structure with ABO_3. In this work, we have studied the phase transition behavior of $[Ba_{1-x}Sn_x]$ TiO_3 (for x = 0.5) ceramics obtained by the dry-route method.

Materials and Methods

The perovskite samples of pure and Sn doped Barium strontium Titanate synthesized $(Ba_{1-x}Sn_x)$ TiO_3 compositions containing Ba content, x = 0.50. All the samples were prepared using $BaCO_3$, $SnCl_2$ and TiO_2 with assay 100%, 99.7% and 99% respectively. These compositions in powder form were mixed in desired molar ratios in acetone. These solid mixtures were milled for 6 hours with acetone in an indigenously designed ball-mill to produce a final powder. The powder, thus formed, was dried and then calcinated in an aluminum crucible at 1100 °C for 4 hours. The powder added with 5% PVA (Polyvinyl alcohol) was compacted into disc-shaped pallets having diameter 1.32 cm using a hydraulic press at an optimized load in the range of 70N to 80N. Then, the pellets were sintered at 1300 ˚C for 5 hours. The density and porosity of the pellet were measured using the sample using the liquid displacement method (glycerin displacement). Finally, in order to measure the dielectric properties, the silver paste was painted on the polished ceramic samples as the electrodes and heated at 500 ˚C for 30 minutes. The dielectric properties are studied using the HIOKI 3532-50 LCR HITESTER. The instrument gives only the capacitances at a different frequency which were used to measure dielectric constant.

The synthesis of the BST ceramics and characterization following the dry-route method and outline as in Figure 1.

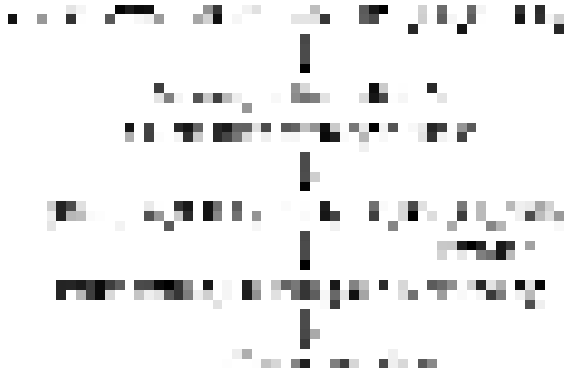

Figure 1: *Details of synthesis of $(Ba_{1-x}Sn_x)$ TiO_3 ceramics by dry route method*

Measurement/characterization techniques

Density and porosity measurement

The density is measured by the liquid displacement method. In the present experiment, glycerin (density 1.255 gm/cc at 20 ˚C) is used as liquid and digital balance is used for taking the weight of the sample and upthrust of the liquid. The whole process depends on the Archimedes principle. The density of the sample can be calculated by using the formula,

For the measurement of porosity, we have plotted a graph between soaking time and percentage densification.

Dielectric measurement

The dielectric properties of the sample are to be studied after electroding. HIOKI 353250 LCR HI-TESTER is used for the study of dielectric properties

using the dual-channel thermometer, temperature controller, sample holder and the instrument. The observed data are then used for the study in our experimental work. The instrument gives directly the capacitances at diferent frequency which are used to measure dielectric constant by the relation

[redacted]

Results and Discussion

Density and porosity measurement

The quality of the ceramic sample is reflected by the percentage of density and porosity. In this study, the weight of the sample in pellet form before electroding is taken by electronic balance which has the accuracy of ± 10^{-3} gm. Then the density of the sample is measured by liquid displacement method using glycerin of density 1.2600 gm/cc at 25 ˚C and of purity of 99.5%. A small amount of porosity is present in all ferroelectric ceramics and is usually considered a defect introduced due to processing imperfections; however, it may also be introduced deliberately to create a composite material system using porosity as a second component [4-6] to provide beneficial effective properties for specific applications. When such a sample is immersed into liquid, liquid molecules inter into the pores resulting in the increase in mass in the given volume. From the measurement of this increased mass, the porosity of the ceramic sample was measured.

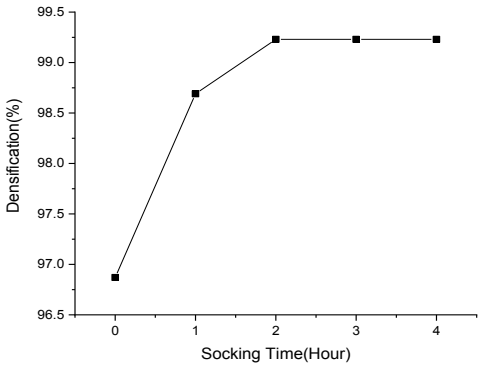

Figure 2: *The variation of densification vs soaking time*

We have measured the porosity of the sample in terms of percentage of density, in another sense, it also measures the amount of water absorbed by the pores of the sample in percentage.

Figure 2 indicates that our sample is more compact due to the carefulness of processing and the increase of doping percentage.

Ferroelectric to paraelectric phase transition

Figure 3 and Figure 4 show the variation of the real and imaginary part of dielectric constant with temperature during heating of BST50 at 100 KHz

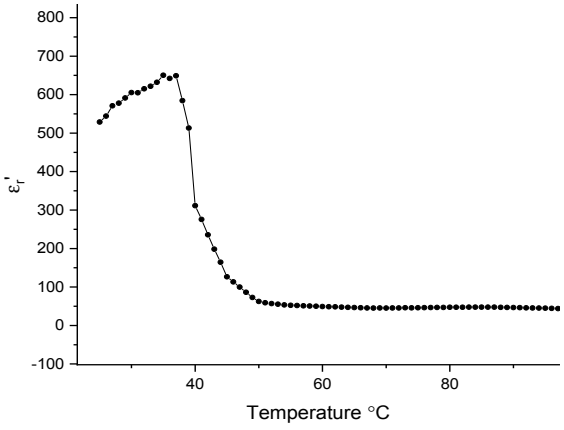

Figure 3: *The variation of real part of dielectric constant with temperature for BST50 at 100 KHz.*

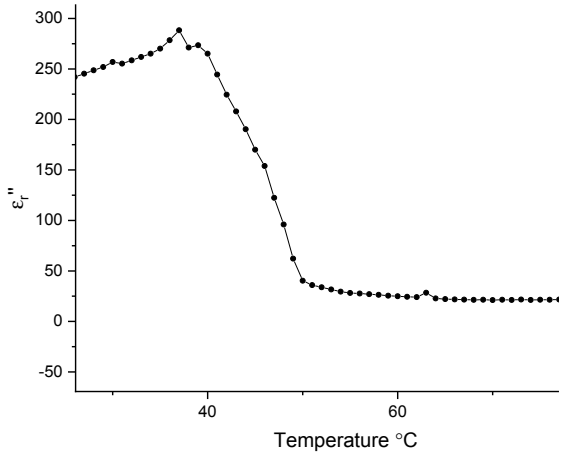

Figure 4: *The variation of imaginary part of dielectric constant with temperature for BST50 at 100 KHz.*

From these figures (iii) & (iv) it is seen that the ferroelectric to paraelectric phase transition occurs at temperatures 37.0934 °C during heating mode. The peak value of dielectric constants for heating mode is 660 whereas the corresponding value of dielectric constant at room temperature (25 °C) is 528.9268 [7].

Curie-Weiss Law

The dielectric constant of BST is known to exhibit Curie-Weiss behavior to temperatures very close to transition temperature [8]. The validity of Curie-Weiss law for BST sample is demonstrated in Figure 5 which depict the variation of dielectric stiffness ($\frac{1}{\varepsilon_r'}$) with temperature followed by the relation;

Where, C is Curie constant and T_0 is Curie temperature. From this figure, we have calculated the Curie constant using the slope of the fitted straight line

To confirm whether the transition is diffuse or regular type, we further use Curie-Weiss like relationship:

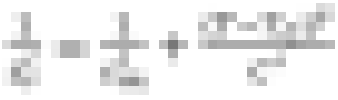

The Curie temperatures observed from the above plot for BST50 is 37 °C which is the intercept value of X-axis in the ε'_r versus temperature plot. The Curie temperature of our sample was less than that of transition temperature in the ferroelectric to paraelectric phase.

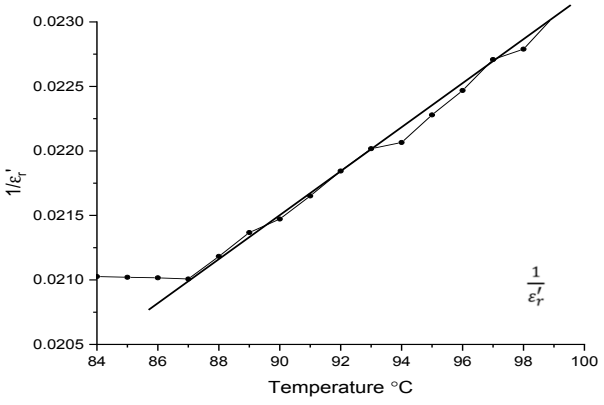

Figure 5: *The variation of dielectric stiffness* $\frac{1}{\varepsilon_r'}$ *with temperature for BST50 at 100 KHz.*

Cole-cole study

To check the polydisperse nature of dielectric relaxation of the dipole, a complex argand plot between ϵ'_r and ϵ''_r called Cole-Cole plot is used [9].

The Cole-Cole plot of electrical quantities of a material is a measure of the various relaxation times for a specific dielectric material.

The complex dielectric constant in such a situation is expressed by the empirical relationship

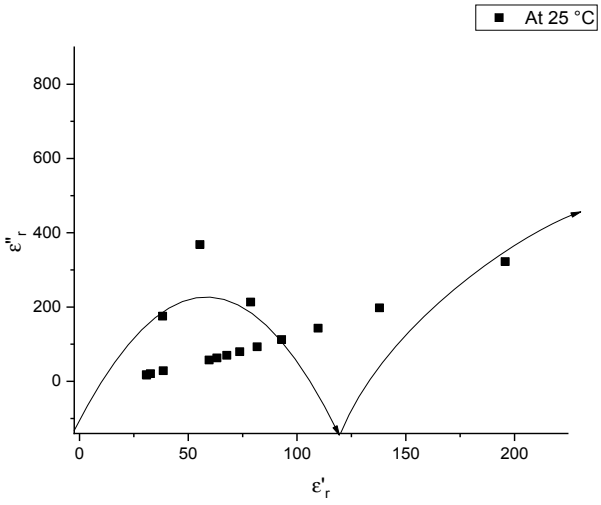

Figure 6: *Cole-Cole plot between* ϵ'_r and ϵ''_r *at 25 ºC.*

It is evident from Figure 6 that the nature of the Cole-Cole plot is changing with temperature. The nature of the curve is narrow semi-circular which indicates the polydisperse nature of our sample.

Conclusion

$(Ba_{1-x}Sn_x)TiO_3$ ( ) powders are prepared by a dry route method. The powders after calcination are compacted in the form of pellets using a hydraulic press at an optimized load above 70 KN. So, obtained pellets are then sintered and fired on silver paint for electroding. The sample thus formed is used for characterization. The main findings of the present work are summarized below:

1. The experimental density of our sample measured by the liquid displacement method with glycerin is 6.1246 gm/cc. whereas theoretical density is found to be 6.3224 gm/cc.

2. The shape is highly dense with low porosity.

3. The structure of BST50 is tetragonal and lattice parameters of the samples a = b = (3.86065$\pm$ 0.00051) Å, c = (4.10234$\pm$ 0.00160) Å and unit cell volume (V) = (61.1440$\pm$0.0206) $Å^3$ with tetragonality 1.063, which shows that on increasing the Sn^{2+} content volume decreases because the size of Sn^{2+} is smaller than that of Ba^{2+} , in comparison to $BaTiO_3$.

Acknowledgements

I owe a great thanks to a great many people who helped and supported me during the research of this work. I would also thank my family, friends, college faculties and Prof. Homnath Poudel (Head of Department of Physics GoldenGate International College) for their continuous support.

References

1. F. H. Riddle, Ceramic spark plug insulators, *Journal of the American Ceramic Society*, 1949, **32**(11), 333-46. (DOI:10.1111/j.1151-2916.1949.tb18909.x).

2. A. Krell, T. Hutzler and J. Klimke, *Journal of the European Ceramic Society*, 2009, **29**, 207-221 (DOI: 10.1016/j.jeurceramsoc. 2008.03.025)

3. T. E. Warner, *Synthesis, properties and mineralogy of important inorganic materials*, John Wiley & Sons, United Kingdom, 2012, 124-144.

4. T. G. Lupeiko and S. S. Lopatin, Old and new problems in piezoelectric materials research and materials with high hydrostatic sensitivity, *Inorganic Materials,* 2004, **40**(1), S19-S32. (DOI: 10.1023/B:INMA.0000036326.98414.3c).

5. R. Kar-Gupta and T. A. Venkatesh, Electromechanical response of porous piezoelectric materials, *Acta Materialia*, 2006, **54**(15), 4063-4078. (DOI: 1016/j.actamat.2006.04.037)

6. R. K. Gupta and T. A. Venkatesh, Electromechanical response of piezoelectric composites: Effects of geometric connectivity and grain size, *Acta Materialia*, 2008, **56**(15), 3810-3823. (DOI: 10.1016/j.actamat.2008.04.031)

7. B. P. Pokharel, Synthesis structure and phase transition behaviour of $(Pb_{1-x}Ba_x)ZrO_3$ ceramics, *Ph. D. Thesis*, Banaras Hindu University, Varanasi, India, 2000.

8. Y. Xu, *Ferroelectric materials and their applications*, 1st Ed. Elsevier Science Publishing Company, London, 1991, 11-15.

9. A. Chelkowski, *Dielectric Physics*, Elsevier Science Publishing Company, London, 1980, 117-123.

JNCS
Journal of Nepal Chemical Society December 2019, Vol. 40, 78-83
ISSN: 2091-0304 (print)
DOI: https://doi.org:10.3126/jncs.v40i0.27287
RESEARCH ARTICLE

Isotherms and Kinetic Studies on the Adsorption of Cd(II) onto Activated Carbon Prepared from Coconut *(Cocos nucifera)* Shell

Rajeshwar Man Shrestha*, Sahira Joshi

Department of Applied Sciences and Chemical Engineering, Pulchowk Engineering Campus, Institute of Engineering, Tribhuvan University, Pulchowk, Lalitpur, Nepal

Corresponding E-mail: rajeshwar@ioe.edu.np
(Received: Sept. 29, 2019; Revised: Dec. 23, 2019 & Accepted: Dec. 29, 2019)

Abstract

Activated carbon prepared Coconutshell using Phosphoric acid as an activating agent was investigated to find the feasibility ofits application for removal of Cd(II) from aqueous solution through the adsorption process. The activated carbon thus prepared has been characterized by SEM, XRD, FTIR. SEM morphology has revealed the pores of different diameters while FTIR showed the presence of surface functional groups such as carboxyl, phenolic and lactones. Batch mode kinetics and isotherm studies were carried out to evaluate the effects of contact time, adsorbent dose and pH. The optimum pH, contact time and adsorbent dose needed for the adsorption of the heavy metal have been found to be 6, 180 minutes and 2 g/L respectively. Langmuir and Freundlich isotherm models have been employed to analyze the adsorption equilibrium data. It was found that the adsorption isotherm of Cd(II) onto the activated carbon was the best described by Langmuir with an adsorption capacity of 33.71 mg/g. Kinetic studies showed that a pseudo second-order model was more suitable than the pseudo first-order model. It has been concluded that the activated carbon prepared from Coconut shell can be used as an effective adsorbent for the removal of Cd(II) from aqueous solution.

Keywords: Activated carbon, adsorption, coconut shell, adsorption isotherms, cadmium

Introduction

Cadmium is one of toxic heavy metals released to the environment through the combustion of fossil fuels, metal production, application of phosphate fertilizers, alloy formation, electroplating, production of batteries, etc. [1,2]. This metal is a non-essential and non-beneficial element for plants, animals and human beings. It has a high affinity for sulfhydryl (-SH) groups of proteins for which it competes with Zn(II) in biological systems and is known as a human carcinogen [3]. Due to its low-concentration-long-term effect in drinking water, cadmium belongs to the chemicals list of endocrine disruptors and priority control pollutants issued by USEPA [4,5]. The toxic implications of cadmium in the environment has made the US Environmental Protection Agency (USEPA) set the level of cadmium in drinking water to 0.002 mgL^{-1} and the World Health Organization (WHO) maximum permissible limit for cadmium in drinking water is 0.003 mgL^{-1} [6-9]. The heavy metalis not biodegradable and tends to accumulate in living organisms, causing various diseases and disorders. As far as cadmium is concerned, it causes serious renal damage anemia, hypertensions, testicular atrophychronic disorders such as "itai–itai", lungs fibrosis etc. [10]. The reduction of the pollutant to an acceptable level is needed when the toxic metal is present in the solution. The physicochemical processes such as precipitation, reverse osmosis, ion exchange, adsorption, membrane filtration, electro dialysis, chemical oxidationetc. are employed to treat cadmium-containing effluents. Theprocesses mentioned above with the exception of adsorption are expensive and also have disadvantages such as incomplete metal removal, high reagent, energy requirements and generation of toxic sludge or other waste products that require proper disposal [11]. Because of the problems this research has been focused on using adsorption since it is cheaper, making use of low cost and local Adsorbents, which are adapted inefficiently removing heavy metal ions found in low concentrations in solution. Many

researchers have used a variety of agricultural wastes for the preparation of low cost activated carbon from cheaper and readily available materials. The wastes such as rice husk [12], apricot stone [13], lapsi seed stone [14], olive stone [15], date stone [16], cotton stalk [17] coconut shell [18], peanut shell etc, [19]. have been tested in the production of activated carbon in developing countries. The use of this raw material in the preparation of activated carbon shows from the past studies that they are available at low cost, contain high carbon content and may be effective in the removal of heavy metals.

The present study explored the use of activated carbon prepared from Coconut shell as an adsorbent for the removal of Cd(II) from aqueous solution. The effect of factors such as contact time, pH, the adsorbent dose was investigated. The adsorption kinetics of Cd(II) onto the activated carbon was analyzed by Pseudo first and pseudo second-order models. Experimental equilibrium data were also analyzed by Langmuir and Freundlich isotherms.

Materials and Methods

Preparation of adsorbent

The precursor used in this work is Coconut shell, the waste material left the consumption of edible part. The coconut shells were washed well with tap water and then with distilled water. The washed materials were dried well at 110 ^{o}C and crushed with an iron mortar and electric grinder to obtain the size of 300 µm.The dried mass was mixed with 50% H_3PO_4 in the ratio of 1:1 and carbonized at 400 ^{o}C for 4 hours and cooled after optimizing the parameters like the percentage of phosphoric acid, the ratio of precursor / phosphoric acid, carbonization time and carbonization temperature. The activated carbon was washed with warm distilled water and dried. The carbon was then cooled and sieved to obtain particles of size 106µm. The activated carbon thus prepared was represented by CSPAAC (coconut shell phosphoric acid activated carbon) and used for the adsorption process.

Chemicals and equipment

The chemicals and reagents used in this work are of analytical grade. The stock solution of heavy metals and other solutions were prepared using the distilled water prepared in the laboratory. pH of the solutions was adjusted by 0.1M HCl and 0.1 M NaOH. The adsorption experiments were carried out by using Shaker (Digital VDRL Rotator-RPM-S). The concentrations of heavy metal (II) ions were determined by atomic absorption spectrophotometer (AAS –VARIAN-AA240FS). Digital pH meter was used to measure the pH of solutions.

Adsorption experiment

In order to investigate adsorption, batch experiments were carried out in 50 mL stoppered conical flasks. The flasks were agitated on Digital VDRL Rotator-RPM-S at 225 rpm for identified time intervals. The effect of contact time, adsorbent dose and solution pH was studied. Each experiment was carried out by suspending 0.05 g of adsorbent in 25 mL adsorbate solution taken in the conical flasks under the optimum conditions set out for the experiments. Since pH is a critical parameter in the process; therefore, the pH of the solutions was adjusted by the addition of 0.1M NaOH and 0.1M HCl. The number of metal ions

$$q_e = (C_o - C_e) \times V/W \quad \text{.....(1)}$$

adsorbed can be calculated by the following equation.

Where C_o and C_e = initial and equilibrium concentration of metal ion (mg / L) respectively,

W= the mass of adsorbent in gram (g) and

V = the volume of the solution in a liter (L).

$$\text{Rem \%} = (C_o - C_e) \times 100/C_o \quad \text{.....(2)}$$

The percentage of removed metal ions (Rem %) in solution is calculated by using the following formula

Results and Discussion

Scanning electron microscope (SEM)

Scanning Electron Microscope (SEM) of the carbon prepared without activating agent and activated prepared with H_3PO_4 as activating agent 50 % H_3PO_4 is presented in Figure 1 and Figure 2 respectively. Figure 1 is the SEM of carbon prepared from Coconut shell without any activating agent. The surface is heterogeneous and hardly any pores are visible. Figure 2 is the SEM images of activatedcarbon prepared by using H_3PO_4 as an activation agent. In the SEM image of Figure 2, a number of pores with different diameters are observed [20]. This development of porous structure may be attributed to the dehydrating effect of H_3PO_4.

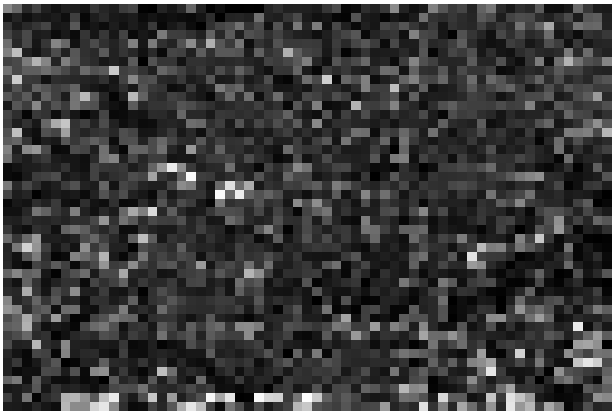

Figure 1: *SEM of carbon without activating agent*

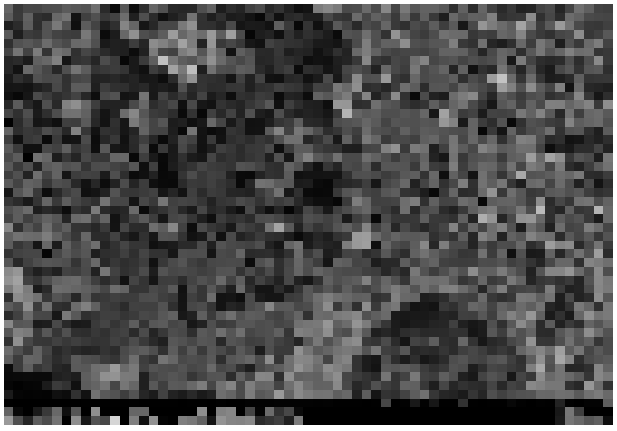

Figure 2: *SEM of activated carbon*

Phosphoric acid being a strong dehydrating agent removes oxygen and hydrogen from coconut shells as water, and that promotes the development of the porous structure.

Fourier transform infrared (FTIR) spectroscopy

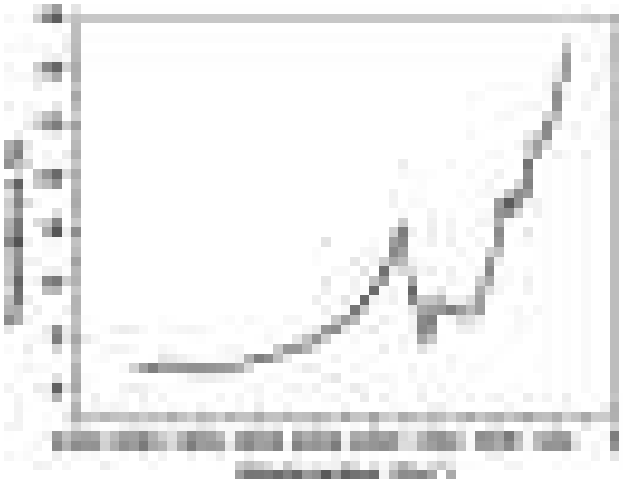

Figure 3: *FTIR spectra of activating agent*

Figure 4: *FTIR spectra of activating carbon*

The FTIR spectra of activated carbon as shown in Figure 4 exhibit a broad band at 3419 cm^{-1} due to the presence of hydroxyl groups on the adsorbent surface. The band located at 1725 cm^{-1} is ascribed to the stretching vibrations of carboxylic groups or to conjugated carbonyl groups (C=O in carboxylic and lactones groups). Asymmetric stretching vibrations of ionic carboxylic groups (-COO-) appeared at 1571 cm^{-1}. The functional groups play an important role in the adsorption of the metal ions by donating electrons to heavy metal ions. These bands observed in the activated carbon are not seen in the carbon prepared without activating agent as shown in Figure 3.

X-ray diffraction (XRD)

XRD of the started as shown shows that the two broad diffraction peaks located near $2\theta = 25.5^{o}$ and 43^{o} reflected from 002 and 100 planes as shown in Figure 5. The appearance of the broad peaks shows

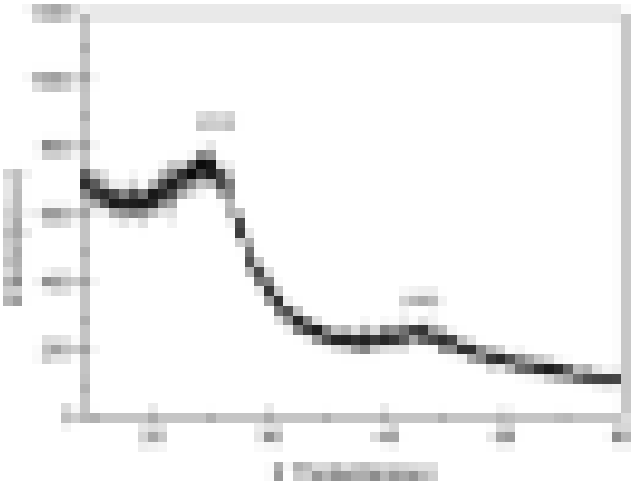

Figure 5: *XRD of activated carbon*

that the activated carbon is amorphous that is the good property of activated carbon for the adsorption.

Adsorption isotherms

Adsorption isotherms are mathematical models that describe the distribution of the adsorbate species among liquid and solid phases, based on a set of assumptions that are related to the heterogeneity/ homogeneity of the solid surface, the type of coverage, and the possibility of interaction between the adsorbate species. In the present study equilibrium data were analyzed using Langmuir and Freundlich isotherms.

Langmuir isotherm

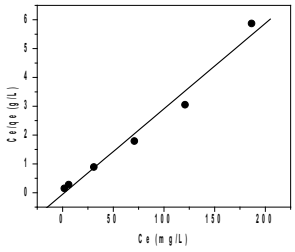

Figure 6: *Langmiur adsorption isotherm for adsorption of Cd (II) on CSAAC*

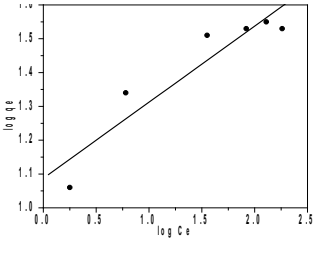

Figure 7: *Freundelich adsorption isotherm for adsorption of Cd (II) on CSAAC*

The Langmuir model assumes that the sorption of metal ions happens on a homogenous surface by monolayer adsorption with no interaction between adsorbed ions. The linear form of Langmuir adsorption isotherm is represented by the following equation.

$$C_e/q_e = (1/ bq_m)+ C_e/q_m \text{.....}\ldots\text{.....}\ldots(3)$$

Where, Ce = is the equilibrium concentration of the adsorbate (mg/L)

qe = the amount of the adsorbate adsorbed at equilibrium

qm = the monolayer adsorption capacity (mg /g)

b = Langmuir constant [21].

Adsorption capacity and Langmuir constant can be calculated from the slope and intercept of the plot C_e/q_e versus C_e as shown in Figure 6.

Freundlich isotherm

The Freundlich equation is an empirical equation based on adsorption on a heterogeneous surface. The linear form of the Freundlich isotherm equation can be represented as follows.

$$\log q_e = \log K_f + (1/n) \log C_e \text{.....}(4)$$

Where, K_f and n = the Freundlich constants related to adsorption capacity and intensity. qe and Ce = the amount of adsorbate adsorbed and equilibrium concentration of the adsorbate respectively.

The values of K_f and 1/n can be determined from the intercept and slope of the plot of log qe versus log Ce as shown in Figure 8. The Langmuir and Freundlich adsorption isotherm parameters are shown in Table 1.

Table 1: *Langmiur and Freundlich parameters of CSAAC*

Heavy metal ions	Langmuir parameters		R^2	Freundlich parameters		R^2
	Q_{max} (mg/g)	b		K_f(mg/g)	n	
Cd (II)	33.71	0.527	0.985	0.031	4.446	0.875

Adsorption kinetics

Adsorption kinetics plays an important role to determine the efficiency of adsorption. Most commonly used two kinetic models like pseudo first-order and second-order kinetic models have been applied to the adsorption kinetic data to analyze the rate of adsorption.

Pseudo first-order

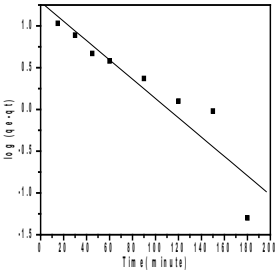

Figure 8: *Pseudo first order kinetics of adsorption of Cd (II) on CSAAC*

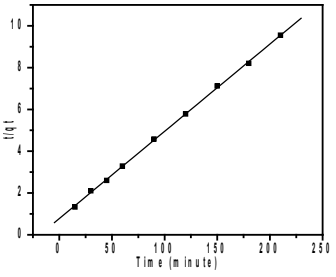

Figure 9: *Pseudo second order kinetics of adsorption of Cd (II) on CSAAC*

The pseudo first-order model was given by Legergren in 1898 [21]. According to him the first-order equation is represented as follows.

$$dqt/ dt = K_1 (q_e - q_t) \text{.....}(5)$$

Where qe = Equilibrium concentration of the metal ions adsorbed (mg/g)

qt = the amount of the metal ions adsorbed at the time 't' (mg/g)

K_1= the pseudo first-order rate constant (L min^{-1}).

On integration the equation (5) will take the form as follows:

$$\log (q_e - q_t) = \log q_e - (K_1/2.303)\, t \quad \text{.....(6)}$$

The plot of the value of $\log (q_e - q_t)$ against 't' as shown in Figure 8 has been applied to test the validity of the kinetic model.

Pseudo second-order

The pseudo second-order model is also called Ho second-order model. The rate equation of pseudo second-order is as follows.

$$dqt/dt = K_2 (q_e - q_t)^2 \quad \text{.....(7)}$$

Where k_2 =second order rate constant of adsorption (g mg $^{-1}$ min $^{-1}$).

The equation (7) after integration takes the form as follows.

$$1/(q_e - q_t) = 1/(q_e \times K_2) + 1/q_e \quad \text{.....(8)}$$

By rearranging the equation (8) will be as follows

$$1/qt = 1/(q_e^2 \times K_2) + 1/q_e \quad \text{……..(9)}$$

The plot of the value of 't/qt' against 't' as given in Figure 9 has been applied to test the validity of the kinetics.

Table 2: *Parameters of Pseudo first and second order kinetics*

Pseudo First-order Model			Pseudo Second-order Model		
q_e (mg/g)	K_1 (1/min)	R^2	q_e (mg/g)	K_2 (g/mg min)	R^2
19.349	0.027	0.865	23.940	2.257×10^{-3}	0.999

The slopes and intercepts of the curves have been applied to calculate the kinetic parameters such as k_1 and equilibrium adsorption capacity. The constants of the kinetic models are given in Table 2.

Conclusion

Adsorption isotherms and adsorption kinetics for the adsorption of Pb (II) have been investigated using the activated carbon prepared from coconut shell. The adsorption of the metal ions has been found to be dependent on pH and the maximum adsorption has been observed at pH 6. Optimal contact time and adsorbent dose have been found to be 180 minutes and 2 g/L respectively. The SEM of the activated carbon has shown the pores of different diameters. Broad peaks in the activated carbon were investigated by XRD. The equilibrium data were best described by Langmuir adsorption isotherm with a higher correlation coefficient (R^2=0.985) than that of Freundlich isotherm (R^2=0.875) showing a maximum adsorption uptake of 33.71 mg/g. Analysis of adsorption kinetic data has shown that the Pseudo second- order model was found to describe adsorption much better with high correlations coefficient (R^2= 0.999) than that of Pseudo first- order model (R^2= 0.865). The results of the present study show that Coconut shell based activated carbon can be used as an efficient adsorbent for the removal of cadmium ions from aqueous solution.

References

1. Y. C. Sharma, Thermodynamics of removal of cadmium by adsorption on an indigenous clay, *Chemical Engineering Journal*, 2008, **145**, 64-68.
2. A. B. Perez-Marin, V. M. Zapata, J. F. Ortuno, M. Aguilar, J. Saez and M. Lorens, Removal of cadmium from aqueous solutions by adsorption onto orange waste, *Journal of Hazardous Materials*, 2007, **139,** 122-131.
3. WHO, *Exposure to Cadmium: a major public health concern, preventing disease through environments*, 2010.
4. X. Huang, N. Gao and Q. Zhang, Thermodynamics and kinetics of cadmium adsorption onto oxidized granular activated carbon, *Journal of Environmental Sciences*, 2007, **19**(11), 1287-1292.
5. USEPA, *United States Environmental Protection Agency-Cadmium Compounds*, 2016.
6. K. S. Rao, M. Mahapatra, S. Anand, and P. Venkateswarlu, Review on cadmium removal from aqueous solutions, *International Journal of Engineering Science and Technology,* 2010, **2**(7), 81-103.
7. Y. Xi, Y. Luo, J. Luo, and X. Luo, Removal of cadmium(II) from wastewater using novel cadmium ion-imprinted polymers, *Journal of Chemical Engineering Data*, 2015, **60**, 3253-3261.
8. WHO, *Cadmium in Drinking Water,* Background document for development of WHO guidelines for drinking water-quality, 2011.
9. A. Mahvi, J. Nouri, G. A. Omrani and F. Gholami, Application of *Platinus orientalis* leaves in the

removal of cadmium from aqueous solution, *World Applied Science Journal,* 2007, **2**, 40-44.

10. J. Ketcha Mbadcam, H. Ngomo Manga, C. Tcheka, A. Ntieche Rahman, H. S. Djoyo and D. Kouotou, Batch adsorption of cyanides from aqueous solution onto copper and nickel-impregnated powder activated carbon and clay, *International Journal of Production Science*, 2009, **3**, 53-57.
11. K. Srinivasan, K. Balsubramaniam and T. V. Ramkrishnan, Studies on chromium removal by rice husk, *Industrial and Engineering Chemistry Research,* 1998, **39**, 376-387.
12. M. Lotfi, M. Djoudi, B. Abdelkrim and B. Lazhar, Adsorption of Pb(II) from aqueous solutions using activated carbon developed from Apricot stone, *Desalination,* 2011, **276**, 148-153.
13. R. M. Shrestha, A. P. Yadav, B. P. Pokharel and R. R. Pradhananga, Preparation and characterization of activated carbon from Lapsi (*Choerospondias axillaris*) seed stone by chemical activation with phosphoric acid, *Research Journal of Chemical Sciences*, 2012, **2**(10), 80-86.
14. T. A. Bohli, N. F. Ouederni and I. Villaescusa, Uptake of Cd^{+2} and Ni^{+2} metal ions from aqueous solutions by activated carbons from waste olive stones, *International Journal of Chemical Engineering and Applications*, 2012, **3**(4), 232-236.
15. J. A. Muthanna, Preparation of activated carbons from date stones by chemical activation method using $FeCl_3$ and $ZnCl_2$ as activating agents, *Journal of Engineering,* 2011, **17**(4), 1007-1022.
16. L. Kunquan, Z. Zhen and L. Ye, Characterization and lead adsorption properties of activated carbons prepared from cotton stalk by one-step H_3PO_4 activation, *Journal of Hazardous Materials*, 2010,**181**, 440 - 447.
17. M. Sekar, V. Sakthi and S. Rengarag, Kinetics and equilibrium adsorption study of lead (II) onto activated carbon prepared from coconut shell, *Journal Colloid and Interface Science*, 2004, **279**, 307-317.
18. W. K. Anna, G. S. Roman and M. Szymon, Biosorption of heavy metals from aqueous solutions onto peanut shell as a low cost biosorbent, *Desalination*, 2011, **265**, 126-134.
19. R. M. Shrestha, Removal of Cd(II) ions from aqueous solution by adsorption on activated carbon prepared from Lapsi (*Choerospondias axillaris*) seed stone, *Journal of the Institute of Engineering*, 2015, **11**(1), 140-150.
20. T. M. Elmorsi, Z. H. Mohamed, W. Shopak and A. M. Ismaiel, Kinetic and equilibrium isotherms studies of adsorption of Pb(II) from water onto natural adsorbent, *Journal of Environmental Protection*, 2014, **5**, 1667-1681.
21. Y. S. Ho, Citation review of Legergren kinetic rate equation on adsorption reactions, *Scienctometrics*, 2004, **59**(1), 171-177.